

**Technical Report  
997**

**Exponential Decay in Windblown  
Radar Ground Clutter Doppler Spectra:  
Multifrequency Measurements and Model**

**J.B. Billingsley**

**DTIC QUALITY INSPECTED 4**

**29 July 1996**

---

**Lincoln Laboratory**  
MASSACHUSETTS INSTITUTE OF TECHNOLOGY  
*LEXINGTON, MASSACHUSETTS*

---

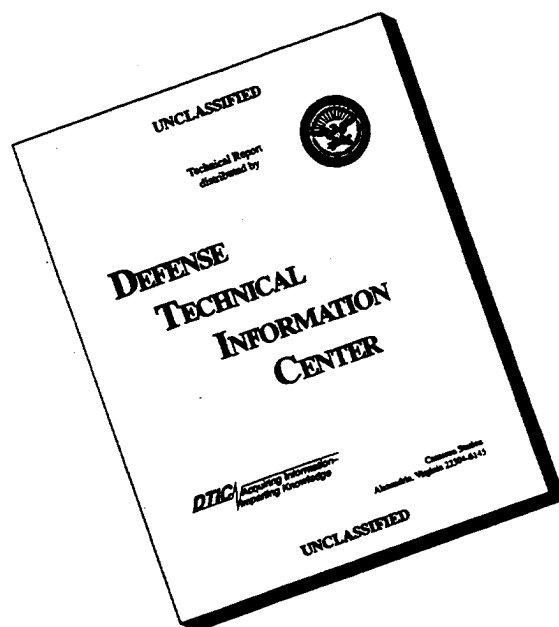


Prepared for the Department of the Air Force and the Defense Advanced  
Research Projects Agency under Air Force Contract F19628-95-C-0002.

Approved for public release; distribution is unlimited.

**19960820 064**

# DISCLAIMER NOTICE



**THIS DOCUMENT IS BEST QUALITY AVAILABLE. THE COPY FURNISHED TO DTIC CONTAINED A SIGNIFICANT NUMBER OF PAGES WHICH DO NOT REPRODUCE LEGIBLY.**

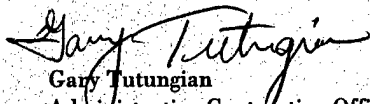
**This report is based on studies performed at Lincoln Laboratory, a center for research operated by Massachusetts Institute of Technology. The work was sponsored by the Department of the Air Force and the Defense Advanced Research Projects Agency under Air Force Contract F19628-95-C-0002.**

**This report may be reproduced to satisfy needs of U.S. Government agencies.**

**The ESC Public Affairs Office has reviewed this report, and it is releasable to the National Technical Information Service, where it will be available to the general public, including foreign nationals.**

**This technical report has been reviewed and is approved for publication.**

**FOR THE COMMANDER**

  
**Gary Tutungian**  
**Administrative Contracting Officer**  
**Contracted Support Management**

## ABSTRACT

A new empirical model for windblown radar ground clutter Doppler spectra is developed based on many clutter spectral measurements obtained with Lincoln Laboratory's L-Band Clutter Experiment (LCE) and Phase One five-frequency (i.e., VHF, UHF, L-, S-, and X-band) instrumentation radars over spectral dynamic ranges reaching 60 to 80 dB below zero-Doppler peaks. The model includes both ac and dc spectral components. Ac spectral shape is specified as exponential, with the Doppler-velocity exponential shape factor strongly dependent on wind speed but independent of radar frequency, VHF to X-band. The exponential shape is intermediate in spectral extent between the Gaussian shape of historical usage (now acknowledged as being too narrow) and power-law shapes of more recent usage (which are too wide when extrapolated to levels 60 to 80 dB down). The ratio of dc to ac spectral power in the model is determined by an empirically derived analytic expression that captures the strong dependencies of dc/ac ratio on both wind speed and radar frequency in the measurement data. Many examples of windblown clutter spectra are provided and compared with model predictions, encompassing variations in wind speed and radar frequency, as well as in other parameters such as polarization, range, cell size, grazing angle, wind direction, measurement site, and season of the year. Although the exponential model is explicitly derived to be applicable to windblown trees, examples are also provided of measured clutter spectra from scrub desert, rangeland, and cropland vegetations which indicate that the model can also perform adequately for other windblown vegetation types by suitably adjusting its dc/ac term. In addition, the moving target indicator (MTI) improvement factor for a single delay-line canceller in exponentially distributed clutter is derived and compared with that for Gaussian clutter; and the theoretical and experimental literature on windblown radar clutter is reviewed, including the somewhat apocryphal evidence that spectral tails very much wider than exponential might exist at spectral power levels well below LCE and Phase One radar sensitivities.

## **PREFACE**

The exponential clutter spectral model presented herein has now been serving Air Vehicle Survivability Evaluation program needs at Lincoln Laboratory for several years. This report documents and disseminates this model to other potential users, provides a complete elaboration of the development of the model so that other users may be able to independently assess its appropriateness and expected accuracy for their particular applications, and compares and contrasts the current exponential model with the existing technical literature on the subject of windblown radar clutter spectra, both theoretical and experimental.

## ACKNOWLEDGMENTS

It is a pleasure to acknowledge Air Force and DARPA sponsorship and Lincoln Laboratory management for conceiving and implementing radar ground clutter measurement activities at Lincoln Laboratory and for providing follow-on support over a number of years in the analysis of the resulting ground clutter spectral data bases leading to the general spectral model of this report. The radar clutter data at Lincoln Laboratory were shared with the governments of Canada and the U.K. under the auspices of The Technical Cooperation Program, and considerable additional spectral analyses of the data have been undertaken under their sponsorship. In particular, many helpful exchanges concerning the spectral information in these data have occurred between the author and Dr. H.C. Chan of Defence Research Establishment Ottawa. At Lincoln Laboratory, John F. Larrabee (Lockheed Martin Corporation) has provided invaluable assistance in the day-to-day management, reduction, and analyses of the clutter spectral data. Others assisting in data reduction and analysis activities at Lincoln have included Dr. Seichoong Chang, Reese Straw, William Dustin, Carol Bernhard, Joanne Bradley and Bob Graham-Munn. The manuscript was skillfully prepared by Pat DeCuir and kindly and efficiently reviewed by Mr. C.E. Muehe who provided a number of constructive suggestions.

## TABLE OF CONTENTS

Abstract	iii
Preface	v
Acknowledgments	vii
List of Illustrations	xi
List of Tables	xiii
 1. INTRODUCTION	 1
 2. WINDBLOWN CLUTTER SPECTRAL MODEL	 3
2.1 ac Spectral Shape	3
2.2 dc/ac Ratio	5
2.3 Model Scope	6
 3. MEASUREMENT BASIS FOR CLUTTER SPECTRAL MODEL	 9
3.1 Radar Instrumentation and Data Reduction	9
3.2 Measurements Illustrating ac Spectral Shape	15
3.3 Measured Ratios of dc/ac Spectral Power	29
 4. USE OF CLUTTER SPECTRAL MODEL	 35
4.1 Spreading of $\sigma^0$ in Doppler	35
4.2 Two Regions of Spectral Approximation	35
4.3 Cells in Partially Open or Open Terrain	39
4.4 MTI Improvement Factor	49
 5. HISTORICAL REVIEW	 55
5.1 Three Analytic Spectral Shapes	55
5.2 Reports of Unusually Long Spectral Tails	82
 6. SUMMARY	 93
 REFERENCES	 97

## LIST OF ILLUSTRATIONS

Figure No.		Page
1	Exponential model for windblown forest ac clutter spectral shape, parameterized by wind speed.	4
2	Modeling information specifying ratio of dc to ac spectral power in windblown forest clutter spectra versus wind speed and radar frequency.	6
3	Four measured power spectra from "stationary" targets exhibiting little or no discernible spectral spreading to levels 70 to 80 dB down.	13
4	Highly exponential decay ( $\beta = 5.2$ ) in a forest clutter spectrum measured under windy conditions.	16
5	Approximate exponential decay in a forest clutter spectrum measured under breezy conditions.	17
6	Approximate exponential decay in a forest clutter spectrum measured under light wind conditions.	18
7	Variation of LCE windblown forest clutter spectra with wind speed.	19
8	Scaled estimate of windblown forest clutter spectrum under gale force winds.	20
9	Variation of windblown forest clutter spectra with radar frequency under windy conditions.	22
10	Variation of Phase One windblown forest clutter spectra with radar frequency under breezy conditions, UHF, L-, and S-band.	23
11	Variation of LCE windblown forest clutter spectra with polarization.	24
12	Variation of LCE windblown forest clutter spectra with time.	25
13	Variation of Phase One L-band windblown forest clutter spectra with time.	26
14	Similar LCE and Phase One forest clutter spectra measured under windy conditions at two different sites.	28
15	An LCE windblown forest clutter spectrum measured under light wind conditions.	30
16	LCE measurements showing ratio of dc to ac spectral power versus wind speed in L-band windblown forest clutter spectra.	31
17	A Phase One windblown forest clutter spectrum at VHF.	32
18	Phase One measurements showing ratio of dc to ac spectral power versus radar frequency under windy conditions at three forested sites.	33
19	Modeling of clutter spectra.	36
20	Highly exponential decay in four measured windblown forest clutter spectra.	37
21	An LCE measured clutter spectrum from desert terrain under windy conditions.	39



## LIST OF ILLUSTRATIONS (Continued)

Figure No.		Page
22	Comparisons of ac spectral shapes of LCE desert and forest clutter spectra under windy conditions.	41
23	Phase One X-band desert clutter spectral measurements.	42
24	Phase One five-frequency clutter spectra from North Dakota wheatland measured on four different days.	44
25	Phase One S-band cropland clutter spectrum from Beiseker, Alta.	47
26	Three analytic spectral shapes each normalized to unit spectral power.	55
27	Measurements of radar ground clutter power spectra by Barlow.	57
28	A measured radar ground clutter power spectrum by Fishbein et al.	60
29	Two measurements of radar ground clutter power spectra by Warden and Wyndham.	61
30	Measurements of radar ground clutter power spectra by Kapitanov et al.	62
31	Measurements of radar ground clutter power spectra by Andrianov, Bondarenko, et al.	63
32	Measurements of radar ground clutter power spectra by Andrianov, Armand, and Kibardina.	64
33	Measurements of radar ground clutter power spectra by Simkins et al.	66
34	Measurements of radar ground clutter power spectra by Chan.	71
35	Phase One ground clutter spectra from Wainwright, Alta. as processed by Sarno.	72
36	Phase One ground clutter spectra from Wainwright, Alta. as processed at Lincoln Laboratory.	73
37	Measurements of radar ground clutter power spectra by Cartledge et al.	75
38	Comparison of an LCE windblown forest clutter spectrum with the Fishbein et al. power-law model.	78
39	Two windblown forest clutter spectra for which exponential fits are compared with power-law fits.	79
40	Comparison of exponential and power-law spectral shapes.	81
41	Chan's conceptual composite clutter model, including a fast-diffuse component.	83
42	Measurements of radar ground clutter power spectra by Goldstein under gale force winds.	87
43	A radar ground clutter power spectrum computed from Goldstein's measured correlation function by Wong et al.	88
44	Measurements of radar ground clutter power spectra by Armand et al.	90

## LIST OF TABLES

Table No.		Page
1	Exponential ac Shape Parameter $\beta$ vs Wind Speed	4
2	Radar System Parameters	10
3	Phase One Clutter Spectra Parameters; Katahdin Hill Data	11
4	Variation of dc/ac Ratio with Length of CPI for LCE Clutter Measurements from Windblown Trees	15
5	Measured vs Modeled Ratios of dc/ac Spectral Power in Four Windblown Forest Measured Clutter Spectra	38
6	Phase One-Measured Ratios of dc/ac Clutter Spectral Power in Beulah, N. Dakota, Wheatland	46
7	Improvement Factor $I_\beta$ in Exponential Clutter for an X-Band Radar	52
8	Improvement Factor $I_g$ in Gaussian Clutter for an X-Band Radar	53
9	Comparison of Ewell and Fishbein Power-Law Clutter Spectral Shape Parameters	69
10	Exponential Approximations to Wainwright Clutter Spectra	74

# 1. INTRODUCTION

Moving target indication (MTI) radar utilizes Doppler processing to separate small moving targets from large clutter returns. Any intrinsic motion of the clutter sources causes the clutter returns to fluctuate with time and the received clutter power to spread from zero-Doppler in the frequency domain. As a result, intrinsic clutter motion degrades and limits MTI performance. Current MTI design objectives can require clutter rejection in the 60- to 80-dB range or more, and can be implemented not only by using conventional fixed-parameter MTI filter design [1,2] but also through modern adaptive Doppler-processing techniques [3,4]. However implemented, successful clutter rejection to such low levels requires accurate definition of the detailed shape of the intrinsic-motion clutter spectrum. The most pervasive source of intrinsic fluctuation in ground clutter is the wind-induced motion of tree foliage and branches or other vegetative land cover. The shape of windblown tree clutter spectra has been a subject of investigation since the early days of radar development. Although this subject continues to be important today, it has generally remained rather poorly understood, largely because of the difficulty of accurately measuring clutter spectra to very low spectral power levels.

Radar ground clutter power spectra were originally thought to be of Gaussian shape [5–8]. Later, with measurement radars of increased spectral sensitivity, it became apparent that spectral tails wider than Gaussian existed that could be modeled as power law over the spectral ranges of power—typically 35 to 40 dB below the peak zero-Doppler level—then available [9–10]. A number of measurements of clutter spectra all generally characterized as power law followed [11–22], and much current discussion continues to focus on power-law representation of spectral shape. If real when extrapolated to low levels, power-law spectral tails would severely limit MTI Doppler-processor performance against small targets and would reduce motivation for suppressing radar phase noise to lower levels. Recent measurements of windblown ground clutter power spectra at Lincoln Laboratory to levels substantially lower (i.e., 60 to 80 dB down) than most earlier measurements indicate spectral shapes that fall off much more rapidly than constant power-law at rates of decay often approaching exponential [23–31]. It has become reasonably well known that Lincoln Laboratory observes exponential spectral shapes, but it is not well understood how these observations are reconcilable with the earlier power-law observations. One purpose of this report is to resolve these apparently conflicting results.

The most salient aspect of Lincoln Laboratory's measurements of windblown ground clutter power spectra is their rapid decay to levels 60 to 80 dB down from zero Doppler. This report provides a simple model with exponential decay characteristics for the Doppler-velocity power spectrum of radar returns from cells containing windblown trees. This exponential model empirically captures, at least in general measure and occasionally very accurately, the major attributes of the measured phenomenon. The exponential shape (a) is somewhat wider than the historic Gaussian shape, as required by the general consensus of experimental evidence; (b) is very much narrower at lower power levels (i.e., 60 to 80 dB down) than more recent power-law representations when they are extrapolated to such low levels; and (c) at higher power levels (35 to 40 dB down) finds gross equivalence in spectral level and extent with a number of reported results modeled as power law at these higher levels. Important effects of wind speed and radar frequency (VHF to X-band) on windblown ground clutter spectra are also described and incorporated in the model.

This report presents the exponential model in Section 2. The general validity of the postulated model is demonstrated in Section 3 by comparing with numerous measurements. Section 4 briefly discusses (a) how to use the exponential clutter spectral model to calculate the absolute level of clutter power in any radar Doppler cell; (b) differentiation of quasi-dc and -ac regions of spectral approximation; (c) how the exponential model can perform adequately not only in forested but also in nonforested terrain (farmland, desert) by suitably adjusting the dc/ac term of the model; and (d) comparison of the MTI improvement factors for a single delay-line canceller in exponential versus Gaussian clutter. Section 5 is a detailed historical review that compares and contrasts current clutter spectral results with those previously reported. Section 6 is a summary.

## 2. WINDBLOWN CLUTTER SPECTRAL MODEL

Consider a radar spatial resolution cell containing windblown trees. Such a cell contains both fixed scatterers (ground, rocks, tree trunks) and moving scatterers (leaves, branches). The returned signal correspondingly contains both a constant (or steady) and a varying component. The steady component gives rise to a dc or zero-Doppler term in the power spectrum of the returned signal, and the varying component gives rise to an ac term in the spectrum. Thus a suitable general analytic representation for the total spectral power density  $P_{tot}(\nu)$  in the Doppler-velocity power spectrum from a cell containing windblown vegetation is provided by

$$P_{tot}(\nu) = \frac{r}{r+1} \cdot \delta(\nu) + \frac{1}{r+1} P_{ac}(\nu), -\infty < \nu < \infty \quad (1)$$

where  $\nu$  is Doppler velocity in m/s,  $r$  is the ratio of dc power to ac power in the spectrum,  $\delta(\nu)$  is the Dirac delta function, which properly represents the shape of the dc component in the spectrum, and  $P_{ac}(\nu)$  represents the shape of the ac component of the spectrum, normalized such that  $\int_{-\infty}^{\infty} P_{ac}(\nu) d\nu = 1$ . Since by definition  $\int_{-\infty}^{\infty} \delta(\nu) d\nu = 1$ , it follows that normalization in Equation (1) is to unit total spectral power, i.e.,  $\int_{-\infty}^{\infty} P_{tot}(\nu) d\nu = 1$ .

It is apparent from Equation (1) that for  $|\nu| > 0$ ,  $P_{tot}(\nu) = [1/(r+1)] P_{ac}(\nu)$ . In considering analytic spectral shapes,  $P_{ac}(\nu)$  is the fundamental quantity, whereas in measured results  $P_{tot}(\nu)$  is the fundamental quantity. On a decibel scale, the level of an analytic spectral shape function  $10 \log_{10} P_{ac}$  must be reduced by  $10 \log_{10} (r+1)$  before comparison with directly measured data  $10 \log_{10} P_{tot}$ . Or the level of directly measured data  $10 \log_{10} P_{tot}$  must be raised by  $10 \log_{10} (r+1)$  before considering its ac spectral shape. Such normalization adjustments obviously depend on the dc/ac ratio  $r$ , a highly variable quantity in measured clutter spectra. In this report, either  $P_{tot}$  or  $P_{ac}$  can represent measured or modeled data, depending on context.

### 2.1 AC SPECTRAL SHAPE

Radar ground clutter spectral measurements at Lincoln Laboratory to levels 60 to 80 dB below the peak zero-Doppler level indicate that the shapes of the spectra often decay at rates close to exponential. The two-sided exponential spectral shape may be represented analytically as

$$P_{ac}(\nu) = \frac{\beta}{2} \cdot \exp(-\beta|\nu|), -\infty < \nu < \infty, \quad (2)$$

where  $\beta$  is the exponential shape parameter. Table 1 provides values of  $\beta$  as a function of wind conditions. The terminology used here to describe wind conditions borrows from but does not strictly adhere to that of the Beaufort wind scale [17,21]. The current Lincoln spectral measurements include no examples under gale force wind conditions, but Table 1 includes a scaled estimate of what is expected for spectral extent under such conditions. The current measurements of clutter spectra range from VHF to X-band. These multifrequency measurements indicate that the information specifying spectral shape  $P_{ac}(\nu)$  in Table 1 is largely independent of radar carrier frequency over this range. The exponential shapes specified in the table are plotted in Figure 1.

**Table 1.**  
**Exponential ac Shape Parameter  $\beta$  vs Wind Speed**

Wind Conditions	Wind Speed (mph)	Exponential ac Shape Parameter $\beta$ (m/s) <sup>-1</sup>	
		Typical	Worst Case
Light air	1–7	12	—
Breezy	7–15	8	—
Windy	15–30	5.7	5.2
Gale force (est.)	30–50	4.3	3.8

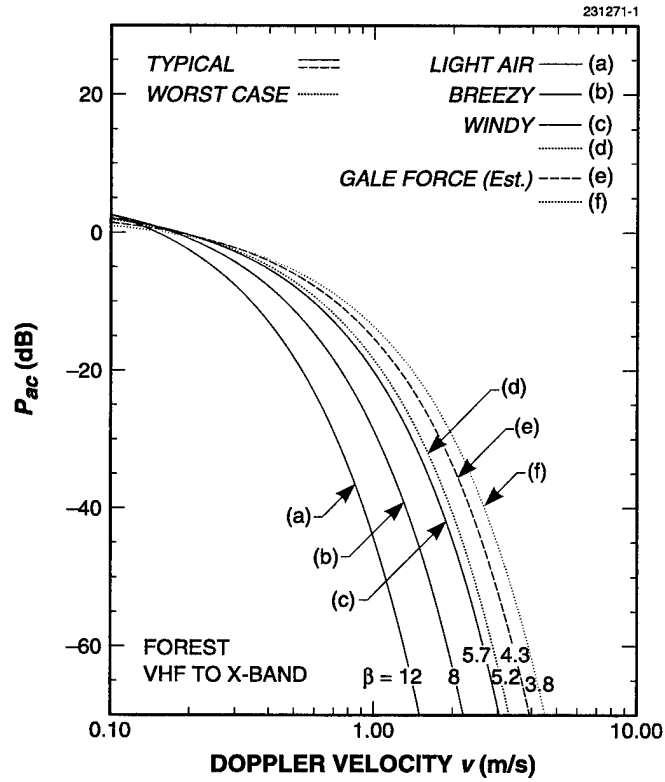


Figure 1. Exponential model for windblown forest ac clutter spectral shape, parameterized by wind speed. Applicable VHF to X-band.

Doppler frequency  $f$  in Hertz and radial Doppler velocity  $v$  in m/s are fundamentally related as  $f = 2v/\lambda$ , where  $\lambda$  is radar wavelength. It follows that if the Doppler velocity extent of measured clutter spectra from windblown vegetation is largely invariant with radar frequency, the Doppler frequency extent from windblown vegetation must scale approximately linearly with radar frequency. In this report clutter spectra are plotted using a Doppler velocity abscissa as opposed to the more commonly used Doppler frequency abscissa to allow direct comparison of spectral shape and extent at different radar frequencies with the linear scaling factor normalized out.

## 2.2 DC/AC RATIO

Although  $P_{ac}(v)$  in Equation (2) is largely independent of radar frequency, the value of dc/ac ratio  $r$  in Equation (1) is strongly dependent on both wind speed and radar frequency. An analytic expression for  $r$  empirically derived from the current Lincoln measurements which generally captures these dependencies is provided by

$$10 \log_{10} r = -15.5 \log_{10} w - 12.1 \log_{10} f_0 + 63.2 \quad , \quad (3)$$

where  $w$  is wind speed in miles per hour, and  $f_0$  is radar carrier frequency in megahertz. Equation (3) applies to cells containing windblown trees. The data base from which it was derived covers the frequency range from 170 MHz (i.e., VHF) to 9200 MHz (i.e., X-band) and includes measurements from many forested cells under various wind conditions. The variation of  $r$  with wind speed and radar frequency as specified by Equation (3) is plotted in Figure 2. The quantity  $r$  in Equation (3) is also the ratio of steady to random average power (originally defined as  $m^2$  by Goldstein [8]) in the Ricean distribution describing the temporal amplitude statistics of the clutter.

In measured clutter spectra from windblown trees, not only does the maximum spectral power almost always occur in the zero-th Doppler bin, but high spectral power levels are also often resolved in neighboring Doppler bins that are very near but not right at zero Doppler. In this report, such near zero-Doppler spectral power is called quasi-dc power. The near zero-Doppler regime of quasi-dc power is usually  $0 < |v| < 0.25$  m/s. Excess quasi-dc power exists in the quasi-dc region when the spectral power initially decays rapidly but continuously from the peak power level right at zero Doppler at a rate much faster than the exponential rate evident at lower power levels in the spectral tail. The spectral power that is resolved in the zero-th Doppler bin in such spectra may be coming from relatively motionless parts of the tree trunks near ground level as well as from the ground surface itself, whereas the spectral power resolved as quasi-dc may be coming from higher parts of tree trunks and major limbs flexing slightly at very slow rates. Including the excess quasi-dc spectral power as part of the ac spectral power degrades the goodness-of-fit of the exponential shape function in the spectral tail. That is, in these circumstances even though the value of  $\beta$  in Equation (2) is correctly selected to match the relative shape  $P_{ac}(v)$  in the spectral tail, the value of  $r$  will be too low, with the result that the absolute level  $[1/(r+1)] P_{ac}(v)$  will be too high. Furthermore, to the extent that wind-blown clutter statistics are nonstationary, besides being too high, this level can also be dependent on the length of coherent processing interval (CPI) employed. Therefore, in this report where excess (above the approximating exponential) quasi-dc power occurs in the data, it is included with the Dirac delta function as dc power in the model. This approach to quantifying dc/ac ratio  $r$  has been followed in the processing underlying the statistics upon which Equation (3) is based (see Section 4.2). The major consequence of this

approach is that the preceding spectral model will approximate the exponential spectral tail region correctly, in both relative shape and absolute level, and independently of the length of CPI employed. Examples of windblown forest clutter spectra containing excess quasi-dc power will be presented subsequently, as well as examples of desert and cropland clutter spectra in which a dc component from the absolutely stationary underlying ground surface (as opposed to the moving vegetation) exists as a discrete delta function.

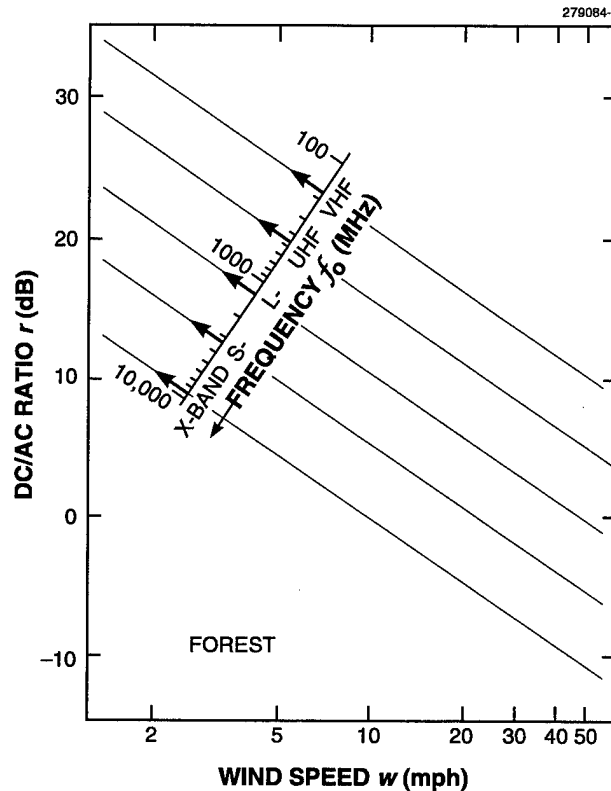


Figure 2. Modeling information specifying ratio of dc to ac spectral power in windblown forest clutter spectra versus wind speed and radar frequency.

### 2.3 MODEL SCOPE

Equations (1), (2), (3), and Table 1 constitute a simple but complete model for characterizing the complex physical phenomenon of windblown clutter spectra over spectral dynamic ranges reaching 60 to 80 dB below the zero-Doppler peak. The test of any model of a physical phenomenon is the degree to which it generally represents the phenomenon while avoiding complicating detail. The important parameters incorporated in the current model of Equations (1), (2), (3), and Table 1 are wind speed and radar frequency; others that might be thought to strongly influence clutter spectra from windblown trees but which appear to be



subsumed within general ranges of statistical variability in the measurement data include (a) the types of trees involved (species, density, growth stage), (b) season of the year (e.g., leaves on vs leaves off), (c) wind direction, (d) cell size, (e) polarization, and (f) angle of illumination. An important requirement in the development of the current model was that its predictions of spectral extent be in the correct general Doppler regime at spectral power levels 60 to 80 dB down. Much uncertainty has existed concerning the location of this regime. The extensive Lincoln data base of windblown clutter spectral measurements without exception indicates ever-increasing rates of spectral decay with decreasing spectral power level as observed on log-Doppler velocity axes such that maximum spectral extents 60 to 80 dB down are limited to Doppler velocities of 3 to 4 m/s. The exponential shape factor properly reflects this important fundamental feature of these measurements. The numerical modeling information specifying the particular exponential shape factor and dc/ac ratio in the current model additionally incorporates representative general trends with wind speed and radar frequency as observed in the measured clutter spectra.

### 3. MEASUREMENT BASIS FOR CLUTTER SPECTRAL MODEL

#### 3.1 RADAR INSTRUMENTATION AND DATA REDUCTION

In recent years Lincoln Laboratory has measured and characterized ground clutter power spectra over wide spectral dynamic ranges using the Phase One and LCE instrumentation radars [23,32]. Important system parameters of these two radars are shown in Table 2. The Phase One radar operated in five frequency bands: VHF, UHF, L, S, and X. Clutter measurements were conducted over a three-year period at 42 different sites of widely varying terrain type [25]. Subsequently, the Phase One equipment was operated at Katahdin Hill at Lincoln Laboratory in eastern Massachusetts once weekly for the following year to provide more depth in the data base with respect to temporal variations associated with wind, weather, and season at a given site. The basic type of Phase One clutter experiment suitable for examining temporal and spectral characteristics of ground clutter was the long-time-dwell experiment in which relatively long sequences of pulses at low pulse repetition frequency (PRF) were recorded over a contiguous set of range gates with a stationary antenna beam. The Phase One instrument used uncoded, pulsed waveforms with two pulse lengths available in each band to provide high- and low-range resolution. Polarization was selectable as vertical or horizontal with transmit and receive antennas always copolarized (i.e., the cross-polarized component in the radar return signal could not be received). The Phase One system activated one combination at a time of frequency, polarization, and pulse length for any particular clutter experiment. External calibration was provided through use of standard gain antennas and corner reflectors mounted on portable towers. Many of the Phase One spectra shown in this report are from long-time-dwell data collected at Katahdin Hill during April and early May, before the leaves had emerged on the deciduous trees. The forested cells from which backscatter was measured at Katahdin Hill are typical of the eastern mixed hardwood forest (oak, maple, beech) with occasional occurrences of conifers (hemlock, pine), all generally 50 or 60 ft high. For these Katahdin Hill measurements, general wind conditions in the neighborhood of the principle cells from which backscatter was recorded were taken from weather information continuously broadcast from nearby Hanscom airfield. At other sites, wind conditions were measured by anemometers located at the radar site and, in many instances, also in the clutter measurement sector.

The LCE radar was a major upgrade at L-band only of the Phase One measurement equipment with substantially reduced phase noise levels [32]. There were two LCE clutter measurement sites. The first was Wachusett Mt., Massachusetts, 32 miles west of Katahdin Hill with similar tree cover. The second was a Nevada site where backscatter data were recorded from sparse scrub vegetation typical of the western desert. In contrast with Phase One, the LCE radar could measure the copolarized and the cross-polarized returns, although not simultaneously. For LCE clutter measurements at Wachusett Mt., wind conditions were measured simultaneously with the clutter measurements at 10-s update intervals with an anemometer stationed on top of a 75-ft tower in a treed clutter cell at range = 7.4 km along one of the three azimuth positions (viz.,  $Az = 166^\circ$ ) selected for clutter measurements there. The measurements were performed in August with the deciduous trees fully in leaf. External calibration of the LCE radar was accomplished using radar repeaters of known radar cross section (RCS) that were sited in open terrain at ranges of several kilometers.

**Table 2.**  
**Radar System Parameters**

Parameter	LCE	Phase One				
	Frequency Band (MHz)					
	L-Band (1230)	VHF (169)	UHF (435)	L-Band (1230)	S-Band (3230)	X-Band (9100)
Antenna gain (dBi)	31	13	25	28.5	35.5	38.5
Antenna beamwidth						
Az (deg)	6	13	5	3	1	1
El (deg)	3	42	15	10	4	3
Peak power (kW)	8	10	10	10	10	50
Polarization	HH,VV,HV,VH	HH,VV				
PRF (Hz)	500	500				
Pulse width (μs)	1	0.1, 0.25, 1				
Waveform	Uncoded CW pulse	Uncoded CW pulse				
A/D converter						
No. of bits	14	13				
Sampling rate (MHz)	2	10, 5, 1				

### 3.1.1 Spectral Processing

LCE long-time-dwell clutter data were acquired with a stationary antenna over 70-s data recording intervals called experiments. Each LCE experiment involved the recording of 80 in-phase (I) and quadrature (Q) sample pairs per pulse repetition interval (PRI) at 2-MHz sampling frequency (i.e., 75-m range gate spacing), leading to a 6-km total recorded range swath. Clutter experiments were usually taken in sequential groups covering the various LCE polarization combinations. Phase One long-time-dwell clutter data were acquired similarly to LCE data. Table 3 provides the specific Phase One clutter data acquisition and spectral processing parameters applicable to the Phase One spectral results shown in this report from Katahdin Hill.

All the LCE clutter power spectra reported herein were computed directly as fast Fourier transforms (FFTs) of the sampled temporal pulse-by-pulse return, including the dc component. A four-term Blackman-Harris window function was utilized, with highest sidelobe level at -92 dB [33]. Each temporal record of 30,720 pulses (first 61.44 s of each 70-s experiment) was divided into contiguous groups of 5120 samples, a 1024-point complex FFT was generated for each group by utilizing every fifth pulse, and the amplitudes

of the resultant set of FFTs were arithmetically averaged together in each Doppler cell to provide the spectrum illustrated. Thus each LCE spectrum shown is the result of averaging six individual spectra (each from a 1024-point FFT) from an overall record of 1.024-min duration, using an effective 10-ms PRI and an effective 100-Hz PRF. The CPI for each FFT was 10.24 s. Previous measurement results [23] indicated that the typical correlation time for windblown trees at L-band is  $\approx 1$  s (see Table 3). Thus the CPI utilized in LCE spectral formation, usually being  $\approx 10$  times the correlation time, is more than adequate to allow the random process to fully develop. The Phase One clutter spectra shown were computed similarly to the LCE spectra. Table 3 provides the particular Phase One spectral processing parameters utilized in generating the Phase One clutter spectra from Katahdin Hill. Table 3 includes both the CPI (i.e., time dwell per FFT) used and the typical correlation time of windblown trees for each Phase One frequency band. These numbers indicate that the CPI covers many correlation periods at each of the five Phase One radar frequencies.

**Table 3.**  
**Phase One Clutter Spectra Parameters; Katahdin Hill Data**  
**(Principle Clutter Cell = 2.8-km Range)**

Parameter	Frequency Band (MHz)				
	VHF (169)	UHF (435)	L-Band (1230)	S-Band (3230)	X-Band (9100)
<b>Experiment</b>	<b>17 Apr/33.7</b>	<b>17 Apr/33.8</b>	<b>3 May/37.2, 38.3</b>	<b>17 Apr/34.4</b>	<b>4 Apr/28.2</b>
Polarization	HH	HH	VV, HH	HH	VV
Range resolution (m)	150	150	15	150	150
No. of pulses recorded	30,720	30,720	30,720	30,720	30,720
PRF (Hz)					
Emit	500	500	500	500	500
Record	500	100 (1/5)	100 (1/5)	167 (1/3)	500
FFT (2048 pt)	33.33 (1/15)	33.33 (1/3)	100	167	500
Time dwell(s)					
Total recorded	61.44	307.20	307.20	184.32	61.44
Per FFT	61.44	61.44	20.48	12.29	4.096
Correlation time (s) [23]	5.04	0.94	0.95	0.081	0.049
No. of FFTs averaged per spectral plot	1	5	15	15	15

### 3.1.2 System Stability

For a steady target, the spectral processing of either the Phase One or LCE radar yields a very narrow spectrum containing only dc power at zero-Doppler velocity. Figure 3 shows results from such steady targets. Figure 3(a) shows the measured LCE clutter spectrum from a desert terrain cell under very still (0 mph) wind conditions. Figures 3(b) and (c) show measured Phase One spectra from a large municipal water tower at L- and X-bands, respectively; in each case, clutter from trees in the same cell as the water tower just begins to broaden the spectrum near the base of the water-tower dc spike. Figure 3(d) shows the measured Phase One VHF spectrum from a cell containing tall grass; the windblown motion of the grass is completely indiscernible in this VHF measurement. In all these results, the width of the dc spectral component from the steady target is essentially the limit of spectral resolution provided by the Blackman-Harris window function, which is cleanly maintained over the full spectral dynamic range of the radar down to the system noise level (i.e., 71 to 77 dB down for Phase One, 80 dB down for LCE). The window function sidelobes occur below the noise level of either system.

### 3.1.3 Spectral Normalization

This report shows measured clutter spectra normalized to compare with analytic representations of clutter spectral density. The first step in spectral normalization is to convert the FFT output from power per spectral resolution cell to power/(m/s) so as to be directly comparable with analytic spectral shapes defining continuous density functions. This conversion is performed by dividing each point in the FFT velocity spectrum by the width of the Doppler velocity resolution cell  $\Delta v$ . The Doppler velocity resolution cell is wider than the sampling interval by a factor equal to the equivalent noise bandwidth *ENBW* of the window function. Thus  $\Delta v = (\lambda/2) \cdot (PRF/N) \cdot ENBW$ , where *N* is the number of points in the FFT. For the four-term Blackman-Harris window used here, *ENBW* = 2.004 [33]. The second step in spectral normalization is to bring the power in the measured spectrum to unity for comparison with analytic spectral shapes for which the integral over the entire velocity domain is unity. In some circumstances total power in the spectrum is brought to unity by dividing each spectral point by total spectral power. In other circumstances, where concern is only with the ac spectral shape and not the particular amount of dc power present, the ac power in the spectrum is brought to unity by dividing each spectral point by total spectral power times  $1/(r + 1)$ .

### 3.1.4 Spectral Power

Total, dc, and ac spectral power were computed in the time domain for the Phase One and LCE spectral results. Total power over the temporal record of each FFT is  $1/N$  times the sum of the squares of the I and Q samples of received power. The dc power over the same temporal record is the square of  $1/N$  times the sum of the I samples plus the square of  $1/N$  times the sum of the Q samples (i.e., coherent sum). The ac power over the same temporal record is total power minus dc power. These computations were performed over each FFT contributing to each spectrum. The final time-domain quantities for total, dc, and ac spectral power are each means of the resulting set of values, one value per FFT, applicable to each spectrum.

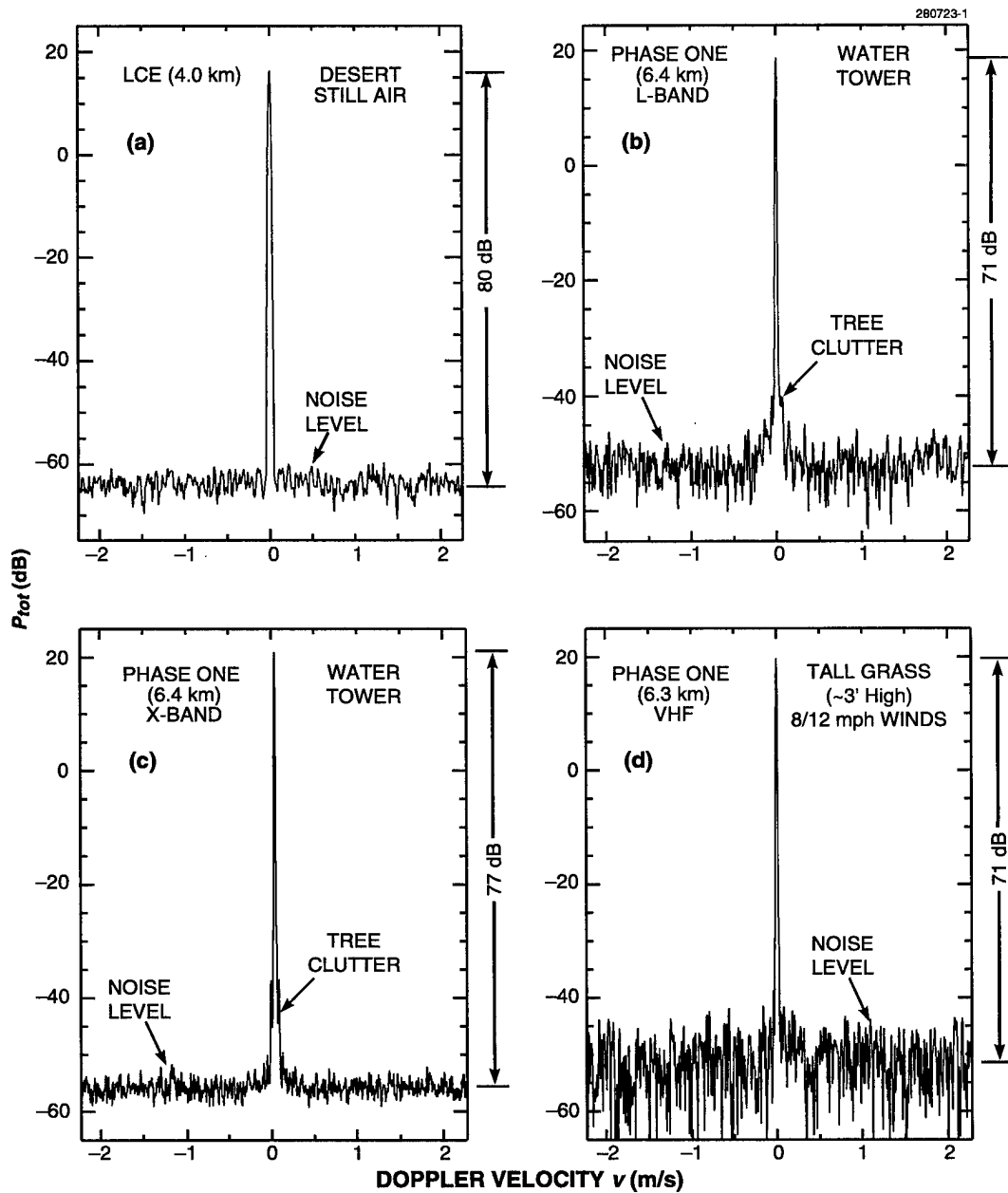


Figure 3. Four measured power spectra from "stationary" targets exhibiting little or no discernible spectral spreading to levels 70 to 80 dB down: (a) LCE, (b), (c), (d) Phase One; L-, X-, VHF bands, respectively.

The dc power obtained by summing coherently over a temporal record of backscatter from wind-blown trees depends on the length of the record (the CPI) over which the summation is performed. If the random process were well behaved (i.e., stationary), the coherent sum would converge and be largely independent of record length for lengths much greater than the correlation period of the process. However, wind-blown clutter backscatter records are not rigorously stationary. The statistics of the process sometimes appear to be characterized as intervals of stability separated by abrupt transitions from one stable state to another. Such abrupt changes might be caused, for example, by large tree limbs suddenly shifting position. In any event, because the coherent sum does not always converge, the ratio of dc/ac power computed in the time domain is dependent on CPI duration. Table 4 provides two examples of the dc/ac ratio obtained as a function of CPI duration for two LCE long-time-dwell backscatter measurements from cells containing windblown trees, one taken under very light wind conditions and the other under very windy conditions. The correlation times for these two experiments are estimated to be  $\approx 4$  s for the light-air data and  $\approx 1$  s for the windy data. The clutter spectra from these two measurements are discussed in Section 3.2.1. It is evident that a significant dc component exists in the light-air data in Table 4 and very little dc power exists in the windy data. The results in the table may be interpreted in terms of decreasing sampling bandwidth of the zero-velocity Doppler filter with increasing CPI, where sampling interval bandwidth is given by  $\lambda/(2 \times \text{CPI})$ . Because no weighting is employed in these time-domain computations, the filter has a  $\sin x/x$  response.

In the frequency domain, the zero-th Doppler bin can contain both a singular dc power component existing as a discrete delta function and ac power existing as a continuous density function. The ac power in the zero-th Doppler bin decreases with increasing resolution (i.e., with increasing CPI duration), whereas the singular dc component is theoretically independent of resolution. However, in all the measured clutter spectra shown here, normalization (division) of power/cell by  $\Delta\nu$  was performed for all cells, including the zero-Doppler cell. First-order credibility checks of the reasonableness of dc/ac ratios provided in this report for spectra containing strong dc components (i.e., strong dc spikes, for example, in desert or cropland or at VHF) should therefore be performed by first decreasing the height of the spike by  $|\Delta\nu|$  dB before estimating the resultant dc/ac ratio. Note that the peak spectral level at zero Doppler (before or after division by  $\Delta\nu$ ) is not itself used in any direct way in this report to normalize measured spectral data (measured spectra are never simply aligned by peak level). One reason that the zero-Doppler cell is not normalized differently from others is to maintain the relative shape of the raw FFT before normalization (whatever is done to one cell is done to all cells). Another reason is that the power in the zero-Doppler cell of windblown foliage spectra is often not dominated by a singular dc (i.e., delta function) component, in which circumstances the continuous power in the zero-Doppler cell requires normalization by  $\Delta\nu$  similarly to all other Doppler cells.

Excess quasi-dc power in Doppler resolution cells near the zero-Doppler cell is included as dc power in computing the dc/ac power ratio used as spectral modeling information in spectra where excess quasi-dc power exists. The dc/ac ratio in which the excess quasi-dc component is included in the singular dc term is obtained in the frequency domain by best-fitting the spectral tail at high Doppler velocities with an exponential ac shape function. The excess quasi-dc power is that which exists above the approximating exponential in cells of very low Doppler velocity close to zero Doppler. The fitting process is largely independent of spectral resolution as long as the resolution is adequate to define the exponential spectral tail. As a result, the dc/ac ratio used herein, which is that required for the ac exponential shape function to match the measured spectral tail both in relative shape and in absolute level, is also largely independent of CPI duration and spectral resolution. This fitting process is discussed in Section 4.2. The resulting dc/ac ratios

when the process is applied to the spectra obtained from the two Table 4 measurements are 29.8 dB for the light-air data and 0.7 dB for the windy data.

**Table 4.**  
**Variation of dc/ac Ratio with Length of CPI for**  
**LCE Clutter Measurements from Windblown Trees**

CPI (s)	No. of Points per CPI (PRF = 500 Hz)	No. of CPIs Averaged	Ratio of dc to ac Power (dB) (Time-Domain Computation)	
			Light-Air Measurement (5 Sep, 4.7 km)	Windy Measurement (11 Sep, 7.7 km)
0.032	16	2048	47.2	20.8
0.064	32	1024	43.1	15.0
0.128	64	512	37.9	9.8
0.256	128	256	32.4	5.1
0.512	256	128	27.1	1.8
1.02	512	64	22.4	-1.0
2.05	1024	32	18.9	-3.6
4.10	2048	16	15.7	-5.8
8.19	4096	8	14.0	-9.1
16.4	8192	4	13.2	-10.7
32.8	16384	2	12.0	-18.6
65.5	32768	1	10.5	-19.0

## 3.2 MEASUREMENTS ILLUSTRATING AC SPECTRAL SHAPE

### 3.2.1 Variations with Wind Speed

Figures 4, 5, and 6 are examples of LCE-measured windblown forest clutter spectra under windy, breezy, and light-air conditions, respectively. The data in these figures are normalized to show ac spectral shape  $P_{ac}(v)$  plotted against a logarithmic Doppler velocity axis similar to the modeled curves of Figure 1. Each figure compares the measured ac spectral shape with several exponential shape functions of various values of shape parameter  $\beta$ . In Figure 4, the measured data follow the exponential curve of shape factor  $\beta = 5.2$  remarkably closely over the full spectral dynamic range shown. This match of measured ac spectral shape with exponential is among the best in the current data base, although other examples exist both of LCE and Phase One windy-day clutter spectra with equally good fits to exponential. Furthermore, the



spectrum of Figure 4 is among the widest measured; its shape factor  $\beta = 5.2$  is the basis of the “worst case, windy” specification in Table 1 and Figure 1. Also shown in Figure 4 is a narrower Gaussian spectral shape function. The particular Gaussian shape shown corresponds to Barlow’s much-referenced, 20-dB dynamic range historical measurement [6]. It is evident in Figure 4 that the overall rate of decay in the LCE data is much more exponential than Gaussian in character. Thus these LCE data support the general consensus of agreement subsequently arrived at [9,10,11,17,20,21] of spectral tails wider than Gaussian in windblown clutter spectra. Li [20] explains that tails wider than Gaussian are theoretically required by branches and leaves in oscillatory—as opposed to merely translational—motion.

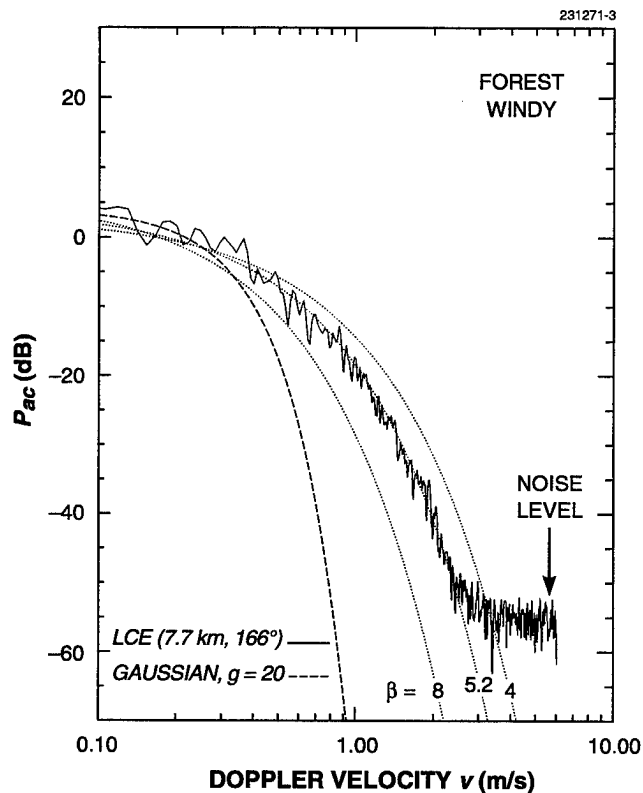


Figure 4. Highly exponential decay ( $\beta = 5.2$ ) in a forest clutter spectrum measured under windy conditions.

The LCE spectral data of Figures 5 and 6 indicate that measured ac spectral shapes remain reasonably well represented by exponential shape functions under less windy conditions, with increasing values of exponential shape factor with decreasing winds (i.e.,  $\beta \approx 8$  for breezy conditions,  $\beta \approx 12$  for light-air conditions). The results of Figures 5 and 6 are representative of many similar spectra measured in other cells on other days. Recall that normalization to  $P_{ac}(v)$  requires raising the  $P_{tot}(v)$  spectrum by  $10 \log_{10}(r + 1)$  decibels on the vertical ordinate. The value of  $r$  applicable in Figures 4, 5, and 6 is 0.7, 18.9, and 29.8 dB, respectively. It is evident in Figures 5 and 6 that the measured data begin to depart from the approximating

exponentials for  $v < 0.2$  m/s as they begin to rise into the quasi-dc region, which contributes to the large values of  $r$  in these data. As the amount of dc spectral power increases, less spectral dynamic range is left for measuring the ac power in the spectral tail, indicated by the rapidly rising effective system noise levels with respect to  $P_{ac}(v)$  as wind speed decreases and dc/ac ratio increases in Figures 4–6.

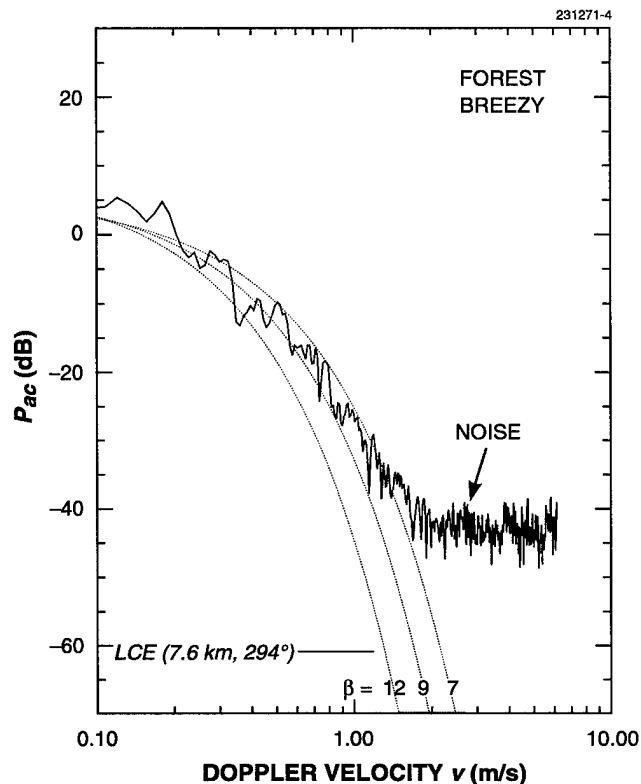


Figure 5. Approximate exponential decay in a forest clutter spectrum measured under breezy conditions.

As discussed later (Section 5.1), power-law spectral tails plot as straight lines in plots of  $10 \log_{10} P$  vs  $\log_{10} v$  such as those of Figures 4–6. Thus a power law of shape  $n = 3$  (30 dB/decade) fits the data of Figure 5 reasonably well down to the  $P_{ac} = -20$ -dB level. However, this  $n = 3$  power law cannot be extrapolated to lower levels. The local power-law (local slope tangent to the data curve) rate of decay in Figure 5 strongly increases (to  $n \cong 6$  or 7) at the lower spectral power levels in Figure 5. Likewise, at first consideration, an  $n = 4$  power law (40 dB/decade) might be thought to be a reasonable match to the measured data of Figure 6. The apparent goodness of this straight-line fit to the data in Figure 6 is heightened by the data beginning to rise above the exponential in the low-Doppler quasi-dc region  $v < 0.2$  m/s, and by the data flaring away from the exponential toward the noise level as they become limited in signal-to-noise (S/N) ratio when approaching to within 10 dB of the noise floor at higher Doppler velocities around 1 m/s. However, these two effects tend to obscure a more fundamental exponential-like rate of decay (increasing local tangent

slope with decreasing power level) as shown in the region  $0.2 < v < 0.7$  m/s in Figure 6, and the upper-level power-law rate of decay can no more be extrapolated to lower levels in the light-air data of Figure 6 than in the windier data of Figures 4 and 5. To do so would lead to physical implausibility as the upper-level light-air power law would extrapolate to lower-level ac power levels (e.g.,  $P_{ac} = -60$  dB) exceeding in spectral width those measured under windy conditions at the same lower levels. The spectra of Figures 4 and 6 are those for which time-domain computations of dc/ac ratio vs CPI duration are provided in Table 4.

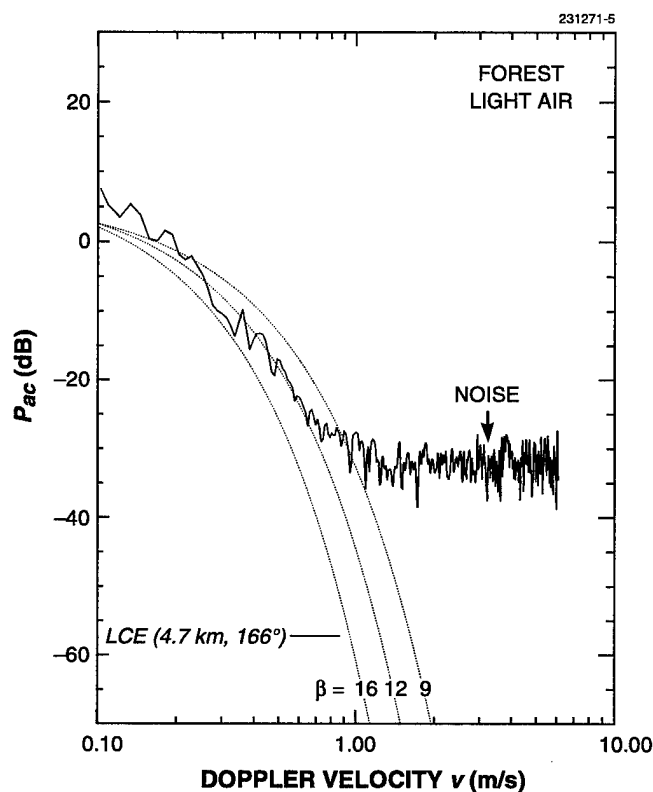


Figure 6. Approximate exponential decay in a forest clutter spectrum measured under light wind conditions.

As shown subsequently, not all the Phase One and LCE clutter spectra measured under breezy and windy conditions are as closely exponential as the measured spectrum in Figure 4. However, like that spectrum, they all demonstrate increasing downward curvature (convex from above) with increasing Doppler velocity and decreasing power level as their most characteristic general feature in plots of  $10 \log P$  vs  $\log v$  such as that of Figure 4. The main reason the exponential form is used herein for modeling clutter spectral shapes is that it, too, when plotted as  $10 \log P$  vs  $\log v$  possesses this increasingly downward curving shape (see Figure 1) while remaining wider than Gaussian as required by the measured data (see Figure 4). In contrast, the spectral tails of power-law functions do not have increasing downward curvature

on  $10 \log P$  vs  $\log v$  axes but plot linearly (i.e., extrapolate rapidly to excessive spectral width) on such axes. (This matter is further elaborated upon in Section 5.1.)

To be clear as to the reader's expectations for the forthcoming measurement data in this report, most of the Phase One- and LCE-measured clutter spectra are not completely and precisely representable by any simple analytic function over their full spectral ranges. Many of these measured spectra are somewhat wider than exponential (i.e., are concave from above in  $10 \log P$  vs  $v$  plots), but they are almost always much narrower than power law (i.e., are convex from above in  $10 \log P$  vs  $\log v$  plots). Even in such circumstances, absorbing excess quasi-dc power in the dc term usually gives the exponential model the flexibility to match the relative shapes and absolute levels of the measured spectra over extensive spectral tail regions.

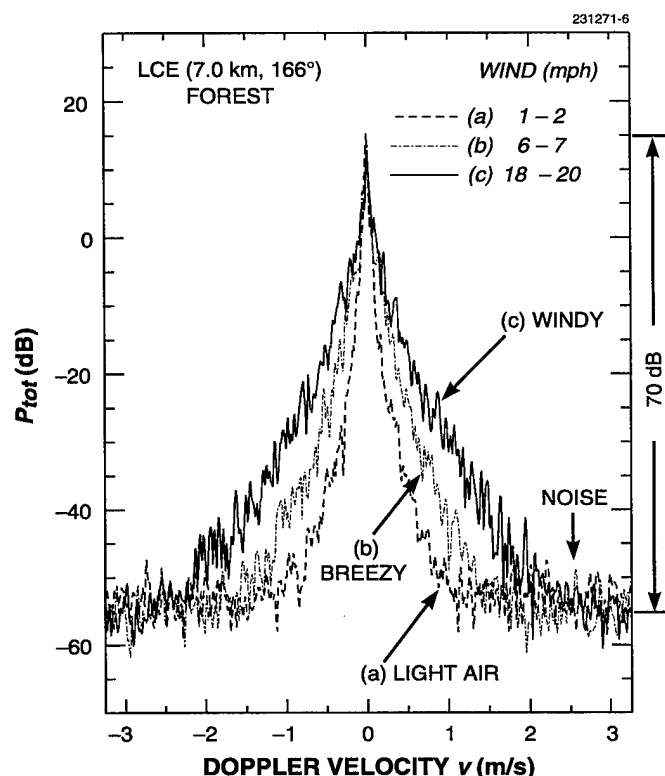


Figure 7. Variation of LCE windblown forest clutter spectra with wind speed. Common range gate (7 km).

**Gale Force Winds (Scaled Estimate).** Figure 7 shows an additional set of three LCE-measured wind-blown-forest clutter spectra under light-air, breezy, and windy conditions, displayed as  $10 \log P_{tot}$  vs  $v$ . In contrast to the light-air, breezy, and windy spectra of Figures 4-6 (which come from three different range cells) the spectra shown in Figure 7 are from the same 7-km range cell on three different measurement days. Thus these Figure 7 spectra clearly indicate that spectral extent from a given range cell increases strongly

with increasing wind speed. In very approximate measure, these data of Figure 7 indicate similar-sized steps of increasing spectral width for wind speeds increasing by approximate factors of 3 (from 1–2 to 6–7 mph, and from 6–7 to 18–20 mph). The maximum spectral extent in these data 70 dB down from their zero-Doppler peaks is  $\approx 1, 2,$  and  $3$  m/s for the light-air, breezy, and windy spectra, respectively. In these results, as ac clutter power increases and spreads out with increasing wind speed, dc clutter power decreases, as indicated by dc/ac ratios  $r$  of  $+0.1, -1.5,$  and  $-4.5$  dB for the light-air, breezy, and windy spectra, respectively.

Figure 8 shows the same three spectra of Figure 7, now displayed as  $10 \log P_{tot}$  vs  $\log v$ . Figure 8 also shows a scaled extrapolation to higher wind speeds by a further factor of 3, that is, from the 18–20 mph of the “windy” spectrum to 54–60 mph gale force wind speeds. This estimate was obtained by finite-difference extrapolation of the light-air, breezy, and windy Doppler velocities, say  $v_a, v_b,$  and  $v_c,$  to  $v_d,$  the estimated gale force Doppler velocity, at multiple spectral power levels, assuming constant factors-of-3 increases in wind speed throughout. As indicated in Figure 8, this gale force spectral estimate is well modeled by an exponential curve of shape factor  $\beta = 4.3$  and is the basis of the “typical” gale force exponential ac shape parameter specification  $\beta = 4.3$  in the clutter model of Section 2. Increasing gale force  $\beta$  in this model from its typical specification based on the scaled estimate shown in Figure 8 to a worst-case specification of  $\beta = 3.8$  brings it into very close agreement (in terms of gross spectral extent at the  $-14$  dB level) with the only known measurement of windblown clutter under actual gale force wind conditions, namely, the very early measurement of Goldstein [8] that is further discussed in Section 5.2.5.

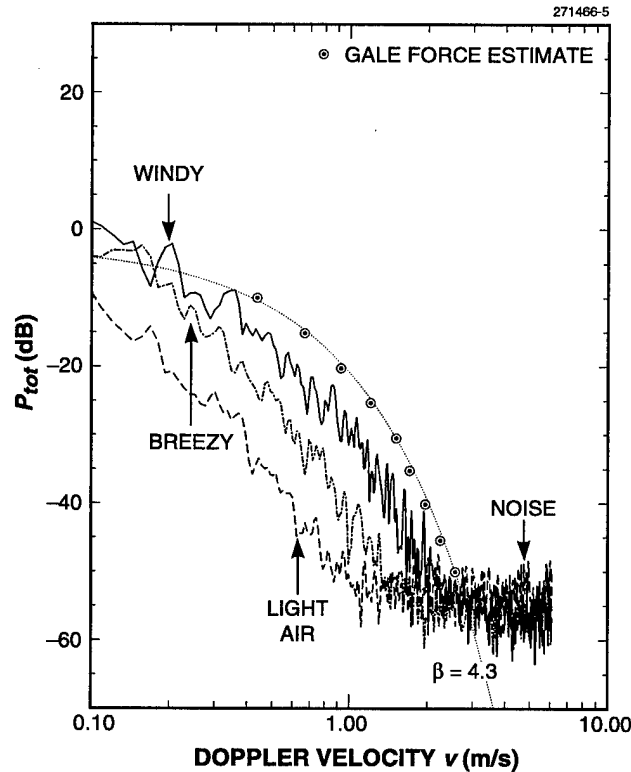


Figure 8. Scaled estimate of windblown forest clutter spectrum under gale force winds (54–60 mph).

### 3.2.2 Invariance with Radar Frequency

The idea that spectral extents of windblown ground clutter Doppler-velocity spectra are in large measure invariant with radar frequency, or equivalently (and as more commonly described), that spectral widths in Doppler-frequency spectra are approximately proportional to radar frequency, has been discussed in the technical literature of the subject since the early days of radar development. For example, early work in comparing spectral widths with radar frequency conducted at the MIT Radiation Laboratory during World War II by Herbert Goldstein and others [5,7,8] is summarized by Goldstein's conclusion that "The widths of the [Doppler-frequency] spectra ... increase with wind speed and ... appear to be essentially proportional to [radar] frequency" [7]. This conclusion remains true in the LCE and Phase One spectral results, as indicated in Figures 9 and 10—Figure 9 shows VHF, L-, and X-band Doppler-velocity forest spectra under windy conditions; Figure 10 shows UHF, L-, and S-band forest spectra under breezy conditions. However, the early Radiation Laboratory results were mainly in the 1- to 10-cm range of wavelengths and, by today's standards, over very limited spectral dynamic ranges ( $\approx 20$  dB). The results of Figures 9 and 10 extend the idea of frequency invariance of windblown clutter Doppler-velocity ac spectral shape over very much greater spectral dynamic ranges ( $> 60$  dB) and to very much longer radar wavelengths [from X-band ( $\lambda = 3.3$  cm) and S-band (9.3 cm) down through L-band (24.4 cm) to include UHF (0.69 m) and even VHF (1.8 m)]. These results are rather surprising, since the dominant, wavelength-sized scatterers at VHF (large branches, limbs) are presumably different than those at X-band (leaves, twigs). As will be shown, much more dc power exists in VHF windblown clutter spectra than at higher radar frequencies, for one reason because the VHF energy partially penetrates the foliage to reach the underlying stationary tree trunks and ground surface. As a result, the ac spectral power at VHF is measured at lower levels in the available spectral dynamic range. Still, over very many spectral measurements of windblown trees at VHF and UHF and as measured over much longer CPIs as required by the longer correlation times at VHF and UHF, ac spectral spreading caused by internal motion in windblown clutter does generally exist at VHF and UHF at lower absolute levels of  $P_{tot}(\nu)$  but roughly equivalently in the relative shape and extent of  $P_{ac}(\nu)$  to that observed in the higher, L-, S-, and X- microwave bands.

In Figure 9, the VHF and X-band spectra were measured by the Phase One radar at Katahdin Hill under windy conditions on two different days in April at 2.8-km range (see Table 3). The L-band spectrum was measured by the LCE radar at Wachusett Mt. on 11 September at 6-km range ( $Az = 294^\circ$ ). The Figure 10 spectra were all measured by the Phase One radar at Katahdin Hill also at 2.8-km range under breezy conditions in late April or early May. In gross measure, the three windy-day spectra of Figure 9 are essentially identical in overall ac spectral shape, as are the three breezy-day spectra of Figure 10. Of course, temporal (minute-to-minute, hour-to-hour) and spatial (cell-to-cell, site-to-site) variability exist in LCE- and Phase One-measured clutter spectra under nominally similar wind conditions, and not all such measurements overlay one another as exactly as those shown in Figures 9 and 10. Examples of LCE and Phase One spectral variability are shown later in this report and elsewhere [23]. Concerning variability, consider that even in the results of Figures 9 and 10 for which the same nominal range and azimuth apply, the spatial cells still encompass quite different overlapping ground areas due to the different azimuth beamwidths (see Table 2). Also, "... there are the usual uncertainties [because of the lack of] ... simultaneity of the measurements in time" [8]. Furthermore, in considering possible means by which variations with radar frequency might be introduced in clutter velocity spectra, amplitude fluctuations caused by scatterer rotation and the wig-wag

shadowing of background leaves by leaves in the foreground have been discussed [13,20,30,34] as possible mechanisms that might complicate clutter spectra over and above phase fluctuations caused by the scatterer velocity distribution. However, one theoretical model exists [13] that incorporates scatterer rotational and shadowing effects and still provides radar frequency-independent clutter Doppler-velocity spectral shapes (i.e., “to a first approximation, the spectrum ... depends only on the product  $\lambda f$ ” [13]). In any event, it is not suggested here that if multifrequency spectra could somehow be measured simultaneously from exactly the same spatial assemblage of windblown foliage, fine-scaled specific differences would not be observed in ac spectral shape with radar frequency. However, in looking across all the LCE- and Phase One-measured spectral data and the variations that exist therein, no significant trend is observed in ac spectral shape with radar frequency, VHF to X-band, as opposed, for example, to the strong trend seen in ac spectral shape with wind speed.

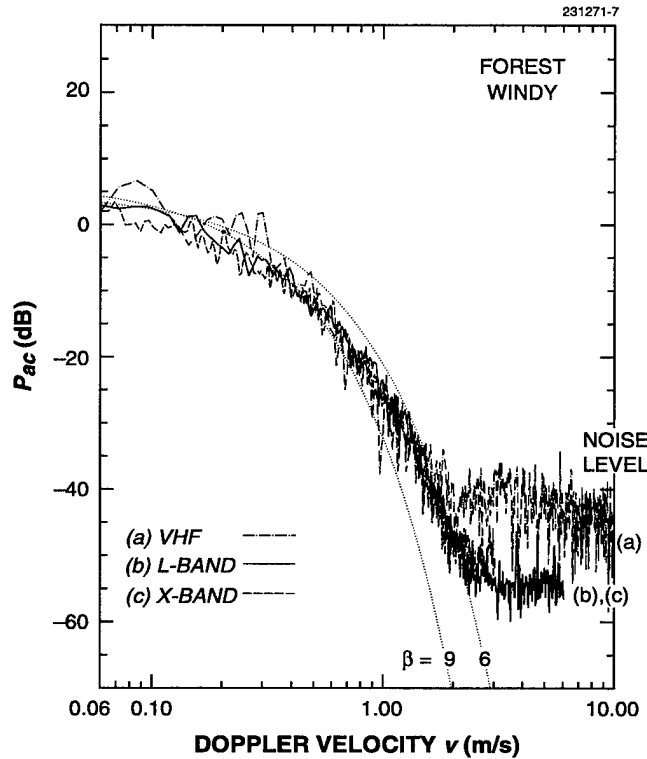


Figure 9. Variation of windblown forest clutter spectra with radar frequency under windy conditions: (a) VHF, Phase One, (b) L-band, LCE, and (c) X-band, Phase One.

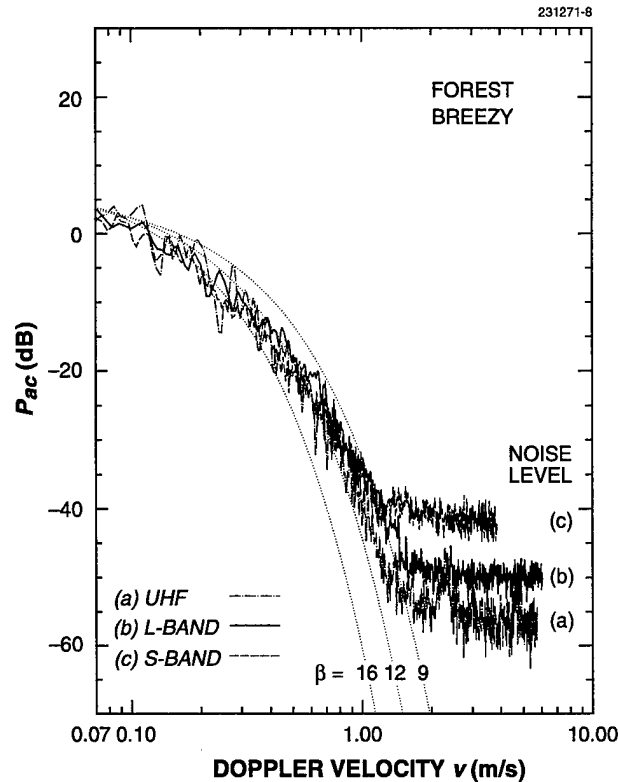


Figure 10. Variation of Phase One windblown forest clutter spectra with radar frequency under breezy conditions, UHF, L-, and S-bands.

### 3.2.3 Invariance with Polarization

The LCE and Phase One clutter spectral data indicate that clutter spectral shape from windblown vegetation is largely independent of radar polarization. In assessing polarization variability in ground clutter spectra on the basis of the LCE and Phase One measurements, small variations in spectral shape with time due to changing wind conditions can often have occurred between measurements of differing polarization to distort the picture. Figure 11 shows one set of three sequential LCE measurements of windblown treed-cell ground clutter spectra at VV-, HH-, and HV-polarizations obtained at approximately 2-min intervals, which are of essentially identical spectral shape. Figure 11 data were obtained from the same cell at Wachusett Mt. that contained the anemometer equipment. The fourth measurement from this cell of this set, which was at VH-polarization and commenced 2 min 30 s after the third, resulted in a spectrum slightly narrower than the others. The spectral artifact in the HV-pol. spectrum of Figure 11 at  $\approx 2.8$  m/s is probably a bird. Many other LCE and Phase One VV- and HH-pol. spectra were compared from common cells selected from other sites and experiments (see Billingsley and Larrabee [23]). A number of these showed little or no variation in spectral shape with polarization, as in Figure 11. Among others for which variations



of spectral shape with polarization did occur, such variations were usually relatively random with little evidence for the existence of any strong general effect on spectral shape with polarization.

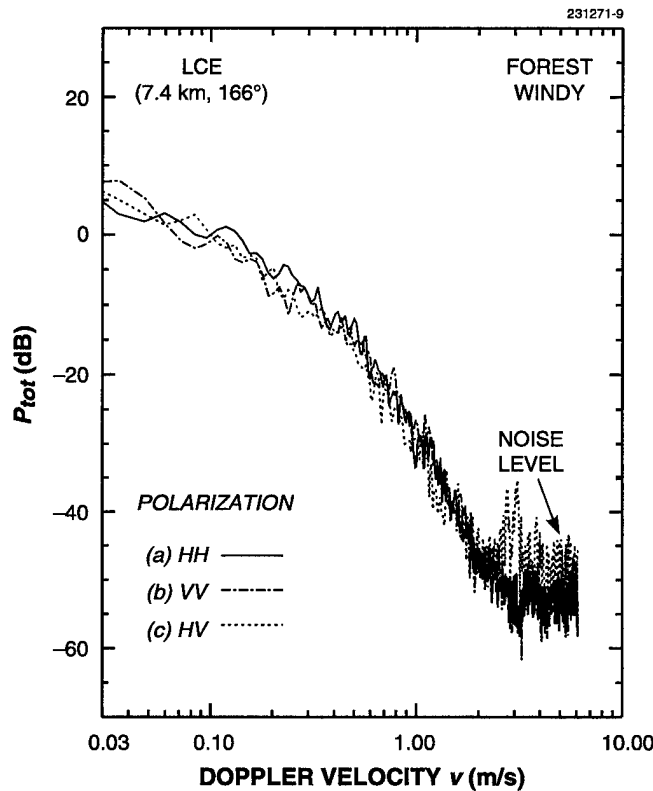


Figure 11. Variation of LCE windblown forest clutter spectra with polarization: (a) pol. = HH, winds (mean/gusts) = 10/18 mph; (b) pol. = VV, 2 min later, winds = 13/19 mph; (c) pol. = HV, 4 min later, winds = 10/16 mph.

Other investigators have also found little effect on windblown clutter spectral shape with polarization. For example, Kapitanov et al. [12] observed that “The spectra of [X-band] echo signals from forest for different polarizations [vertical and circular] ... are on the average similar.” They also observed significant depolarization of the signals and an indication of little correlation between orthogonally polarized components. More recent X-band windblown clutter spectral results by Ewell [22] at VV-, HH-, and circular polarizations in desert terrain also indicated no consistent differences in the spectral shapes obtained at the various polarizations.

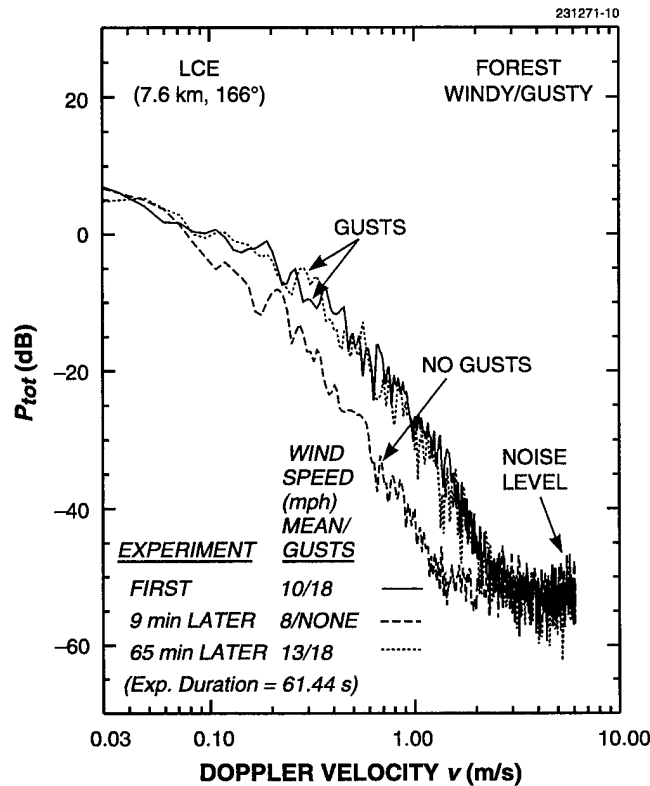


Figure 12. Variation of LCE windblown forest clutter spectra with time: Wachusett Mt., 11 Sep 1991.

### 3.2.4 Temporal Variation

All LCE clutter spectra in this report are averages of six individual 1024-point FFTs, each formed from a 10.24-s duration temporal backscatter record. The 7.4-km clutter-cell anemometer readings collected simultaneously with the LCE radar data at 10-s update intervals indicate that windy-day wind conditions frequently vary considerably from one 10-s interval to the next. Elsewhere [23] it was shown that such variability of windy-day conditions within a treed resolution cell from one 10.24-s interval to the next leads to correspondingly large variability over a set of 30 individual L-band clutter spectra formed from 30 sequential 10.24-s dwells. That is, windy-day treed-cell L-band clutter spectra are not very stationary at 10-s periodicity. However, the results of Figures 12 and 13 indicate that over longer periods of 60- to 80-s, windy-day treed-cell clutter spectra can be expected to become more stationary. Figure 12 shows LCE treed-cell clutter spectra for three repeated experiments on a windy day, each of which is formed from an overall temporal record of 61.44-s (100-Hz PRF, 1024-point FFTs, 6 FFTs averaged). The shape of the spectrum from the first experiment is essentially identically replicated by the shape of the spectrum from a following experiment begun 65 min later, suggesting that enough averaging of wind variations occurs within 1 min to lead to some degree of convergence in average spectral shape. Of course, wind is an extremely

nonstationary dynamic random process with complex short- and long-term variation. For example, on the windy/gusty day on which the data of Figure 12 were collected, the gusts (as measured by the 7.4-km clutter-cell anemometer) happened to die down over the 70-s interval covering the second experiment (begun 9 min after the first), and the spectrum formed from that data is indeed considerably narrower than the other two. On the preceding measurement day, which was also windy (but somewhat less so), two spectra from the same cell as that of Figure 12 formed from 61.44-s experiments 15 min apart also had identical spectral shapes (somewhat narrower than the wider spectra of Figure 12).

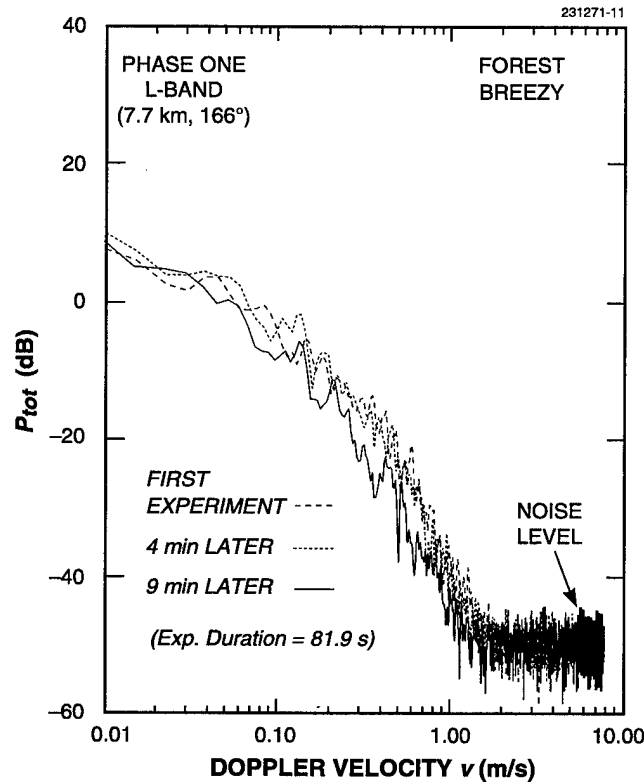


Figure 13. Variation of Phase One L-band windblown forest clutter spectra with time: Wachusett Mt., 22 Aug 1984.

Figure 13 shows Phase One L-band clutter spectra for three repeated breezy-day experiments for very nearly the same treed cell at Wachusett Mt. from which the LCE data of Figure 12 were obtained. Each of these Phase One spectra is formed from a temporal record of 81.9-s duration (125-Hz PRF, 2048-point FFTs, 5 FFTs averaged). The spectrum from the first experiment is nearly identical to that of the second experiment, begun 4 min later. The spectrum from the third experiment, begun 9 min after the first, is somewhat narrower. In a similar set of five sequential experiments begun 15 min before those of Figure 13, the range of variability of spectral shape (here formed by averaging over 61.44-s temporal records) was similar to that of Figure 13, with the spectrum of the third experiment being somewhat narrower than the first and

fifth (the second and fourth were of intermediate width). Thus the slightly changing average wind conditions within 60- to 80-s intervals can be followed in this manner over this complete set of eight spectra in total covering 32 min. The main observation is that the range of variability in clutter spectra formed by averaging over 60- to 80-s data intervals within this 32-min period is quite low, compared with the much more variable individual FFTs formed from 12- to 16-s data intervals during the same period.

### 3.2.5 Effects of Site/Season/Tree Species/Cell Size

It has been observed that extrapolation of early results modeled as power law compared with recent Lincoln results modeled as exponential leads to extremely large differences at very low spectral power levels. Possible reasons that have been advanced to account for these differences have included different (a) kinds of trees, (b) seasons, (c) measurement geometries (range, depression angle), (d) resolution cell sizes, and (e) measurement instrumentation and/or data processing. The Phase One and LCE spectral data indicate that all these factors have little or no significant general influence on spectral shape or extent within the dynamic ranges of these instruments. The large differences in these modeled results are simply due to non-valid extrapolation of power-law models obtained from early measurement data of limited spectral dynamic range to much lower levels.

The Phase One and LCE radars mimic long-range ground-based surveillance radars in the relatively long ranges, large resolution cell sizes, and low illumination angles of their measurements. If, for example, 7 km is taken as a typical range to a clutter measurement cell for these instruments, then for Phase One at L-band the resolution cell size is 367 m cross range  $\times$  150 m (or 15 m) down range; and for LCE the resolution cell size is 733 m cross range  $\times$  150 m down range. These cell sizes are large enough to encompass a large spatial ensemble of scatterers (many trees) as well as variable local wind currents within the cell. Because of the complexity of the scattering ensemble and nonuniform winds within such large cells and the variability of the ensemble from cell to cell over large numbers of cells, it is difficult to discern significant site-to-site differences or significant trends with season and/or tree species in the Phase One and LCE spectral data. It is not surprising that other, more fine-scaled investigations, both historical [12–15] and recent [35–37], involving small illumination spot sizes (e.g., 1.8-m diameter [37]) on individual trees at short ranges (e.g., 30 m [37]; 50 m [15]), provide results showing variation on treed-cell spectral shape with the type or species of trees. Presumably such fine-scaled measurements could also show small differences with radar frequency and season (leaves on vs leaves off). However, such small differences are largely absorbed within the general ranges of statistical variability in the Phase One and LCE measurements and are thus of limited consequence for the longer ranges and larger cells of surveillance radars.

It is not difficult to find Phase One and LCE spectra of essentially identical exponential spectral shape—two are shown in Figure 14. The LCE spectrum (a) measured on 10 September 1991 (leaves on deciduous trees) at Wachusett Mt. at 7.9-km range, HH-pol., 150-m range resolution, and 2° depression angle essentially overlays and replicates the Phase One spectrum (b) which was measured on 3 May 1985 (leaves not yet emerged) at Katahdin Hill at 2.4-km range, VV-pol., 15-m range resolution, and 0.5° depression angle. Note that these two measurements were obtained with different radar receivers, and the two spectra were produced using different computers and different data reduction and processing software, indicating that the results were not colored by the instruments or processing. Thus commonality can exist in spectral shape, in large measure because of the large cells and large degree of spatial averaging involved, despite a

host of underlying differences including measurement instrumentation and parameters (range, cell size, illumination angle, polarization), site, and time of year.

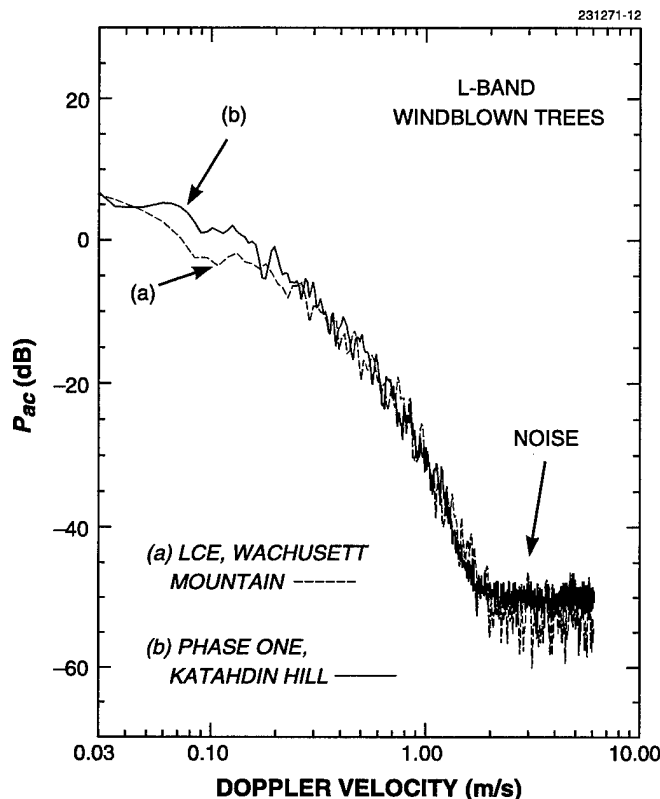


Figure 14. Similar LCE and Phase One forest clutter spectra measured under windy conditions at two different sites: (a) LCE, Wachusett Mt., 10 Sep 1991, and (b) Phase One (L-band), Katahdin Hill, 3 May 1985.

Because strong variations are not observed in windblown clutter spectral shape with radar frequency or season does not mean that one should accept as a “logical consequence” that “X-band backscatter must come from branches, not leaves.” Leaves certainly provide a major contribution to the backscatter from tree foliage in summer season at X-band, but the spectral differences between X-band backscatter, predominantly from leaves of trees in summer vs bare twigs and branches in winter are small; and the ac spectral differences between X-band backscatter from leaves and/or small branches vs VHF backscatter from larger branches and major limbs are also small.

**Early Phase One Studies.** The extensive Phase One data base allows further, more specific commentary on the influence of different sites, seasons, and cell sizes on clutter spectra. From the Phase One Katahdin Hill measurements acquired from a specific set of forested cells once a week over a nine-

month period [23,25], L-band spectra were examined for seasonal variations in three wind regimes, viz., calm to light-air conditions, light-air to breezy, and windy. The data base was of sufficient depth to provide reasonably significant results by season in each wind regime. These results marginally showed that in each wind regime, spectral widths 60 to 70 dB down were only very slightly wider by no more than  $\approx 0.5$  m/s for summer measurements (leaves on deciduous trees) than for winter measurements (leaves off deciduous trees).

An early study of Phase One spectra involved eight forested sites, four in western Canada and four in the eastern U.S. For the western Canadian sites, the dominant tree species were aspen and spruce. For the eastern U.S. sites, the forest was mixed (oak, beech, maple, hemlock, pine). Measured Doppler-velocity spectra generally showed no significant major differences in shape or extent from one forested measurement site to another, either within each group or from group to group. Since it is just marginally possible to determine small seasonal differences in Phase One windblown treed-cell clutter spectra, it is understandable that higher-order differences caused by differing mixes of tree species are not observed.

No significant discernible difference has been observed in the shapes of Phase One spectra from cells of 150-m range resolution compared with cells of 15-m range resolution, nor has any significant discernible difference been observed in the shapes of Phase One clutter spectra obtained with different azimuthal beam-widths (i.e.,  $1^\circ$  to  $13^\circ$ , X-band to VHF). That is, independent of particular cell-size parameters, the Phase One cell sizes are all large enough so that effects of variations in cell size on clutter spectral shape are not significant.

### 3.3 MEASURED RATIOS OF DC/AC SPECTRAL POWER

#### 3.3.1 Variation with Wind Speed

Forested ground clutter cells contain many scatterers. Each scatterer is positioned randomly within the cell and hence produces an elemental scattered signal of random relative phase with respect to the other scatterers. Some of the scatterers, such as leaves and smaller branches, move in the wind, producing fluctuating signals with time-varying phases. Other scatterers, such as tree trunks and larger limbs, are more stationary, producing steady signals of fixed phase. The total clutter signal is the sum of all the elemental backscattered signals, both steady and fluctuating. At high wind speeds, most of the foliage is in motion, and the ratio  $r$  of dc to ac power in the clutter spectrum is relatively low. In such circumstances, and in the higher microwave bands where little foliage penetration occurs, the steady component can become vanishingly small, whereupon Equation (1) simplifies to  $P_{tot}(\nu) \cong P_{ac}(\nu)$ . Goldstein correctly anticipated, however, that "As the wind velocity decreases, ... the steady-to-random ratio [i.e.,  $r$ ] would be expected to increase" [8]. Thus under light winds, a large proportion  $r/(r+1)$  of the clutter power is at dc. Even so, the small proportion of clutter power  $1/(r+1)$  that, under light winds, remains at ac can still troublesomely interfere with desired target signals. Therefore it is necessary that a windblown clutter spectral model quantify the dc/ac ratio  $r$  expected from forested or other types of vegetated cells as a function of wind speed.

Figure 15 shows an LCE-measured clutter spectrum from a treed cell under very light wind conditions (previously shown in Figure 6). The most striking characteristic of the light winds spectrum of Figure 15 is its extreme narrowness, with spectral spreading occurring only at relatively low power levels and to relatively small extent in Doppler. This spectrum contains a large steady or dc component, and since the spectral

density decays smoothly and continuously (albeit rapidly) away from the peak zero-Doppler level, it also contains high levels of quasi-dc power at very low but nonzero Doppler velocities. This spectrum may be approximately modeled utilizing a value of  $r = 29.8$  dB in which excess quasi-dc power is included in the dc term, and an exponential shape function for the spectral tail of shape parameter  $\beta = 12$  (see Figure 6). The spectrum of Figure 15 is generally representative of many, similarly narrow LCE and Phase One L-band clutter spectra measured in other treed cells and on other light wind days.

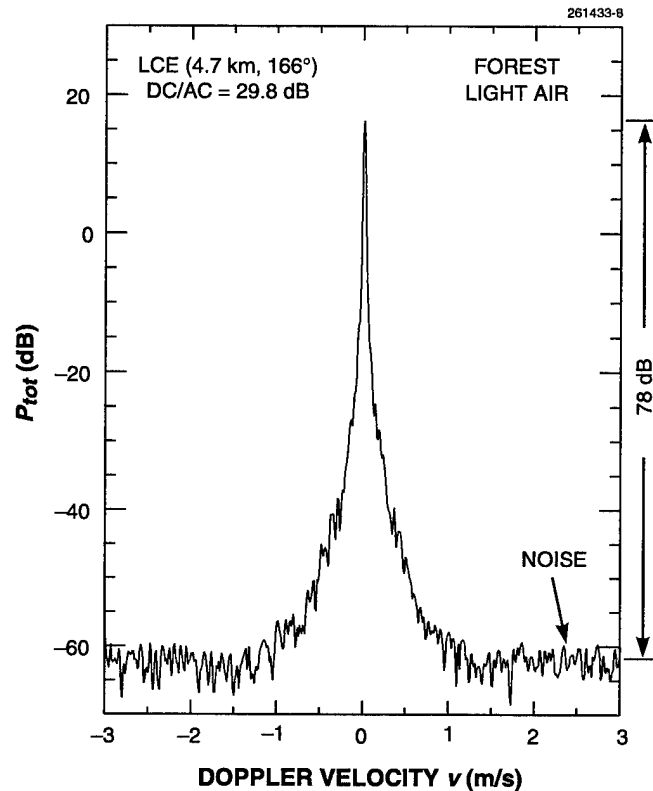


Figure 15. An LCE windblown forest clutter spectrum measured under light wind conditions

The particular value of dc/ac ratio  $r$  applicable to any given treed clutter cell is highly variable. Such variability is illustrated in the results shown in Figure 16, in which ratios of dc to ac spectral power obtained from LCE clutter measurements from many treed cells are shown as a function of wind speed. There is some difficulty in precise specification of wind speed in such results since the remote anemometer used in LCE measurements provides only a one-point-in-space indication of wind conditions for the total test area. Still, Figure 16 indicates that much variability exists in the ratio of dc to ac spectral power in measurements of windblown clutter spectra within common regimes of wind speed. Over and above this inherent variability, however, Figure 16 also clearly indicates a strong trend in the data such that the ratio of dc to ac spectral power increases rapidly with decreasing wind speed.

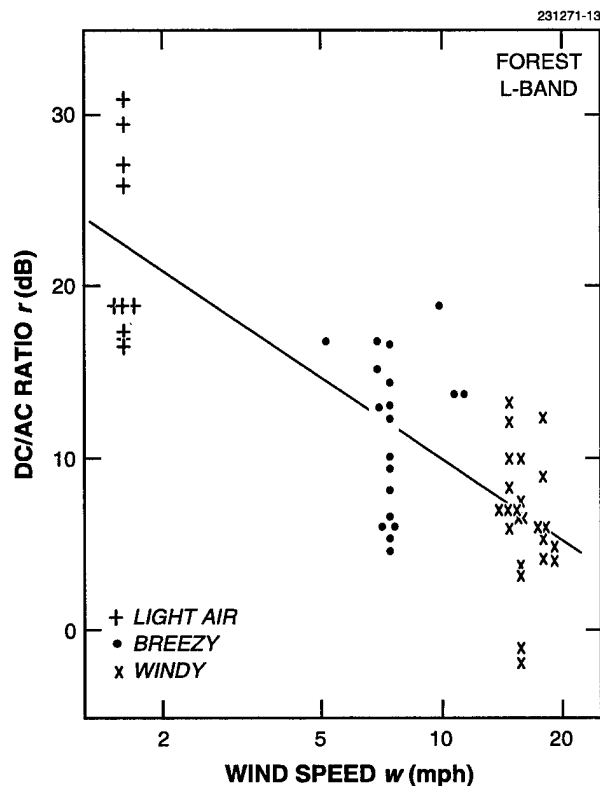


Figure 16. LCE measurements showing ratio of dc to ac spectral power vs wind speed in L-band windblown forest clutter spectra.

### 3.3.2 Variation with Radar Frequency

Whether a scatterer in a forested clutter cell is classified as stationary or in motion depends on the radar wavelength. A back-and-forth scatterer motion of 3 cm would produce a steady signal of essentially fixed phase at VHF, but a fluctuating signal passing through all possible phases at X-band. Furthermore, at VHF and UHF, significant energy penetrates the foliage to scatter from the stationary underlying ground surface, whereas at X-band little or no energy reaches the ground. Again, Goldstein correctly anticipated that, because of such effects, the dc to ac ratio in windblown clutter spectra "... should therefore decrease with wavelength" [8]. Figure 17 shows a Phase One-measured spectrum at VHF from a treed cell under windy conditions (see Table 3). This spectrum was previously shown in Figure 9. It is evident in Figure 17 that a large dc component exists in this VHF clutter signal such that the ratio of dc to ac power in the spectrum is 14.8 dB. In contrast to the large dc component in the light winds spectrum of Figure 15 in which significant quasi-dc spectral power also occurs, in the lower frequency VHF spectrum of Figure 17 the dc component exists largely as a discrete delta function at the spectral resolution of the processing in the zero-Doppler bin. On the same windy measurement day on which the VHF data of Figure 17 were obtained, a



much smaller dc component occurred in measured spectra at higher radar frequencies from the same forested cell. Although there is a large dc component in the VHF spectrum, it also contains a significant amount of ac power of considerable spectral extent. This VHF spectrum appears rather erratic because it comes from a single FFT of 61.44-s CPI, as required to provide adequate spectral resolution at this relatively low radar frequency. The VHF spectrum of Figure 17 is representative of many other Phase One-measured VHF clutter spectra from other forested cells and on other windy days.

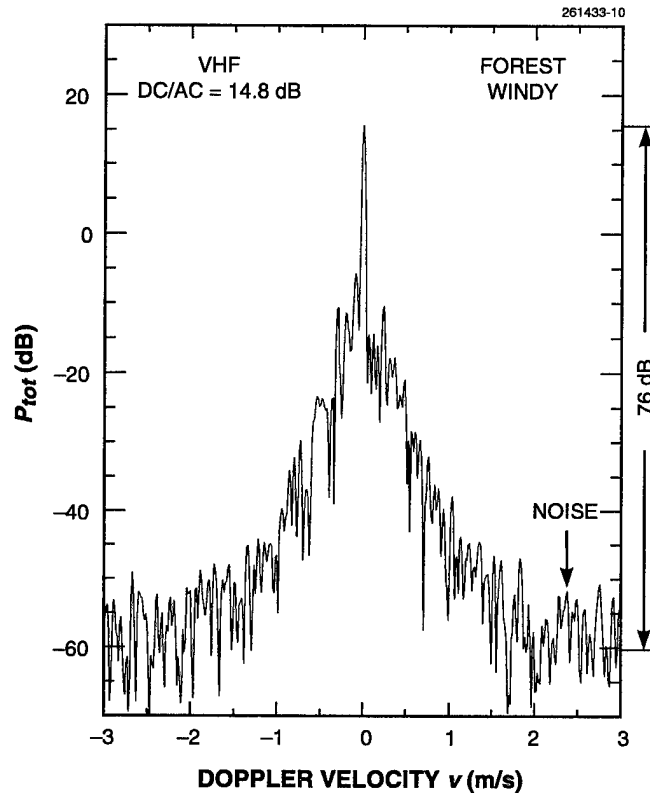


Figure 17. A Phase One windblown forest clutter spectrum at VHF.

Figure 18 shows ratios of dc to ac spectral power vs radar frequency, VHF to X-band, obtained from Phase One clutter measurements under windy conditions at three forested sites. The solid line in the figure joins the median positions of each in-band cluster of data points; the dashed line joins the median positions of the bounding VHF and X-band clusters only. These lines indicate that over and above the inherent variability in the data, there is a strong trend of increasing dc to ac ratio with decreasing radar frequency. Thus at X-band in Figure 18, virtually all the spectral power is ac, whereas at VHF the ac power occurs at levels 15 to 25 dB below the dc power. The information shown in Figures 16 and 18 substantiates the early expectations [8] in these matters. Such information was used to develop the empirical relationship given by Equation (3), which relates dc to ac ratio in windblown clutter spectra with wind speed and radar frequency.

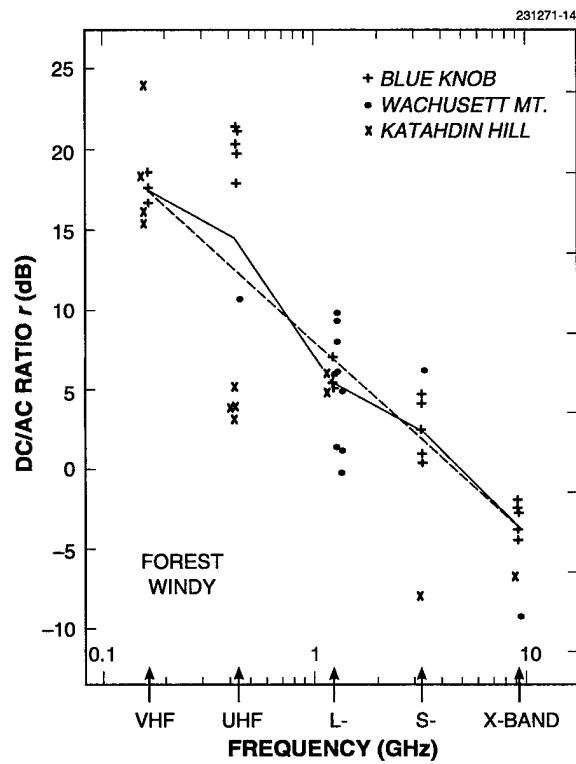


Figure 18. Phase One measurements showing ratio of dc to ac spectral power vs radar frequency under windy conditions at three forested sites.

## 4. USE OF CLUTTER SPECTRAL MODEL

### 4.1 SPREADING OF $\sigma^\circ$ IN DOPPLER

Two important issues concerning the effects of ground clutter on radar system performance are the strength of the clutter, which determines how much interfering clutter power is received, and the spreading of received clutter power in Doppler. Thus predicting ac clutter power in a given Doppler cell requires predicting the backscattering clutter coefficient  $\sigma^\circ$ , predicting the dc to ac power ratio in the spectrum, and predicting the ac spectral shape factor  $P_{ac}(v)$ . The clutter coefficient  $\sigma^\circ$  was defined by Goldstein [8] to be radar cross section per unit ground area in the spatial resolution cell under consideration.

Let  $\sigma_{trees}^\circ$  be the clutter coefficient for windblown trees. Equation (1) shows that  $[\sigma_{trees}^\circ \cdot P_{tot}(v)]$  specifies the spreading of  $\sigma_{trees}^\circ$  in Doppler, i.e.,  $\int_{-\infty}^{\infty} [\sigma_{trees}^\circ \cdot P_{tot}(v)] dv = \sigma_{trees}^\circ$ , so  $[\sigma_{trees}^\circ \cdot P_{tot}(v)]$  represents the normalized density of windblown tree clutter power occurring at Doppler velocity  $v$  in units of  $[(m^2/m^2)/(m/s)]$ . For  $|v| > 0$ ,  $[\sigma_{trees}^\circ \cdot P_{tot}(v)]$  becomes  $[(\sigma_{trees}^\circ / (r + 1)) \cdot P_{ac}(v)]$ . Let  $n = 0, 1, 2, \dots, N$  be the Doppler cell index, where  $n = 0$  is the zero-Doppler cell. Then the amount of windblown-tree clutter cross section  $\sigma_{trees}(n)$  that occurs in the  $n$ th Doppler cell is given by:

$$\sigma_{trees}(n) = \frac{\sigma_{trees}^\circ \lambda}{2(r + 1)} \cdot \Delta f \cdot \Delta A \cdot P_{ac}(f_n), \quad n > 0, \quad (4)$$

where  $\sigma_{trees}(n)$  is in units of  $[m^2]$ , and  $f_n$  is the Doppler frequency [Hz] in the center of the  $n$ th Doppler cell. In Equation (4),  $\Delta f$  = Doppler cell width [Hz];  $\lambda$  = radar wavelength [m];  $\Delta A$  = spatial resolution cell area  $[m^2] = R \cdot \Delta R \cdot \Delta \theta$  where  $R$  = range [m],  $\Delta R$  = range resolution [m], and  $\Delta \theta$  = azimuth beamwidth [rd];  $r$  = ratio of dc/ac spectral power [as given by Equation (3)]; and  $P_{ac}(f_n)$  is the value at  $f = f_n$  of the ac spectral shape function [as given by Equation (2) and Table 1].

Comprehensive information specifying the clutter coefficient  $\sigma_{trees}^\circ$  in Equation (4) is available for low illumination angles typical of ground-sited radar, for radar frequencies from VHF to X-band, and for both VV- and HH-polarizations, on the basis of the Phase One clutter measurement data base [25,29,38]. Phase One clutter data are not available at cross-polarization. However, the LCE clutter data at Wachusett Mt. indicate that in forest, cross-pol. clutter coefficients are generally 3 to 6 dB but occasionally as little as 0 dB or as much as 8 dB less than the co-pol. clutter coefficients. Similar depolarization effects in forest clutter data have been observed previously [12].

### 4.2 TWO REGIONS OF SPECTRAL APPROXIMATION

Figure 19 shows an idealized representation of a typical windblown clutter spectrum (solid line). As is often observed in measured spectral data, this representation consists of two distinct regions, namely, a quasi-dc region near zero-Doppler velocity and an ac spectral tail region at greater Doppler velocities. Also shown is a spectral model (dashed lines) as given by Equation (1). The model uses a delta function at  $v = 0$  to represent the dc spectral component and the exponential shape function as given by Equation (2) to represent the ac spectral tail. In a plot of  $10 \log_{10} P_{tot}$  vs  $v$  such as that of the figure, the exponential shape plots

as a straight line of slope  $4.34 \beta$  (where  $4.34 = 10 \log_{10} e$  and  $e = 2.718 \dots$ ). Also, both the data and the model in Figure 19 are normalized to unit total spectral power, i.e.,  $\int_{-\infty}^{\infty} P_{tot}(\nu) d\nu = 1$ . In these circumstances, the model is matched to the data as follows: first,  $\beta$  is selected so that the slope [i.e., dB/(m/s)] of the model matches that of the data in the ac spectral tail region. Next, the value of dc/ac ratio  $r$  in the model is assigned to provide a y-intercept  $[1/(r+1)](\beta/2)$  so that the exponential model overlays and matches the ac region of the data in absolute power level  $P_{tot}(\nu)$  (i.e., vertical position) as well as slope. Because of the normalizations involved, this procedure results in the excess power from the quasi-dc region of the data being included in the dc Dirac delta function term  $[r/(r+1)]\delta(\nu)$  of the model, where by excess quasi-dc power is meant the power in the quasi-dc region of the data that exists above the approximating exponential of the model.

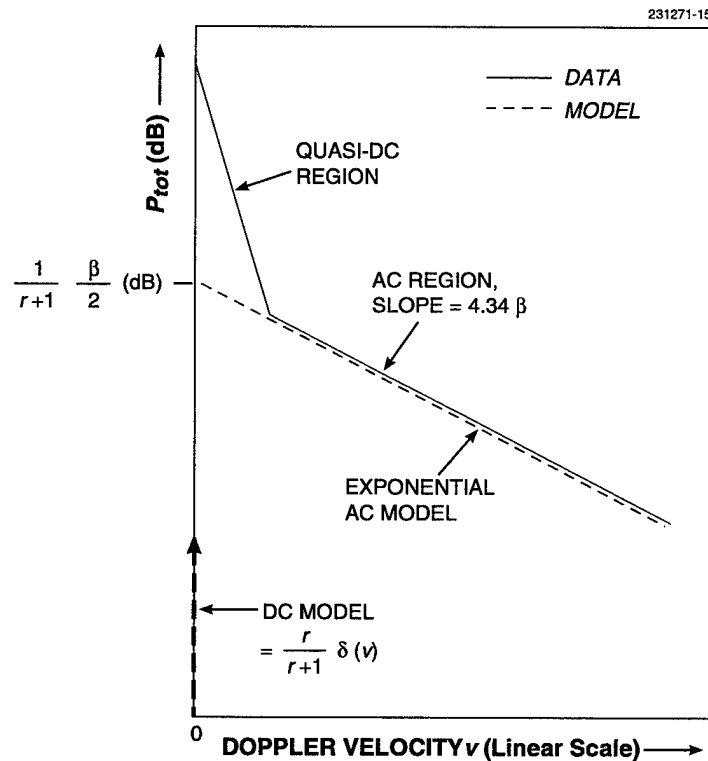


Figure 19. Modeling of clutter spectra.

Figure 20 shows four examples of measured windblown clutter spectra presented as  $10 \log P_{tot}(\nu)$  vs  $\nu$  to illustrate quasi-dc and ac spectral regions in actual measured data. Figure 20(a) shows an LCE spectrum; Figures 20(b) through (d) show Phase One spectra at L-, X-, and UHF bands, respectively. Each spectrum has an approximating exponential model shown as a straight line through the right side of the data. It is evident that each spectrum in Figure 20 contains excess power above the approximating exponential in a quasi-dc region near zero-Doppler. Note the very fine resolution ( $\approx 0.01$  m/s, see Table 3), so in every case quasi-dc spectral power is resolved at levels well above the zero-Doppler window function limiting resolution. It is further evident in the figure that absorbing the excess quasi-dc power of the data in the delta

function dc term of the model in these examples allows extremely good fits of the ac spectral tail regions with exponential shape functions over regions of wide Doppler extent in the spectral tails.

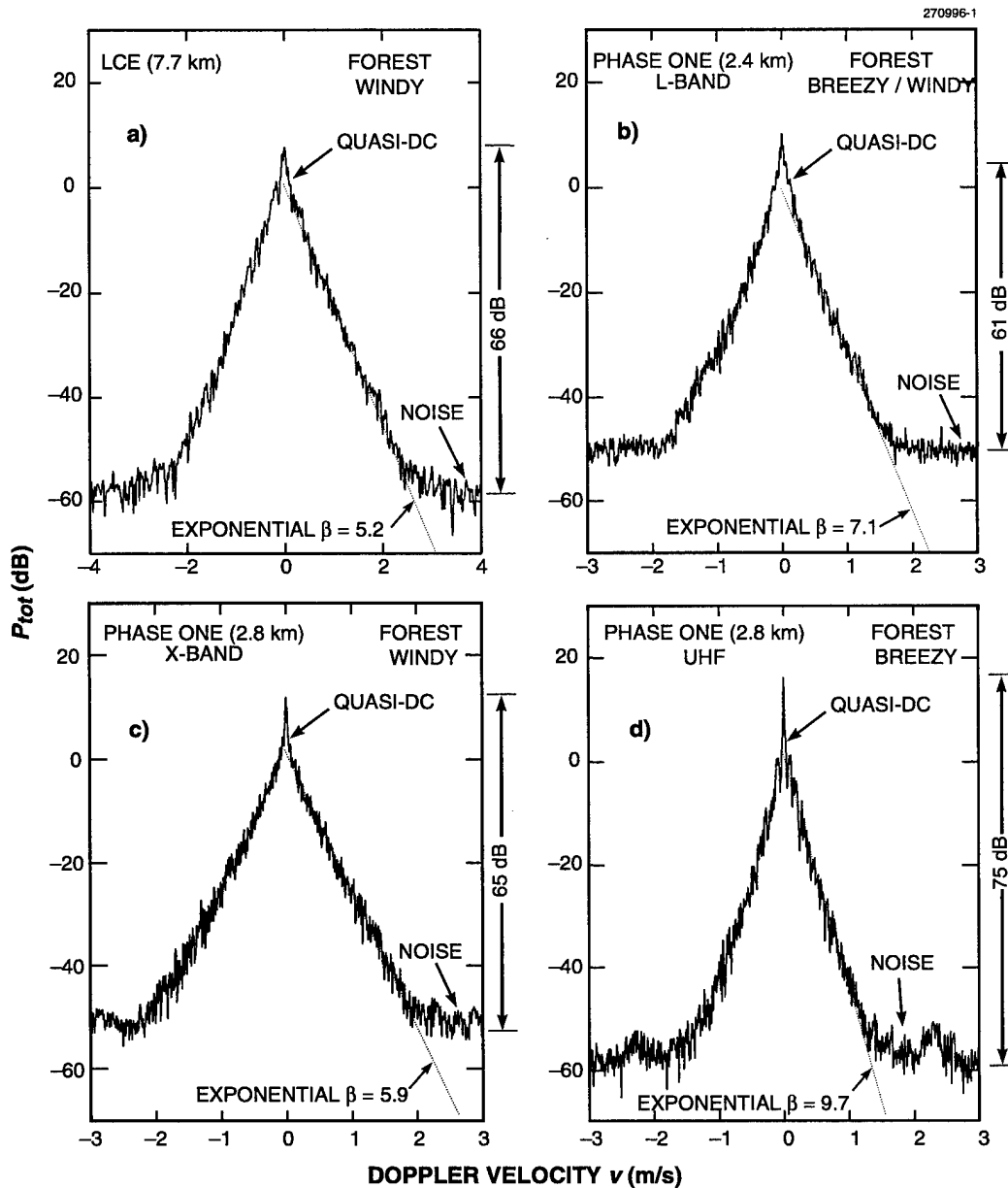


Figure 20. Highly exponential decay in four measured windblown forest clutter spectra: (a) LCE; (b), (c), and (d) are Phase One, L-, X-, and UHF bands, respectively. Regions of excess quasi-dc power are also indicated.

As computed directly in the time domain, the zero-Doppler cell contains relatively little dc power compared with the total ac power from all the non-zero Doppler cells, for each of the examples shown in Figure 20. The dc/ac ratios  $r$  that result both from direct time-domain computation  $r_{\text{measured}}$  and as required to include the excess quasi-dc power in the modeled dc term  $r_{\text{modeled}}$  are shown in Table 5 for each example of Figure 20. Recall that  $r_{\text{measured}}$  is dependent on CPI duration. It is apparent in Table 5 that  $r_{\text{modeled}}$  increases compared with  $r_{\text{measured}}$  as a result of absorbing the excess quasi-dc power in the modeled dc term. This increase in  $r_{\text{modeled}}$  over  $r_{\text{measured}}$  causes the exponential straight-line fits to the data in the examples of Figure 20 to be shifted downwards by  $10 \log(r_{\text{modeled}} + 1) - 10 \log(r_{\text{measured}} + 1)$  decibels, resulting in the exponential models overlaying the measured data in these examples throughout the extensive ac spectral tail regions. The spectral examples of Figures 20(c) and (d) were previously shown in Figures 9 and 10, respectively, in which the data were normalized to  $P_{ac}(v)$  using  $r_{\text{measured}}$ . The spectral example of Figure 20(a) was previously shown in Figure 4, but in this case the data were normalized to  $P_{ac}(v)$  using  $r_{\text{modeled}}$ . Equation (3) which specifies  $r_{\text{modeled}}$  was developed from data in which excess quasi-dc power was absorbed in the dc term to gain the benefit of improved fidelity in modeling spectral tails. Not all Phase One- and LCE-measured spectra are as closely exponential as the examples of Figure 20.

**Table 5.**  
**Measured vs Modeled Ratios of dc/ac Spectral Power in Four**  
**Windblown Forest Measured Clutter Spectra**

Clutter Spectrum (see Figure 20)	CPI (s)	dc/ac Ratio $r$ (dB)	
		Measured (Direct Time-Domain Computation)	Modeled (Excess Quasi-dc Power in dc Delta Function Term)
(a) L-band (LCE)	10.24	-10.7	0.7
(b) L-band (Phase One)	20.48	-9.9	4.3
(c) X-band (Phase One)	4.096	-10.1	1.9
(d) UHF (Phase One)	61.44	-0.4	8.0

No simple ac model (i.e., analytic expression), including exponential, can adequately represent both the quasi-dc region  $|v| < 0.25$  m/s and the ac region  $|v| > 0.25$  m/s of the data in Figures 19 and 20. The objective of this report is realistic representation of the ac region or spectral tail of the data. Even the simplest single-delay-line MTI filter can usually sufficiently reject dc and quasi-dc clutter power in the region  $|v| < 0.25$  m/s. It is the tail of the clutter spectrum that requires definition to enable, for example, knowledgeable design of the skirts of MTI filter characteristics or other Doppler signal-processing ground clutter rejection techniques in the region  $|v| > 0.25$  m/s. In the modeling information provided herein, excess quasi-dc power is included in the dc term in situations where including it as ac power would degrade representation of the ac spectral tail. Users of this information whose interests in clutter spectra may differ from those just stipulated need to be aware that some of the dc power in the delta function of the current model is often spread slightly into a near-in quasi-dc region  $|v| < 0.25$  m/s in actual measurements.

### 4.3 CELLS IN PARTIALLY OPEN OR OPEN TERRAIN

#### 4.3.1 Desert

Ground clutter spatial resolution cells in which some of the backscattered power comes from stationary scattering elements such as the underlying terrain surface itself or large fixed discrete objects (water towers, rock faces) provide correspondingly larger values of dc/ac ratio  $r$  in the resulting clutter spectra. In the ground clutter spectral measurements conducted by the LCE radar at its desert site, portions of barren desert floor were visible between the sparse desert bushes (greasewood, creosote) typically of heights of 3 or 4 ft. Figure 21 illustrates a typical LCE clutter spectrum measured at this desert site under windy conditions (wind speed  $\cong 20$  mph). It is evident that this desert clutter spectrum contains a large dc component at zero-Doppler velocity, presumably the result of backscatter from the stationary desert floor.

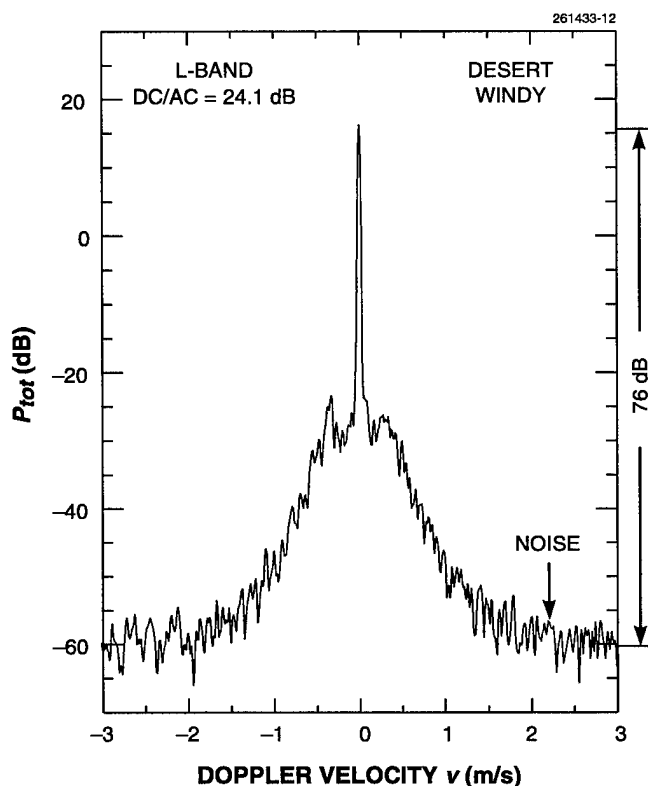


Figure 21. An LCE-measured clutter spectrum from desert terrain (scrub/brush, partially open) under windy conditions.

The ratio of dc/ac power computed directly in the time domain for the desert spectrum of Figure 21 is 24.1 dB. Normalization of measured spectral data to  $P_{tot}(\nu)$  involves division of power per resolution cell by the width of the cell  $\Delta\nu$ . For the data of Figure 21,  $\Delta\nu$  equals -16.22 dB, so this procedure raises the power in each cell by 16.22 dB. For spectra like that of this figure with a large dc component, the power in the zero-Doppler cell is not distributed over  $\Delta\nu$  but exists as a singular dc component. Reducing the zero-Doppler peak by 16.2 dB allows more straightforward interpretation of  $r = 24.1$  dB as simply the ratio of the reduced zero-Doppler peak to the total ac power (i.e., the power level of the step function existing in the unit interval  $-0.5 < \nu < +0.5$  m/s and containing the same total ac spectral power as the measured spectrum).

In addition to the desert/windy clutter spectrum of Figure 21 containing a large dc component, it also contains extensive ac spectral spreading at lower power levels. The low-level ac spectral spreading in these data is due to wind-induced motion of the desert foliage. Other LCE-measured desert spectra from similar cells under light or calm wind conditions showed little or no spectral spreading over as much as 80 dB of spectral dynamic range [see Figure 3(a)]. Unlike the forest/light wind spectrum of Figure 15, which also contains a large dc component but in which the spectral power decays rapidly but broadens continuously away from the zero-Doppler peak, the dc component in the desert/windy spectrum of Figure 21 exists more as a discrete delta function at the spectral resolution of the window function over the higher levels of spectral power.

Figure 22 shows the ac spectral tail region of the desert/windy spectrum of Figure 21 at higher Doppler velocities as  $10 \log P_{ac}(\nu)$  vs  $\log \nu$ . Also shown in Figure 22 is the forest/windy spectrum previously shown in Figures 4 and 20(a). Both measured spectra in Figure 22 are normalized to  $P_{ac}(\nu)$  [i.e., multiplied by  $(1 + r)$ ] using  $r$  as computed directly in the time-domain. Note that the 24-dB dc/ac ratio in the desert spectrum (a) of Figure 22 results in an effective 24-dB loss of sensitivity (i.e., higher noise level) compared with the forest spectrum (b) in measuring ac spectral shape. Otherwise, and perhaps surprisingly, the ac spectral shape of the desert/windy spectrum in Figure 22 almost exactly overlays that of the forest/windy spectrum over their common interval of available spectral dynamic range. It was previously shown that the exponential shape factor  $\beta = 5.2$  provides an excellent match to the forest/windy spectrum of Figure 22. Thus, at least on the basis of these data, the modeling information of Table 1 and Figure 1 specifying wind-blown clutter ac spectral shape under windy conditions appears reasonable, not only for densely forest-vegetated clutter cells upon which the modeling information was principally based, but also for more open desert-vegetated cells in which a significant proportion of stationary ground was visible and containing very different types of vegetation from forest trees. That is, these data suggest that the ac spectral shape function caused by windblown vegetation in a cell may be, at least to a first-order approximation, somewhat independent of the type of vegetation in the cell and/or how much of the cell area as viewed by the radar contains vegetation. Of course, the dc to ac ratio of clutter spectral power is much higher in partially open desert than in forest terrain.



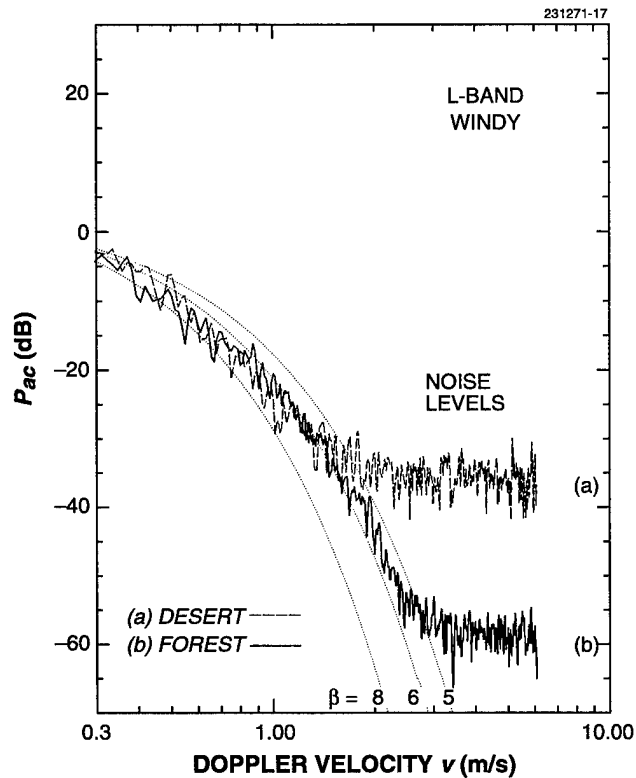


Figure 22. Comparisons of ac spectral shapes of LCE (a) desert (scrub/brush) and (b) forest clutter spectra under windy conditions.

**Knolls, Utah.** Recently, it has been suggested that X-band desert clutter spectral shapes, in particular, might be significantly different and perhaps wider than those observed at lower radar frequencies and from other types of windblown vegetation. Figure 23 shows X-band desert clutter spectra measured by the Phase One radar at two western U.S. desert measurement sites—Booker Mt., Nevada, and Knolls, Utah—in summer 1984. At both sites these spectra were obtained as eight-gate averages, 15 FFTs per gate, 2048-point FFTs, PRF = 500 Hz, hor. pol., gate width = pulse length = 150 m. At Booker Mt., the radar carrier frequency was 8990 MHz; at Knolls, 9200 MHz. The Booker Mt. spectrum of Figure 23(a) was measured from barren level mud flats under calm wind conditions and light rain at 12- to 13.2-km range and  $2.3^\circ$  grazing angle. This Booker Mt. spectrum shows essentially no spectral spreading beyond the window-function resolution over a 60-dB spectral dynamic range, except for the small residual spur indicated at the base of the dc-spike 56 dB down and 4 dB above the noise floor, and again evidences the field capability of the Phase One radar for making X-band clutter spectral measurements [compare with Figure 3(c)].

In contrast to no spectral spreading at Booker Mt. in Figure 23(a), 23(b) and (c) show an X-band desert spectrum from Knolls with significant spectral spreading. The Knolls spectrum was measured from very level terrain containing sparse, low, desert scrub vegetation under 11- to 16-mph wind conditions at

2.5- to 3.7-km range and  $0.5^\circ$  grazing angle. This X-band desert spectrum, although containing a significant dc component, contains less dc power than the LCE L-band Nevada desert spectrum of Figure 21. As a result, more ac spectral dynamic range is available for defining the shape of the X-band desert spectrum in Figure 23(c) than was available for defining the shape of the L-band desert spectrum in Figure 22. Contrary to the preceding suggestion, this X-band Knolls desert spectrum [Figures 23(b), (c)] is very similar to other Phase One and LCE windblown clutter spectra observed at other radar frequencies and from other types of vegetation.

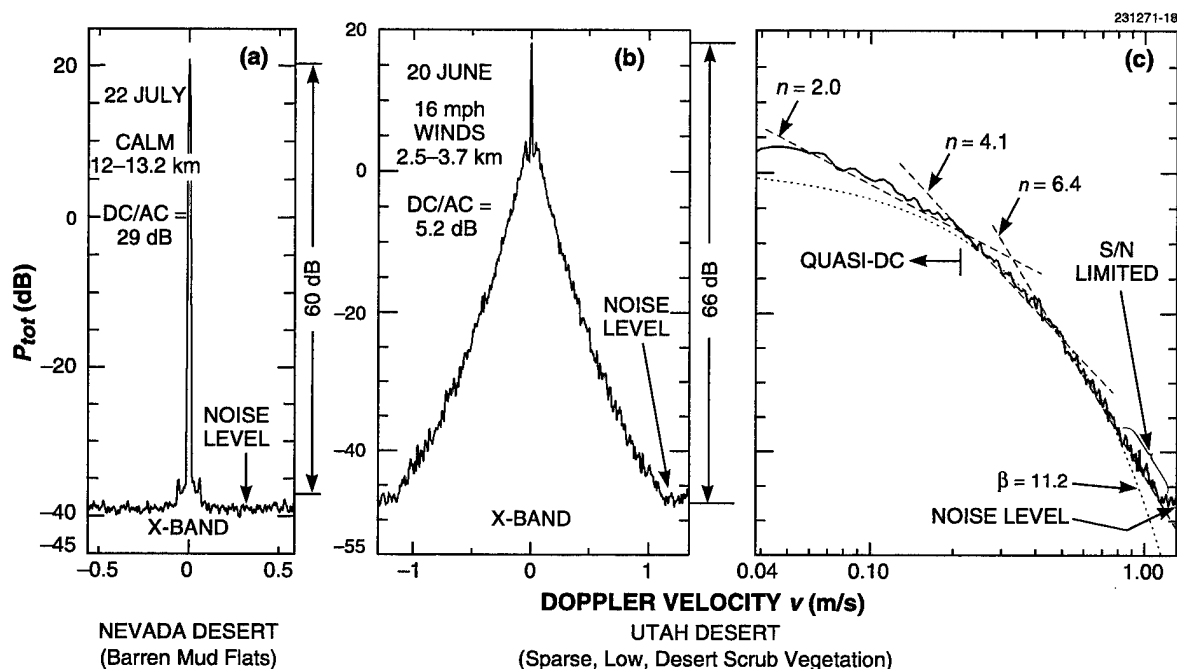


Figure 23. Phase One X-band desert clutter spectral measurements: (a) Booker Mt., Nevada, and (b), (c) Knolls, Utah.

The basic similarities of the Knolls spectrum to other Phase One- and LCE-measured spectra are in the increasing downward curvature with increasing Doppler velocity and decreasing power level displayed in Figure 23(c) on  $10 \log P$  vs  $\log v$  axes. This downward curvature also characterizes the exponential shape factor. Thus through a broad central region of increasing downward curvature in the data of Figure 23(c), the exponential shape factor  $\beta = 11.2$  overlays the data and captures its general shape. At upper levels, the data rise somewhat above the approximating exponential in the quasi-dc region  $|v| < 0.21$  m/s; this excess quasi-dc power is included as dc power in the dc/ac ratio of 5.2 dB ascribed in modeling this spectrum (the time-domain dc/ac ratio for these data was computed as +0.5 dB). The slight broadening beyond exponential at very low levels in Figure 23(c) as the measured data approach to within 10 dB of the noise level is at least partially the result of S/N limitations in this region. In contrast to the exponential shape factor generally capturing the shape of the measured Knolls spectrum of Figures 23(b) and (c), power-law rates of decay [Figure 23 (c)] increase from  $n \cong 2$  (20 dB/decade) at upper levels to  $n \cong 4$  (i.e., 40 dB/decade) at

intermediate levels to  $n > 6$  ( $> 60$  dB/decade) at the lowest levels; in other words, no single power law comes close to capturing the general shape of the X-band desert spectrum shown in Figures 23(b) and (c). The exponential shape factor  $\beta = 11.2$  for the X-band desert spectrum of Figures 23(b) and (c) is somewhat greater than the value of  $\beta = 8$  supplied by the windblown forest exponential spectral model of Section 2 in similar breezy conditions. That is, the Knolls X-band desert spectrum is similar in shape but somewhat narrower than that generally expected for windblown forest spectra under similar wind conditions. Otherwise the Knolls X-band desert spectrum does not stand out as fundamentally different from general Phase One and LCE findings for the behavior of clutter spectra from windblown vegetation.

#### 4.3.2 Cropland

The Phase One radar acquired clutter measurement data at the farmland site of Beulah, N. Dakota, during the first two weeks of June 1984 [25]. The open agricultural fields in the measurement sectors around Beulah were mostly in wheat (with some oats and barley, some sweet clover, some summer fallow). Trees occurred at  $\sim 1\%$  to  $3\%$  incidence by area on the Beulah landscape, for the most part at low-lying elevations along creekbeds. In early June the average height of the wheat was about 1 ft. Wind conditions were measured by an anemometer located at the radar site.

The primary Beulah measurement swath examined comprised 16 contiguous 150-m gates from 4.5- to 6.75-km range. Over this swath, the terrain, rising at slopes as great as  $2^\circ$  to  $3^\circ$  in places, was well illuminated by the Phase One radar at a depression angle of  $\sim 0.4^\circ$ . The main swath principally contained wheat fields, particularly at the higher elevations at longer range. Some of the nearer gates in the swath, at lower elevations, contained some trees. One gate in the swath at longer range (i.e., 6.3 km) contained a strip of high grass. Windblown wheatland clutter spectra were generated for all 16 primary-swath gates at vertical polarization and 1- $\mu$ s pulsewidth in all five Phase One frequency bands. In each band, 2048-point FFTs were generated and averaged to form the spectrum for each gate. The effective PRF and number of FFTs averaged in each band were at X-band, 500-Hz PRF, 15 FFTs; at S-band, 167-Hz PRF, 5 FFTs; at L-band, 100-Hz PRF, 3 FFTs; at UHF, 33.3-Hz PRF, 1 FFT; and at VHF, 12.5-Hz PRF, 1 FFT. Considerable variation occurred in these spectra from gate to gate, although in all bands above VHF, the individual-gate spectra always showed a considerable degree of spectral spreading to either side of a significant dc component.

Six particular gates (10–12 and 14–16) at longer ranges in the primary swath were selected as under strong illumination and essentially containing pure wheat fields within the complete azimuth main beam-width in all bands. Spectra from these gates were averaged in each band to provide a generalized indication of pure windblown wheatland clutter spectra. Figure 24 shows the resultant generalized clutter spectra from pure windblown wheatland in all five Phase One frequency bands. These measurements were obtained on four different days in early June under relatively windy conditions. These results show significant spectral spreading in each of the upper four bands (X, S, L, and UHF) to either side of a strong dc component. Spectral spreading in these bands extends to power levels 60 to 70 dB below zero-Doppler peaks and to corresponding Doppler velocities generally  $< \sim 1$  m/s. In contrast, the VHF wheatland spectrum shows absolutely no spectral spreading to a level 65 dB down under 12-mph winds. Presumably, this complete lack of VHF spectral spreading is due to a combination of (a) a high degree of penetration of the VHF radiation through the wheat stalks to the underlying stationary ground, and/or (b) the amplitude of the 12-mph wind-blown motion of the wheat stems being  $\ll 1\lambda$  at VHF ( $\ll 1.7$  m). Note that the UHF wheatland spectrum, which shows the greatest degree of spreading of any of the four upper-band spectra to a maximum Doppler velocity of  $\sim 1.25$  m/s, was measured under much windier conditions (27 mph) than the VHF spectrum.

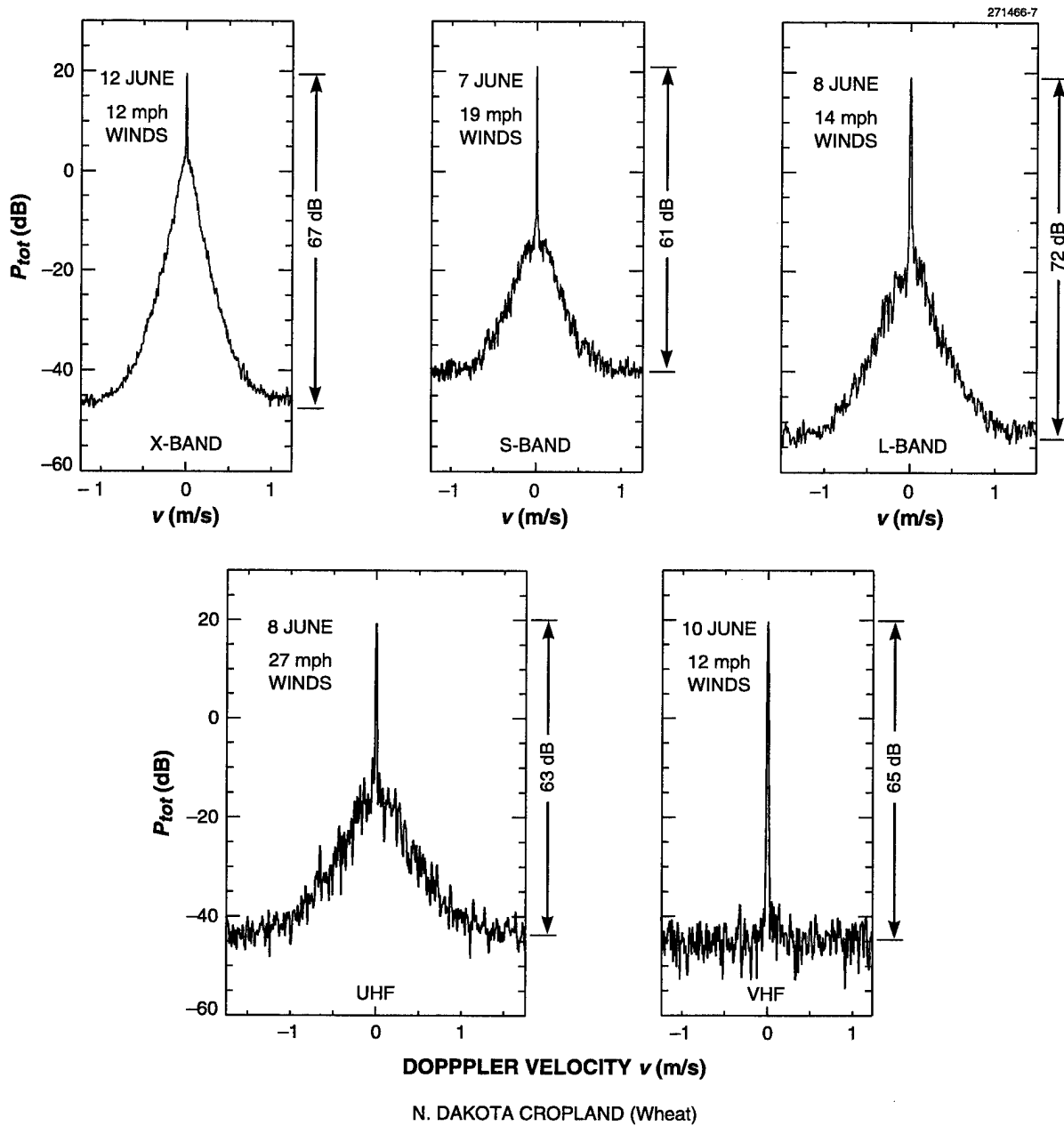


Figure 24. Phase One five-frequency clutter spectra from North Dakota wheatland measured on four different days in early June 1984 under strong breezy or windy conditions.

The ac spectral spreading in the four upper-band wheatland clutter spectra of Figure 24 is highly exponential in shape, as indicated by the relatively linear decay displayed on the  $10 \log P$  vs  $v$  axes used in

Figure 24. The increased spreading (greater than exponential) indicated in the results of Figure 24 at lower spectral power levels within 10 dB of the system noise floors is at least partially caused by inadequate S/N ratio at these low levels. The three ac spectral shapes at S-, L-, and UHF-bands are remarkably exponential, and in fact are reasonably well-fitted by the exponential shape factor  $\beta = 9$ , which although slightly greater (slightly narrower spectra), is not out-of-line with the values provided in Table 1 for windblown forest. Each spectrum also shows a very strong dc component. There is little indication in these three spectra of decreasing foliage penetration (decreasing dc component) with increasing radar frequency. However, the X-band spectrum in Figure 24 does show a much decreased dc component, such that much of the dc power in the lower bands has spread into a quasi-dc region  $|v| \leq 0.25$  m/s.

Field investigation revealed that one of the gates (gate 13, at 6.3-km range) in the primary swath of 16 Beulah range gates contained a strip of high grass as opposed to wheat. The height of the grass (viz., crested wheat grass) was  $\sim 3$  ft. Clutter spectra for this tall-grass gate were reduced in all five Phase One frequency bands from the same experiments and in a manner similar to the spectra of Figure 24. These tall-grass spectra were wider, less exponential, and with less dc component than the corresponding wheat spectra in each of the four upper bands, UHF to X. The VHF tall-grass spectrum continued to show absolutely no spectral spreading, in this case to a noise level 71 dB down [see Figure 3(d)]. In the four upper bands, the tall-grass spectra showed significant concave curvature from above on  $10 \log P$  vs  $v$  axes. Although wider than exponential, none of these spectra were well-fittable with any single power-law shape; the local power-law rates of decay in these spectra ranged from  $n \cong 3$  at upper levels of spectral power to  $n \cong 4$  at mid-levels to  $n \cong 5$  (or  $n \cong 6$  at UHF) at the lower levels measured 65 to 75 dB down from zero-Doppler peaks. Maximum spectral extents at these low levels were to  $|v| \cong 1.5$  m/s in the three upper bands and to  $|v| \cong 2$  m/s in the very windy UHF measurement.

Additional clutter spectra were also reduced in all five Phase One frequency bands in which, for each band, spectra from all 16 range gates in the primary Beulah range swath were averaged together. The same experiments and similar data reduction procedures were used for these 16-gate-averaged spectra as for the pure-wheat spectra of Figure 24. As previously mentioned, a very small incidence of trees occurred over this primary swath, particularly in the nearer gates in the swath and more so for the wider beamwidths (i.e., the lower radar bands) in these nearer gates. The resulting 16-gate-averaged wheat-with-1%- to-3%-trees spectra had significantly lower dc components than the pure-wheat spectra of Figure 24 at all radar frequencies below X-band. The VHF wheat-with-trees spectrum showed spectral spreading beginning at a level 50 dB below the zero-Doppler dc peak and spreading to Doppler velocities  $|v| \cong 1$  m/s at the spectral noise level 69 dB down. Otherwise, these 16-gate-averaged wheat-with-trees spectra were very similar in terms of ac spectral shape and extent to the 6-gate-averaged pure-wheat spectra of Figure 24.

Table 6 shows the ratio of dc to ac clutter spectral power as computed directly in the time domain for all the primary-swath Beulah spectral results previously discussed (the pure-wheat, the wheat-with-trees, and the tall-grass spectra). Also shown in Table 6 is the dc/ac ratio predicted by Equation (3) for windblown trees at the radar frequencies and wind speeds applicable to the five Beulah clutter experiments. One would expect that the dc/ac ratios for the wheat-with-trees spectra would lie intermediately between those for pure wheat and those for forest, and indeed this expectation is largely true in the table. Beyond this, however, the trends in these pure-wheat vs wheat-with-trees vs forest dc/ac ratios are rather erratic. Much more of such data would be required to establish statistically significant trends as a function of percent incidence of trees in generally open terrain.

**Table 6.**  
**Phase One-Measured Ratios of dc/ac Clutter Spectral Power**  
**in Beulah, N. Dakota, Wheatland**

Frequency	Wind Speed at Radar Hilltop Location, Mean/Max (mph)	dc/ac Ratio Computed Directly in the Time Domain (dB)			
		Pure Wheat, ~ 1 ft High (6-gate avg)	Wheatland, 1% to 3% Trees (16-gate avg)	Forest (Exponential Model Prediction)	Tall Grass, ~3 ft High (1 gate)
X-band	7/12	4	4	-1	3
S-band	15/9	17	10	1	1
L-band	8/14	21	14	8	11
UHF	22/27	17	9	9	1
VHF	8/12	33 <sup>a</sup>	28	19	38 <sup>a</sup>
a. Noise-limited (no Doppler spreading of the dc spike occurred in the clutter spectrum down to the radar noise level)					

In the upper three radar bands, the tall-grass dc/ac ratios in Table 6 are very similar to those shown for forest for similar wind speeds. That is, direct application of the complete exponential windblown clutter spectral model, including the dc/ac ratio [Equations (1), (2), and (3); Table 1] as derived from windblown tree measurements, also appears suitable in agricultural terrain containing high crops (like tall grass) at L-, S-, and X-bands. At VHF, as expected, the tall-grass spectrum has a much higher dc/ac ratio (resulting from absolutely no spectral spreading) than the forest spectrum.

**Beiseker, Alberta.** Another agricultural site visited by the Phase One radar in summer season was Beiseker, Alberta—a site-of-concentration visited by the Phase One radar four different times to establish seasonal variations in clutter strength [25]. The Phase One summer visit to Beiseker was in August 1983 when the crops (mostly wheat and other grains) were mature and thus much higher than for the June visit to Beulah. Figure 25 shows an S-band summer-season Beiseker cropland clutter spectrum measured as a 16-gate average, 5 FFTs per gate, 2048-point FFTs, PRF = 500 Hz, ver. pol., gate width = pulse width = 150 m, radar frequency = 3240 MHz. In particular, note that the PRF of 500 Hz used to make this spectrum was higher than the 167 Hz generally used at S-band, resulting in somewhat reduced spectral resolution (the dc spike shown in Figure 25 is ~ 3 times wider than usual). The Beiseker spectrum was measured from rising terrain at 10- to 12.4-km range under 7- to 12-mph winds. The measurement geometry was similar to that at Beulah, with the terrain first falling off with increasing range from the radar, and then rising again over the measurement sector in the distance, resulting in illumination at a depression angle of ~ 0.4°. The 2.4-km Beiseker measurement sector was almost entirely in mature wheat, although the measurement sector was somewhat broken in places and dissected with a stream bed, resulting in a small secondary incidence of her-

baceous rangeland, with minor scrub/brush evident in the air photos at lower elevations along the stream bed.

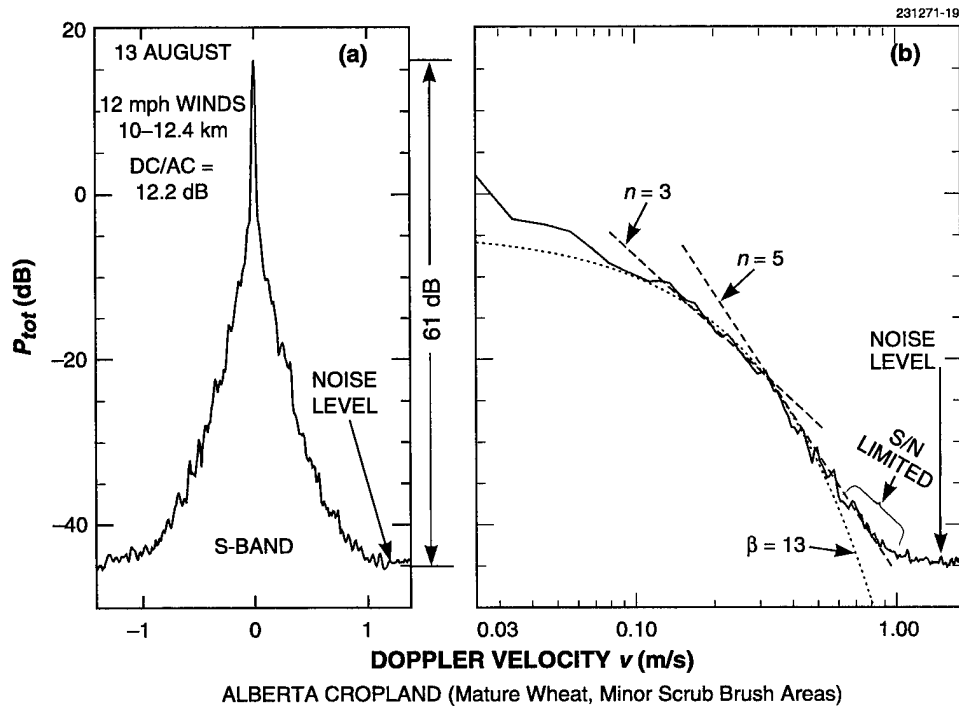


Figure 25. Phase One S-band cropland clutter spectrum from Beiseker, Alberta.

The 16-gate, mature-wheat, Beiseker S-band spectrum of Figure 25 contains less dc power than the 6-gate, young-wheat, Beulah S-band spectrum included in Figure 24. Otherwise the Beiseker spectrum is also well represented as exponential. As shown in Figure 25(b), the exponential shape factor that best represents the Beiseker spectral shape is  $\beta = 13$ , slightly greater than the  $\beta = 9$  Beulah value, indicating a somewhat narrower Beiseker spectrum resulting from the lighter (7 to 12 mph) winds at Beiseker compared with those at Beulah (15 to 19 mph). Some of the increased broadening beyond exponential at very low levels in Figure 25(b) may be attributed to S/N limitations as the measured data approach to within 10 dB of the noise floor. Power-law rates of decay are shown in Figure 25(b) to increase from  $n \approx 3$  (30 dB per decade) at intermediate levels to  $n \approx 5$  (50 dB per decade) at lower levels; that is, no single power law very well represents the shape of this measured cropland spectrum. The dc/ac ratio in which excess quasi-dc power is included as dc power to enable the  $\beta = 13$  shape factor to fit the spectral tail in Figure 25 is 12.2 dB (as computed directly in the time-domain, the dc/ac ratio for this spectrum was 9.8 dB). These Beiseker dc/ac ratios may be compared with the Beulah dc/ac ratios shown in Table 6. In contrast to the Beulah pure-wheat 6-gate spectrum, the Beulah wheatland 16-gate spectrum (not shown, but which included the tall-grass gate and occasional trees in early gates) is essentially identical in all respects (i.e., a direct overlay) to

the Beiseker 16-gate spectrum of Figure 25. That is, although detailed gate-to-gate differences exist in these data caused by variations in topography, crops, and wind speeds, when averaged over broad 2.4-km swaths these results appear to indicate that exponential spectral spreading generally occurs in open cropland terrain without much site-specific variation.

**de Loor's Results.** Much earlier measurements of clutter spectra from windblown crops (including wheat) made with a noncoherent X-band system were reported by de Loor, Jurriens, and Gravesteijn [39]. The one example shown by de Loor et al. is an ac spectrum for full-grown wheat under 5- to 7-mph winds of ~40-dB spectral dynamic range. This spectrum appears to be highly exponential (i.e., its shape is convex from above as shown plotted in decibels against a log-Doppler frequency axis) and is very similar in shape to the Phase One-measured Beulah pure-wheat spectra of Figure 24. The spectral width of the example shown by de Loor et al. is ~0.32 m/s at the -40-dB level; i.e., is somewhat narrower than the higher-wind-speed Beulah X-band spectrum of Figure 24. Spectral widths at the -3- and -10-dB levels as a function of wind speed for winds up to 22 mph are also provided by de Loor et al. [39] in composite plots covering four different crop types (wheat, alfalfa, sugar beets, potatoes) for which the maximum -10-dB widths were ~0.67 m/s. However, de Loor et al. "could not conclusively [show] significant [spectral] differences between different crop types." Also, de Loor et al. state that in their spectral measurements from crops, the -25-dB level never exceeded 1.6 m/s Doppler velocity. Although matching the de Loor et al. maximum extent points of 0.67 m/s at -10 dB and 1.6 m/s at -25 dB requires gale force winds in the current windblown-tree exponential model of Section 2, the de Loor et al. spectral results are noncoherent and are therefore wider by a factor of ~1.4 (see Section 5.1.1) than corresponding coherent data. Reducing the de Loor et al. maximum extent points by a factor of ~1.4 yields reduced points of maximal extent of ~0.5 m/s at -10 dB and ~1.1 m/s at -25 dB. These reduced points fall in very closely with the predictions of the current windblown-tree exponential model at corresponding -10- and -25-dB levels under windy conditions (see Figure 1). Such comparisons of Phase One spectral results with those of de Loor et al. reinforce Phase One indications suggesting no gross differences in ac spectral shape or extent at microwave frequencies between windblown tree spectra and windblown crop spectra, or indeed, between windblown crops at different stages of maturity, from different sites, and of different crop types, under windy conditions. However, there is a strong effect of increasing spectral width with increasing wind speed for both windblown trees and windblown crops.

### 4.3.3 Summary

It is not possible to generalize information for dc/ac spectral power ratio  $r$  for all possible varieties of physical cells from which significant proportions of backscattered clutter power come from stationary scattering elements. LCE measurements of clutter spectra at L-band in partially open desert terrain and Phase One measurements of clutter spectra at X-, S-, L-, and UHF bands in open agricultural (wheatland) terrain, although indicating much larger values of dc/ac spectral power ratio when compared with forest terrain, also indicate that the residual ac spectral shape function  $P_{ac}(v)$  is similar to that of forest (also corroborated by the X-band cropland spectral results of de Loor et al.). Additional corroborative multifrequency Phase One spectral measurements in partially open rangeland terrain at Wainwright, Alberta, are presented subsequently in Section 5.1. Phase One measurements performed in urban terrain indicate that residential treed areas provide clutter spectra similar to forest, whereas downtown high-rise city centers largely devoid of visible trees provide very narrow spectra ( $r \rightarrow \infty$ ) except for occasional spectral artifacts, for example, such as might be caused if a moving vehicle happens to be in the cell. Thus the spectral model of Equations (1), (2),



and Table 1 may be considered generally applicable at least as a first-order approximation to cells in partially open or open terrain as long as the value of  $r$  is increased appropriately. However, Equation (3) specifying  $r$  was derived only from forested cells, and only some particular examples are provided herein on how to go about increasing  $r$  for cells incompletely filled with trees or in open agricultural terrain.

#### 4.4 MTI IMPROVEMENT FACTOR

A significant advantage of an exponential spectral model for clutter is its analytic tractability. Here an example of this tractability is provided by deriving the MTI improvement factor of a single delay-line canceller operating in an environment of windblown clutter exponentially distributed in Doppler. Also derived is the single delay-line canceller MTI improvement factor that results under the more traditional assumption of Gaussian-distributed clutter, which is then compared with the improvement factor pertaining to exponentially distributed clutter. In deriving those improvement factors, the earlier approaches of Skolnik [1] and Narayanan et al. [37] are followed for deriving improvement factors for Gaussian spectral shapes. However, also explicitly included in the derivations here is the effect of the dc spectral component on the improvement factor.

Note that the power-law function [see Equation (12)] is not so analytically tractable as the exponential and Gaussian functions. For example, attempting to follow the preceding approach to obtain the single delay-line canceller improvement factor for power-law-distributed clutter leads to an infinite integral expression that cannot be simply evaluated analytically.

##### 4.4.1 Preliminary Analysis

The input clutter power within one pulse repetition interval  $T$  entering the single delay-line canceller is given by

$$P_{ic} = \int_{-f_p/2}^{f_p/2} P_{tot}(f) df \quad ,$$

where  $f_p = 1/T$  is the PRF and  $P_{tot}(f)$  is the total clutter spectral power density as given by Equation (1) (transformed from Doppler velocity  $v$  to Doppler frequency  $f$ ). Since  $f_p$  must be much greater than the clutter spectral extent of  $P_{tot}(f)$  for successful MTI operation, the limits of integration in the preceding integral can be further expanded to  $\pm \infty$  without practical consequence on  $P_{ic}$ , whereupon

$$P_{ic} = \int_{-\infty}^{\infty} P_{tot}(f) df = 1 \quad .$$

The equivalence of the infinite integral expression to unity in this equation is required by the definition of  $P_{tot}(f)$  in Equation (1). The frequency response function in the power domain for a delay line of time delay  $T$  is given [1] by

$$|H(f)|^2 = \sin^2(2\pi fT) \quad .$$

Thus the residual clutter power after cancellation is given by

$$P_{oc} = \int_{-\infty}^{\infty} P_{tot}(f) |H(f)|^2 df \quad .$$

In this equation, the sine function in  $|H(f)|^2$  may be replaced by its small-angle approximation (i.e., its argument), again because  $f_p = 1/T$  greatly exceeds the practical spectral extent of  $P_{tot}(f)$ . The result of this substitution is

$$P_{oc} = 4\pi^2 T^2 \int_{-\infty}^{\infty} f^2 P_{tot}(f) df \quad .$$

The total clutter spectral power density  $P_{tot}(f)$  is given by Equation (1) as

$$P_{tot}(f) = \frac{r}{r+1} \delta(f) + \frac{1}{r+1} P_{ac}(f) \quad ,$$

where  $r$  is the ratio of dc to ac power in the clutter spectrum and  $P_{ac}(f)$  is the ac spectral shape factor. Substituting this expression for  $P_{tot}(f)$  into the above equation for  $P_{oc}$  and recognizing that the term involving integration over the delta function term vanishes, the general result is that the output clutter power from a single delay-line canceller is given by

$$P_{oc} = \frac{4\pi^2 T^2}{r+1} \int_{-\infty}^{\infty} f^2 P_{ac}(f) df \quad . \quad (5)$$

The MTI improvement factor  $I$  of the single delay-line canceller is given [1,37] by

$$I = \bar{G} \frac{P_{ic}}{P_{oc}} \quad ,$$

where  $\bar{G}$ , the average gain of the canceller, can be shown [1] to equal 2. Therefore,  $I$  of the single delay-line canceller is given by

$$I = \frac{2}{P_{oc}} \quad ,$$

where  $P_{oc}$  is given by Equation (5).

#### 4.4.2 Exponential Clutter

Clutter distributed exponentially in Doppler frequency  $f$  is given by Equation (2) as

$$P_{ac}(f) = \frac{\beta'}{2} \exp(-\beta' |f|) \quad ,$$

where  $\beta' = (\lambda/2)\beta$  and  $\beta$  is as specified in Table 1. It follows that

$$P_{oc} = \frac{4\pi^2 T^2}{r+1} \beta' \int_0^{\infty} f^2 \exp(-\beta' f) df \quad .$$

Using the standard result  $\int_0^\infty x^2 \exp(-ax) dx = 2a^{-3}$ , the preceding equation reduces to:

$$P_{oc} = \frac{8\pi^2 T^2}{(r+1)\lambda^2} \cdot \left(\frac{2}{\beta}\right)^2 .$$

Representing  $I$  of the single delay-line canceller in exponentially distributed clutter as  $I_\beta$ , it follows that

$$I_\beta = (r+1) \left(\frac{v_p}{\pi}\right)^2 \left(\frac{\beta}{2}\right)^2 , \quad (6)$$

where  $v_p = (\lambda/2)f_p$ .

#### 4.4.3 Gaussian Clutter

Clutter distributed Gaussianly in Doppler frequency  $f$  is given by Equation (11) as

$$P_{ac}(f) = \sqrt{\frac{g'}{\pi}} \exp(-g' f^2) ,$$

where  $g' = (\lambda/2)^2 g$ . It follows that

$$P_{oc} = \frac{8\pi^2 T^2}{r+1} \sqrt{\frac{g'}{\pi}} \int_0^\infty f^2 \exp(-g' f^2) df .$$

Using the standard result  $\int_0^\infty x^2 \exp(-a^2 x^2) dx = \frac{\sqrt{\pi}}{(4a^3)}$ , the preceding equation reduces to:

$$P_{oc} = \frac{8\pi^2 T^2}{(r+1)\lambda^2} \cdot \frac{1}{g} .$$

If  $I$  of the single delay-line canceller in Gaussianly distributed clutter is represented as  $I_g$ , it follows that

$$I_g = (r+1) \left(\frac{v_p}{\pi}\right)^2 g . \quad (7)$$

Except for the inclusion of the term  $(r+1)$ , which explicitly shows the effect on  $I_g$  of nonzero dc/ac spectral power ratio  $r$ , this expression for  $I_g$  is otherwise identical to that provided elsewhere [1,37]. Both Equations (6) and (7) reduce to

$$I = (r+1) \left(\frac{v_p}{\pi}\right)^2 \left(\frac{1}{2\sigma^2}\right) , \quad (8)$$

where  $\sigma$  is the standard deviation in the respective spectrum (i.e., in Gaussian-distributed clutter,  $\sigma = \sigma_g = 1/(\sqrt{2}g)$ ; in exponentially distributed clutter,  $\sigma = \sigma_\beta = (\sqrt{2}/\beta)$ ).

#### 4.4.4 Numerical Examples

It is evident from Equations (6), (7), and (8) that  $I$  obtained in Gaussian clutter exceeds that obtained in exponential clutter by a decibel amount given by

$$10 \log_{10}(I_g/I_\beta) = 10 \log_{10}(4g/\beta^2) = 10 \log_{10}(\sigma_\beta/\sigma_g)^2, \quad (9)$$

assuming that the radar parameters  $\lambda$  and  $f_p$  and the clutter dc/ac ratio  $r$  are the same in both cases. As a numerical example, consider Barlow's [6] much-referenced Gaussian clutter spectrum under windy (20 mph) conditions for which  $g = 20$  (see Section 5.1.1). The value of  $\beta$  from the exponential clutter model of Section 2 for similar windy (15- to 30-mph) conditions is specified in Table 1 as  $\beta = 5.7$ . Applying Equation (9) using these clutter parameters shows that the single delay-line canceller improvement factor obtained in  $g = 20$  Gaussian clutter is 3.9 dB greater than that obtained in  $\beta = 5.7$  exponential clutter, independent of radar frequency and processing-specific parameters such as pulse repetition frequency. That is, the fact that exponential clutter spreads the clutter in Doppler beyond that of the more usually assumed Gaussian clutter results in a 3.9 dB loss in improvement factor. As further numerical examples, the actual values of  $I$  obtained by an X-band radar (i.e.,  $\lambda = 3$  cm) of  $f_p = 1000$  Hz operating in exponential or Gaussian clutter are shown in Tables 7 and 8 as computed from Equations (6) and (7), respectively. The exponential clutter for which Table 7 applies is that of the model of Equations (1), (2), (3) and Table 1 under various wind conditions. The Gaussian clutter for which Table 8 applies is that of Barlow with the further assumption that the dc/ac ratio (unspecified by Barlow) is given by Equation (3).

**Table 7.**  
**Improvement Factor  $I_\beta$  in Exponential Clutter**  
**for an X-Band Radar ( $\lambda = 3$  cm) with PRF = 1000 Hz**

Wind Speed (mph)	Exponential ac Spectral Shape Factor $\beta^a$	Ratio of dc/ac Spectral Power $r$ (dB) <sup>b</sup>	Single Delay-Line Canceller Improvement Factor $I_\beta$ (dB) <sup>c</sup>
5	12	4.0	34.6
10	8	-0.7	28.3
20	5.7	-5.4	23.8
40	4.3	-10.0	20.6
a. From Table 1 b. From Equation (3) c. From Equation (6)			

**Table 8.**  
**Improvement Factor  $I_g$  in Gaussian Clutter**  
**for an X-Band Radar ( $\lambda = 3$  cm) with PRF = 1000 Hz**

Wind Speed (mph)	Gaussian ac Spectral Shape Factor $g^a$	Ratio of dc/ac Spectral Power $r$ (dB) $^b$	Single Delay-Line Canceller Improvement Factor $I_g$ (dB) $^c$
20	20	-5.4	27.7
a. From Barlow [6], see Sec. 5.1.1 b. From Equation (3) c. From Equation (7)			

## 5. HISTORICAL REVIEW

### 5.1 THREE ANALYTIC SPECTRAL SHAPES

In comparing different analytic forms for the shape of the ac component of the windblown clutter Doppler velocity spectrum  $P_{ac}(\nu)$  [see Equation (1)], it is necessary to base the comparison on equivalent total ac spectral power, and it is convenient to maintain total ac spectral power at unity. Such normalization is seldom implemented in representations of clutter spectra. Figure 26 shows examples of the three forms for  $P_{ac}(\nu)$  to be discussed subsequently, namely Gaussian, power law, and exponential, in each of which  $\int_{-\infty}^{\infty} P_{ac}(\nu) d\nu = 1$ . As a result, the power density levels at any value  $\nu$  for these three spectral shapes as shown in Figure 26 are directly comparable on an equivalent total ac power basis.

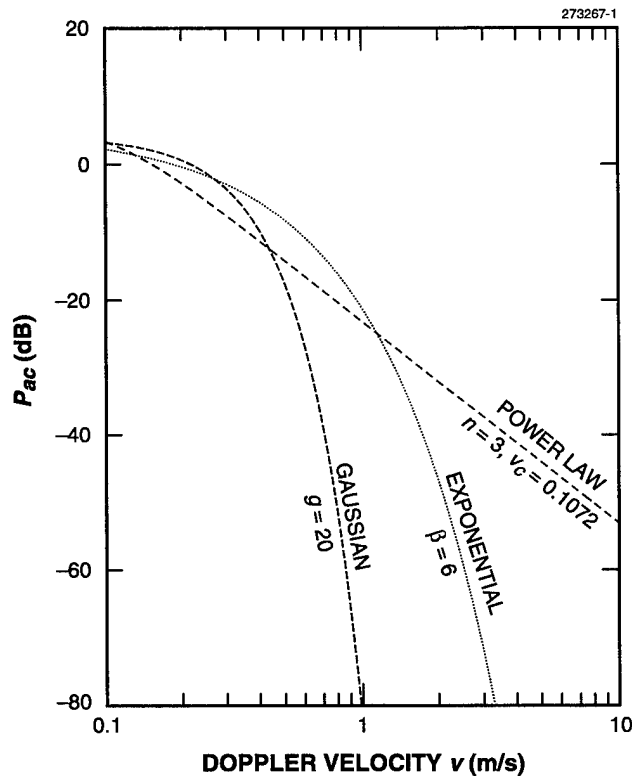


Figure 26. Three analytic spectral shapes, each normalized to unit spectral power.

The ac spectral shape function  $P_{ac}(\nu)$  may be decomposed as

$$P_{ac}(\nu) = K_{\eta} \cdot k_{\eta}(\nu) \quad (10)$$

where  $\eta$  is a shape parameter,  $K_{\eta}$  is a normalization constant set so that  $\int_{-\infty}^{\infty} P_{ac}(\nu) d\nu = 1$ , and  $k_{\eta}(\nu)$  is the unnormalized shape function with  $k_{\eta}(0) = 1$ . Often, historically,  $K_{\eta}$  is omitted and only  $k_{\eta}(\nu)$  is shown in plots such as Figure 26 with the zero-Doppler peak at 0 dB. In such cases, at best the shape parameter  $\eta$  of each individual spectral representation is all that remains for adjustment to equivalent total ac spectral power, where in fact it is the shape parameter that should be used to match to experimental data, or at worst (often the case) no attempt is made to compare spectra on an equivalent total ac spectral power basis at all. In short, in comparing different analytic spectral representations, it is not rigorously proper to simply set their zero-Doppler peaks each at unity (i.e., 0 dB).

It is evident in the examples shown in Figure 26 that spectral extent of the exponential representation lies between that of the Gaussian (narrow) and that of the power law (wide). The following subsections consider the origins of these three analytic expressions that have been used in the past to represent the shape of the Doppler frequency or velocity spectrum of windblown ground clutter, and in particular the rate of decay with increasing Doppler in the tail of the spectrum.

### 5.1.1 Gaussian Spectral Shape

Radar ground clutter power spectra were originally thought to be of approximately Gaussian shape [5–8]. The Gaussian spectral shape may be represented analytically as

$$P_{ac}(\nu) = \sqrt{\frac{g}{\pi}} \cdot \exp(-g\nu^2) , -\infty < \nu < \infty , \quad (11)$$

where  $g$  is the Gaussian shape parameter,  $K = \sqrt{g/\pi}$  is the normalization constant,  $k(\nu) = \exp(-g\nu^2)$ , and  $\int_{-\infty}^{\infty} P_{ac}(\nu) d\nu = 1$ . To convert to  $P_{ac}(f)$  in Equation (11) where  $f$  is Doppler frequency, i.e.,  $P_{ac}(f) df = P_{ac}(\nu) d\nu$ , replace  $\nu$  by  $f$  and  $g$  by  $(\lambda/2)^2 g$ . The standard deviation of the Gaussian spectrum of Equation (11) is given by  $\sigma_g = 1/(\sqrt{2g})$  in units of [m/s]. In a much-referenced [1,17,40] early paper, Barlow [6] presents measured L-band ground clutter power spectra approximated by the Gaussian shape to a level 20 dB below the peak zero-Doppler level and to a maximum Doppler velocity of 0.67 m/s. Figure 27 shows Barlow's ground clutter spectra  $k(\nu)$  as plotted originally, except here vs Doppler velocity  $\nu$  rather than Doppler frequency  $f$ . Recall that  $k(\nu)$  is the unnormalized ac shape function such that  $k(0) = 1$ , so the spectra plotted in Figure 27 are not shown on an equivalent total ac power basis.

Barlow's spectral results were obtained from radar envelope measurements as opposed to coherent processing. For a Gaussian-shaped spectrum, the width of the envelope spectrum is approximately 1.4 times the width of the coherent spectrum [41,42]. That is, in Equation (11),  $g_{\text{coherent}} \approx (1.4)^2 g_{\text{envelope}}$ . On this basis, estimates of the shapes of the coherent spectra corresponding to Barlow's envelope spectra are also shown in Figure 27. The resulting  $g = 20.036$  coherent-spectrum  $k(\nu)$  curve shown in Figure 27 for heavily wooded hills under 20 mph winds corresponds to the Gaussian  $g = 20$   $P_{ac}(\nu)$  curve shown in Figure 26.

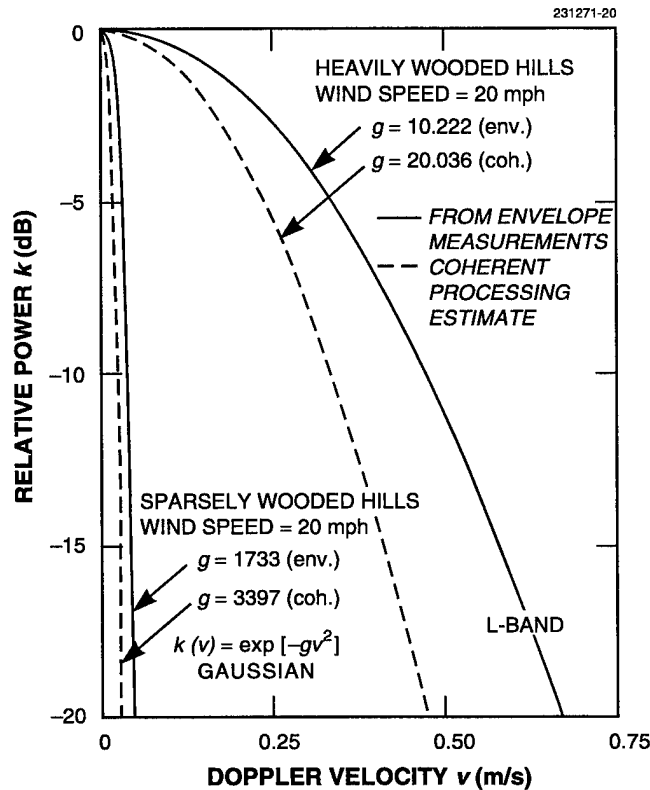


Figure 27. Measurements of radar ground clutter power spectra by Barlow [6], 1949

Early observations at the MIT Radiation Laboratory [7,8] were that the shapes of power spectra from precipitation, chaff, and sea echo were “roughly Gaussian” and that the shape of the spectrum from land clutter was “roughly similar” but with differences from Gaussian shape “somewhat more pronounced.” The explanation for clutter spectra of approximately Gaussian shape is loosely based on the idea that windblown vegetation consists fundamentally of a random array of elemental moving scatterers, each with a constant translational drift velocity. If the distribution of radial velocities of such a group of scatterers were roughly Gaussian, they would generate an approximately Gaussian-shaped power spectrum. However, consider if the motion of the scatterers also were to include an oscillatory component to represent branches and leaves blowing back and forth in the wind. It is well known [43] that simple harmonic angle modulation (frequency or phase) generates an infinite series of sidebands so that an array of oscillating scatterers would be expected to generate a wider spectrum than an array of scatterers each with only a constant drift velocity. Indeed, in 1967 Wong, Reed, and Kaprielian [34] provided an analysis of the scattered signal and power spectrum from an array of scatterers, each with random rotational (oscillatory) motion as well as a constant random drift velocity. Under assumptions of Gaussianly distributed drift and rotational velocities, Wong et al. [34] showed that the power spectrum of the scattered signal is the sum of six components. Li [20] recently provided further interpretation of these six components, as follows. If scatterer rotation is absent, the Wong



et al. expression for the clutter spectrum degenerates to Barlow's simple Gaussian expression, i.e., Equation (11). However, with scatterer rotation present, five additional Gaussian components arise, all of which decay more slowly and all but one of which are offset from zero-Doppler (by  $\pm 2$  and  $\pm 4$  times the rotational velocity). As a result, these five additional Gaussian terms that come into play with scatterer rotation act to "spread" the spectrum beyond that of the simple Gaussian of Equation (11). A recent paper [37] goes back to Wong's formulation of offset Gaussians in modeling some newly acquired X-band windblown clutter spectral measurements.

In 1965, two years before the publication of the Wong et al. paper [34], Bass, Bliokh, and Fuks [44] also provided a theoretical study of scattering from oscillating reradiators to model scattering from wind-blown vegetation. In the Bass et al. paper, the reradiators were modeled to be decaying oscillators randomly positioned on a planar surface. In their analysis, Bass et al. showed that the power spectrum of the scattered radiation from the oscillating reradiators consists of a doubly infinite sum of offset Gaussian functions, but when the reradiators do not oscillate, the power spectrum simplifies to a sum of simple non-offset Gaussians. It is evident that these results have some degree of similarity with those of Wong et al. [34] in that both represent the power spectrum from a group of oscillating random scatterers as sums of Gaussians, the peaks of which are offset from zero-Doppler, and for which the offsets collapse in the absence of oscillation.

Some years following both the Wong et al. [34] and the Bass et al. papers [44], Rosenbaum and Bowles [45] also derived theoretical expressions for windblown clutter spectra based on a physical model in which the backscattering was associated with random permittivity fluctuations superimposed on a lossy background slab. Again with overtones of similarity to both the Wong et al. and the Bass et al. analyses, Rosenbaum and Bowles modeled scatterer motion two ways, first, as a Gaussian process, and second, assuming scatterer motion to be quasi-harmonic, so that the scatterers behave as decaying simple-harmonic oscillators. It has been observed that the Rosenbaum and Bowles spectral results "are ... too complex for radar engineers to use in design practice" [20].

**Status (Gaussian Spectral Shape).** As will be shown, essentially all measurements of ground clutter spectra from 1967 on, with increased sensitivity compared with those of Barlow and the other early investigators, without exception show spectral shapes wider than Barlow's simple Gaussian in their tails. Also, as indicated in the preceding discussion, it had become theoretically well understood, also from 1965–67 on, that scatterer rotational and/or oscillatory motion generates spectra wider than Gaussian. Nevertheless, Barlow's simple Gaussian representation continues to be how clutter spectra are usually represented in radar system engineering, at least as a method of first-approach in representing effects of intrinsic clutter motion. Thus many of the standard radar system engineering and phenomenology textbooks continue to reference Barlow's early results [1,17,40]. Also, Nathanson [21] characterizes ground clutter spectral width in a scatter plot of data from many different sources in which the standard deviation of the best fit of each data source to a Gaussian shape is plotted vs wind velocity. Although it is stated in Nathanson that these results are not intended as a recommendation for the use of Gaussian spectral shape in any system design in which the detailed shape of the spectrum is of consequence, nevertheless Nathanson's results continue to be referenced as justification for the "common assumption ... " [3] that clutter spectral shape is Gaussian. This continuing representation is understandably based on reasons of simplicity, i.e., "the clutter spectrum is often modeled as Gaussian for convenience, but is usually more complex" [46], and analytic tractability, e.g., the Gaussian function is its own Fourier transform [41].

### 5.1.2 Power-Law Spectral Shape

MTI system performance predicted by the assumption of a Gaussian-shaped clutter spectrum was not achieved in practice. In a much referenced later report, Fishbein, Graveline, and Rittenbach [9] introduced the power-law clutter spectral shape. The power-law spectral shape may be generally represented analytically as

$$P_{ac}(v) = \frac{n \sin(\pi/n)}{2\pi v_c} \cdot \frac{1}{1 + \left[\frac{|v|}{v_c}\right]^n}, \quad -\infty < v < \infty. \quad (12)$$

Equation (12) has two power-law shape parameters— $n$ , the power-law exponent, and  $v_c$ , the break-point Doppler velocity where the shape function is 3 dB below its peak zero-Doppler level. The normalization constant  $K$  is equal to  $n \sin(\pi/n)/(2\pi v_c)$ ,  $k(v) = 1/[1 + (|v|/v_c)^n]$ , and  $\int_{-\infty}^{\infty} P_{ac}(v) dv = 1$ . To convert to  $P_{ac}(f)$  in Equation (12), i.e.,  $P_{ac}(f)df = P_{ac}(v) dv$ , replace  $v$  by  $f$  and  $v_c$  by  $f_c = (2/\lambda)v_c$ . For velocities  $v \gg v_c$ , Equation (12) simplifies to  $P_{ac}(v) = (K \cdot v_c^n) v^{-n}$ , which plots as a straight line in a plot of  $10 \log P_{ac}$  vs  $\log v$ . In such a plot,  $n$  defines the slope of the straight-line  $v^{-n}$  power-law spectral tail (slope = dB/decade =  $10n$ ). Because of its two shape parameters, the power-law shape function of Equation (12) has an additional degree of freedom for fitting experimental data compared with the single-parameter Gaussian and exponential shape functions of Equations (11) and (2), respectively. For any power of  $n$ , the power-law shape function may be made as narrow as desired by making  $v_c$  small enough. Still, whatever the values of  $n$  and  $v_c$ , ultimately at low enough power levels (i.e., as  $10 \log P \rightarrow -\infty$ ) the power-law shape always becomes wider than Gaussian or exponential.

Fishbein et al. [9] indicate that measured clutter rejection ratios up to 40 dB are matched under the assumption of a theoretical power-law spectral shape with  $n = 3$ . They also made one actual X-band clutter spectral measurement in 12 knot winds verifying that an  $n = 3$  spectral tail did exist down to a level 35 dB below the zero-Doppler level and out to a maximum Doppler velocity of 1.6 m/s. The graph of these results, shown in Figure 28, appears to very convincingly show the clutter spectrum to be an  $n = 3$  power law, as opposed to Gaussian, and it is widely referenced [17,21].

The Gaussian and power-law curves in Figure 28 are  $k(v)$  curves as originally presented by Fishbein et al. [9] with their zero-Doppler peaks at 0 dB. Such  $k(v)$  curves are generally not of equivalent total ac power. However, the particular Gaussian curve shown in Figure 28 is that resulting when its shape parameter  $g$  is adjusted to the necessary value, viz.,  $g = 46.875$ , to provide equivalent power (not unity) to that contained by the power-law curve of Figure 28. That is, the Gaussian curve in this figure did not arise from direct fitting to measured data. In contrast, Barlow's Gaussian curves of Figure 27 did arise from direct fitting to measured data. It is more fair to compare the Fishbein et al.  $n = 3$  power-law curve of Figure 28 with Barlow's  $g = 10$  and 20 Gaussian curves of Figure 27, all as  $P_{ac}$  curves normalized to unit total ac spectral power for whatever values of shape parameter were required to fit to measured data. The  $g = 20$  Gaussian curve and  $n = 3$ ,  $v_c = 0.1072$  power-law curve shown in Figure 26 are Barlow and Fishbein et al. curves, respectively, plotted as  $P_{ac}$  functions, each properly normalized to equivalent unit total ac spectral power. It is evident that Barlow's  $g = 20$  Gaussian curve would be considerably wider than (i.e., would lie to the right of) the  $g = 46.875$  Gaussian plotted in Figure 28, with the result that the data in Figure 28 become somewhat less convincingly power law.

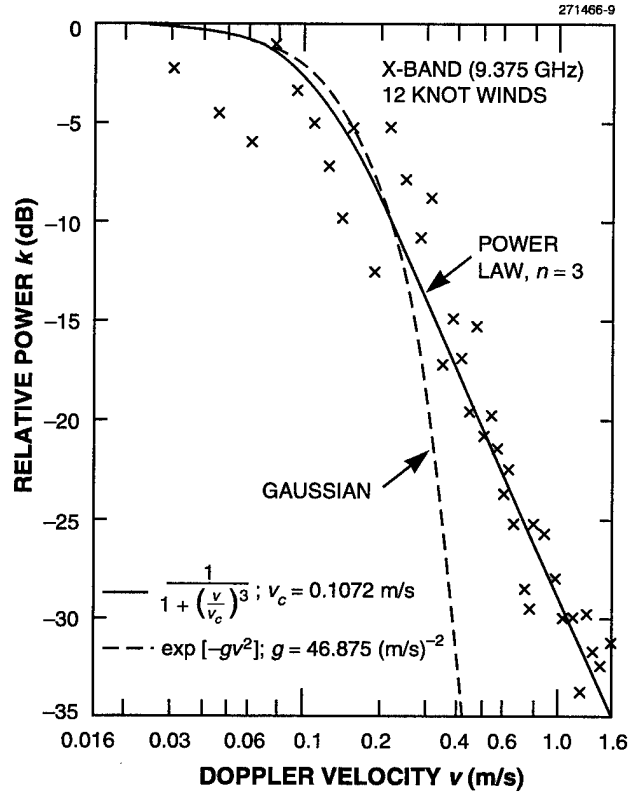


Figure 28. A measured radar ground clutter power spectrum by Fishbein et al. [9], 1967

The Fishbein et al. [9] results were important in establishing the existence of low-level tails wider than Gaussian in ground clutter spectra. Other ground clutter spectral measurements followed in which power-law spectral shapes were observed. For example, shortly after publication of the Fishbein et al. report, Warden and Wyndham [10] briefly mentioned two S-band measurements of clutter spectra, shown in Figure 29. The first was a clutter spectrum for a wooded hillside in 14 to 16 knot winds. The shape of this spectrum, to -29 dB at a maximum Doppler velocity of 0.82 m/s, is wider than Gaussian but narrower than an  $n = 3$  power law. The second was a clutter spectrum for a bare hill in 10 to 12 knot winds. This spectrum is slightly narrower than the first, although still wider than Gaussian in the tail. The authors concluded that an  $n = 3$  power law best fitted their data overall.

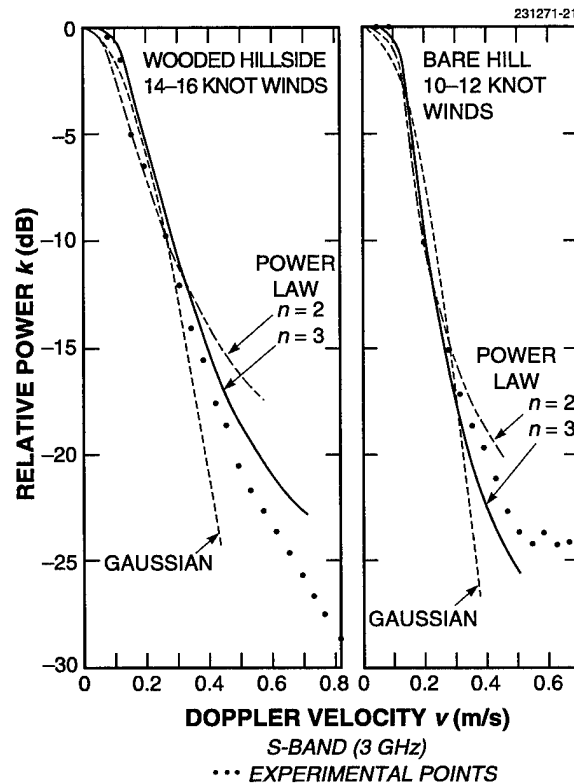


Figure 29. Two measurements of radar ground clutter power spectra by Warden and Wyndham [10], 1969.

Several years later, Currie, Dyer, and Hayes [11] provided measurements of noncoherent clutter spectra from deciduous trees under light air and breezy conditions over a spectral dynamic range of 20 dB at frequencies of 9.5, 16, 35, and 95 GHz. Over this limited spectral dynamic range, they also found their results to be well fitted with power laws of  $n = 3$  in the lower bands and  $n = 4$  at 95 GHz. At both 9.5 and 16.5 GHz, maximum spectral extents under breezy 6- to 15-mph winds at the -20-dB level were  $\sim 0.8$  m/s, which is a close match both to the Fishbein et al. results and to the Phase One and LCE measurements and exponential model (see Figure 1) of this report over similar spectral dynamic ranges and under similar breezy conditions—especially if the Currie et al. spectral widths are reduced by a factor of  $\sim 1.4$  to account for the fact that their measurements were noncoherent. At 35 and 95 GHz, maximum spectral extents under breezy conditions at the -20-dB level were  $\sim 0.5$  m/s, that is,  $\sim 40\%$  narrower than at their lower X- and K<sub>u</sub>-band frequencies. These narrower upper-band spectra appear to indicate that the frequency invariance, VHF to X-band, of Doppler-velocity ac spectral shape of the current exponential model may not extend to frequencies as high as 35 GHz (K<sub>a</sub>-band) and 95 GHz (W-band). The Currie et al. [11] results are also discussed in Appendix B of Long [17] and in Currie and Brown [18]; in the latter discussion, N.C. Currie remarks that “curve-fitting is an inexact science” and goes on to raise the possibility that other spectral shapes might also have been used to equally well fit these data.

A set of papers in the Russian literature [12–15] from the same time period included power law among various analytic representations used in fitting experimental data in different Doppler regimes. Results taken from these Russian papers are shown in Figures 30, 31, and 32. This, at the time, little-known series of Russian papers involving X-band windblown forest spectral measurements was first encountered when searching for earlier reports of exponential shape for windblown clutter power spectra [23]; they have since become better known [21]. In these Russian studies, spectral power was observed to decay at first according to Gaussian [12] or exponential [15] laws to spectral power levels down 10 to 20 dB from zero-Doppler. This initial region of decay was followed by subsequent power-law decay to lower levels and higher Doppler velocities. Spectral widths in these Russian measurements closely match those measured by the Phase One and LCE radars near their limits of sensitivity (down  $\approx 70$  dB).

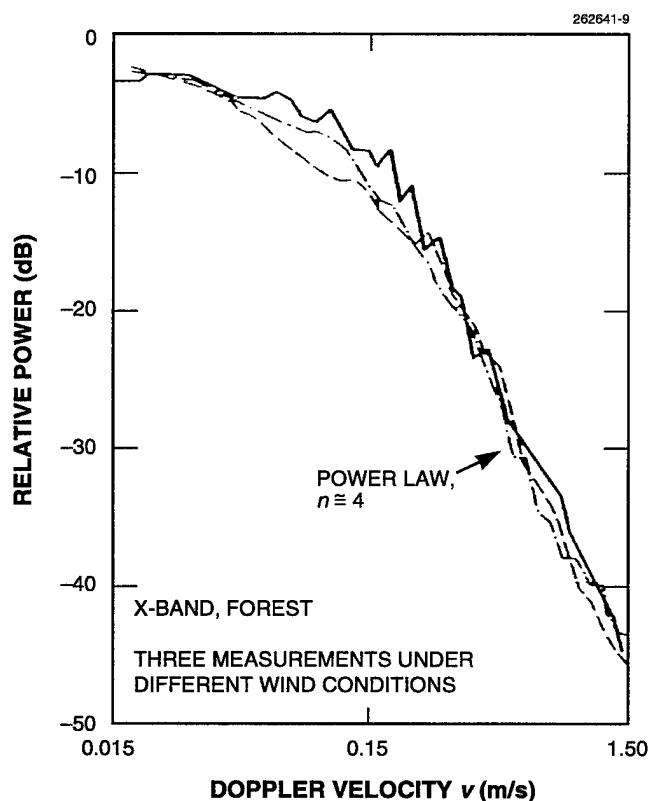


Figure 30. Measurements of radar ground clutter power spectra by Kapitanov et al. [12], 1973.

The Russian investigations included theoretical [12,13] as well as empirical characterizations of windblown clutter spectra. The theoretical studies concluded that shadowing effects (of background leaves and branches by those in the foreground under turbulent wind-induced motion) were important in determining the shapes of spectral tails, over and above oscillatory and rotational effects. A physical model of wind-blown vegetation was initially discussed by Kapitanov et al. [12], which included random oscillation of elementary reflectors (leaves, branches) causing phase fluctuation of returned signals and shadowing of some elementary reflectors by others causing amplitude fluctuation of returns. An expression for the clutter spectrum was obtained based on the correlation properties of the returned signals. This expression consisted

of four terms—the first dependent on the initial positions of the reflectors, the second representing the spectrum of the amplitude fluctuations, and the third describing the spectrum of the phase fluctuations; the fourth term was the convolution of the amplitude and phase fluctuations of the elementary signals and was said to determine “the behavior of the wings [i.e., tails] of the spectrum” [12]. It was believed in this study that the interaction of foliage with turbulent wind flow was beyond the scope of accurate mathematical description, so the authors resorted to experimental measurement of the oscillatory motion of branches in winds through photographic methods. These measurements of branch oscillatory motion led to the prediction of an  $n = 4$  power-law clutter spectral decay associated with phase fluctuation up to a Doppler velocity of  $\approx 0.5$  m/s, with a faster phase fluctuation-induced rate of decay expected at higher Doppler velocities. Since their measurements indicated an  $n = 4$  power-law decay to higher Doppler velocities (i.e., to 1.5 to 3 m/s near their system limits of  $-36$  to  $-40$  dB down from zero-Doppler peaks), they concluded that shadowing-induced amplitude fluctuation must have caused the  $n = 4$  power-law decay continuing to be observed beyond  $\approx 0.5$  m/s.

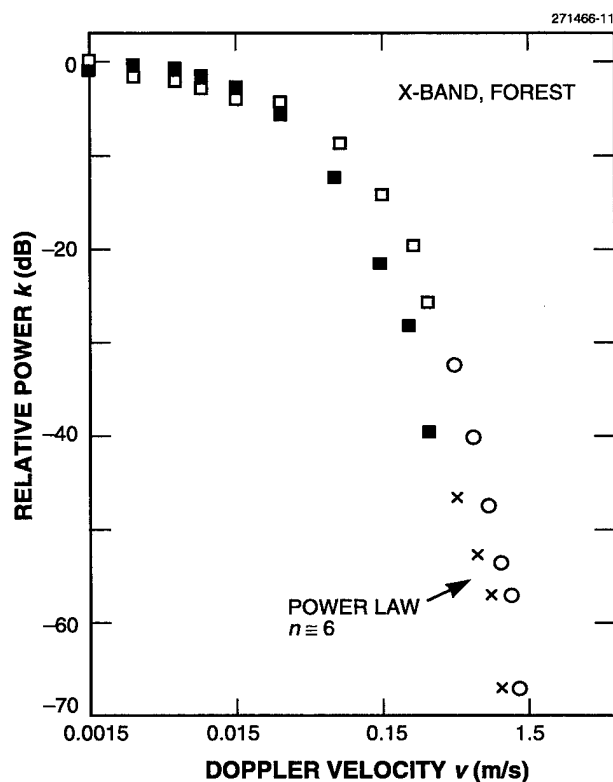


Figure 31. Measurements of radar ground clutter power spectra by Andrianov et al. [14], February 1976.

Armand et al. [13] further developed the Kapitanov et al. [12] physical model by assuming that the elemental scatterers at X-band were primarily leaves and modeling them as metal disks. These elemental scatterers introduced phase fluctuation in returned signals due to oscillatory motion, and amplitude fluctuation due to rotational motion and shadowing effects. A mathematical model of wind-induced scatterer motion including these effects was assumed. The resultant tail of the clutter spectrum was shown to be describable by a negative power series in Doppler frequency  $f$ , including both integer and fractional powers. In the absence of shadowing effects, this expression simplified considerably, leaving only a single dominant power-law term of  $n \cong 5.66$ . Since the authors observed experimental power-law spectral decay of  $n \cong 3$ , they also concluded that shadowing effects had to be at work in determining the shape and extent of wind-blown clutter spectral tails.

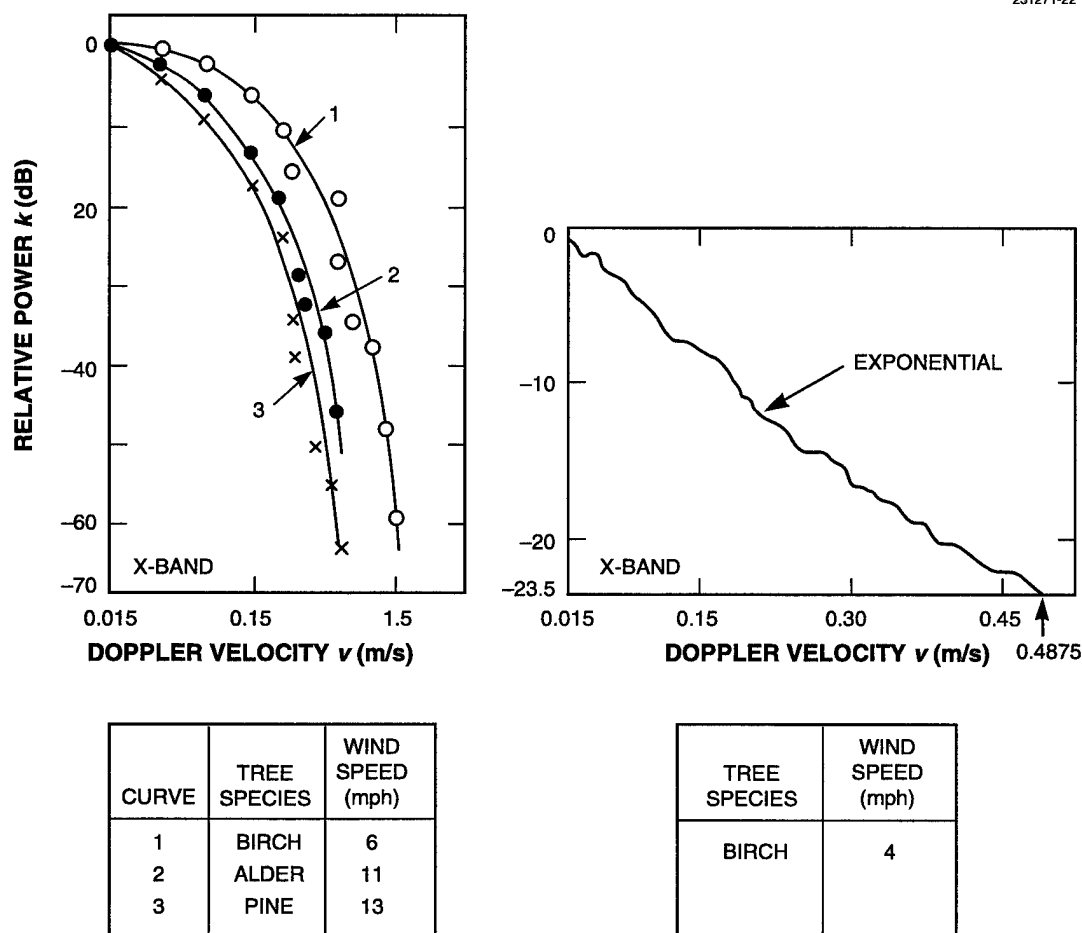
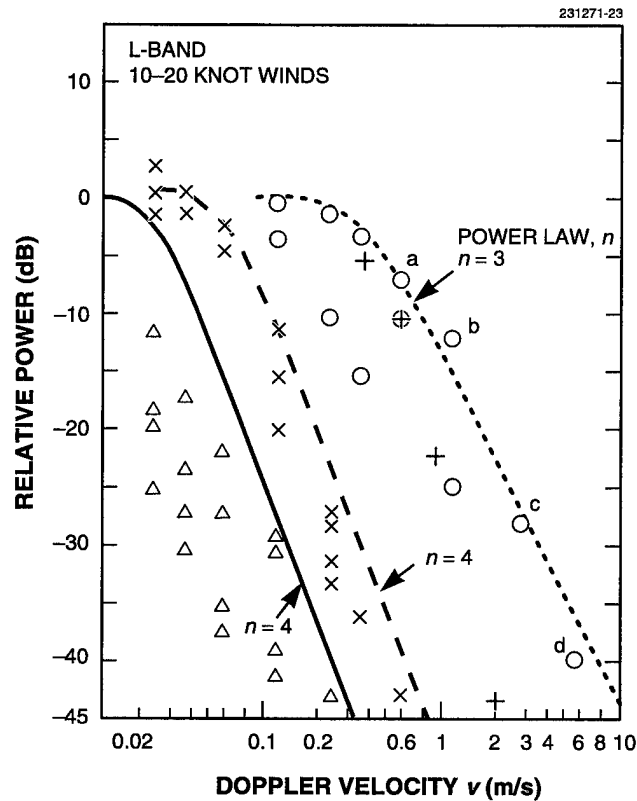


Figure 32. Measurements of radar ground clutter power spectra by Andrianov, Armand, and Kibardina [15], September 1976.

Other results in which power-law spectral decay was observed are those of Simkins, Vannicola, and Ryan [16]. These results were obtained in a clutter measurement task at L-band performed in support of the Seek Igloo radar development program directed toward implementation of minimally attended radar systems at Alaskan surveillance radar sites. These Seek Igloo measurements of ground clutter spectra are shown in Figure 33. In these results, power-law shapes with exponents  $n$  of 3 and 4 were attributed to the measured data which exist to levels 40 to 45 dB below the zero-Doppler peaks. In Figure 33, the “partially wooded hills” power law (given by  $n = 4$ ,  $v_c = 0.058$  m/s) provides spectral widths comparable with those measured by other investigators, but the “heavily wooded valley” power law (given by  $n = 3$ ,  $v_c = 0.34$  m/s) for which the bounding envelope is shown to reach 10.6 m/s at the -45-dB point provides spectral widths very much wider than any other known ground clutter spectral measurement at equivalent spectral power levels. The particular four points in the “heavily wooded valley” data that show excessive spectral width for windblown forest in 20 knot winds are indicated as a, b, c, and d in Figure 33 and labeled ANOMALOUS, by which is meant that they deviate from the general rule as determined by the vast preponderance of other reported measurements in the literature of the subject. The position of the widest Lincoln LCE-measured clutter spectrum is also shown in Figure 33 for comparison. These Seek Igloo results were subsequently extrapolated as  $n = 3$  and  $n = 4$  power laws to lower levels in clutter models for new radar system procurement.

In the 1980s, several research institutes in China investigated backscattering power spectra from windblown vegetation in various microwave radar bands, including X, S, and L [19,20]. In all plots presented, spectral dynamic ranges were  $\leq 30$  dB below zero-Doppler peaks. The focus of interest in these Chinese investigations was on the fact that power spectra from windblown vegetation over such limited spectral dynamic ranges are typically well approximated by power laws, but that no simple physical model or underlying fundamental principle is known that requires spectral shapes to be of power-law form. Thus they wished to bring the power-law basis for spectral decay into better understanding and onto firmer theoretical footing. Jiankang, Zhongzhi, and Zhong [19] presented a first-principles theoretical model for backscattering from vegetation to represent the intrinsic motion or time variation of  $\sigma^\circ$  that occurs in microwave surface remote sensing. This model was based on representing the vegetation as a random medium in which the dielectric constant varied with space and time. A general formulation for the backscattering power spectrum was obtained based on the assumed leaf velocity distribution. Assumptions that the wind was an impulse function and that the leaves were Rayleigh-distributed elemental masses led to a leaf velocity distribution that was shown to be closely similar in form (but not exactly equal) to an  $n = 3$  power law. However, the resulting backscattering power spectrum was of “quite complex form” [19]. Its numerical evaluation and comparison with three measured spectra indicated  $n = 3$  power-law spectral decay over spectral dynamic ranges reaching 30 dB down from zero-Doppler peaks. A further assumption restricting the originally specified elliptic spatial distribution of leaf motion to motion only along the wind direction reduced the complex expression for backscattering power spectrum to the same  $n = 3$  quasi-power-law form as the leaf velocity distribution. This expression was compared with the Fishbein  $n = 3$  power-law results and found to be in good agreement. The authors concluded by claiming that their model provides a theoretical basis for power-law spectral decay, and in addition allows generalization of parametric effects such as wind speed on spectral shape. What their model appears to show is that a theoretical  $n = 3$  quasi-power-law distribution of leaf velocities results in similar  $n = 3$  quasi-power-law clutter spectral shapes.





MEASUREMENTS	MODELS
MOUNTAINS $\Delta$	————
PARTIALLY WOODED HILLS $\times$	- - - -
HEAVILY WOODED VALLEYS (Lowlands) $\circ$	.....
a, b, c, d: ANOMALOUS	
$+$ : WIDEST LINCOLN MEASUREMENT	

Figure 33. Measurements of radar ground clutter power spectra by Simkins et al. [16], 1977.

In a later paper, Li [20] summarized L-band investigations at the Chinese Airforce Radar Institute to characterize Doppler spectra from windblown vegetation to improve design and performance of MTI and MTD (moving target detector) clutter filters. According to Li, the common position reached by Chinese researchers from several research institutes in China was that the radar land clutter spectrum could be represented as a power law with  $n$  ranging from  $< 2$  to  $> 3$ , but that no direct physical explanation for the power-law spectral shape was available in published papers. To help provide such an explanation, Li started with the complex theoretical formulation for the power spectrum from an assemblage of randomly translating and rotating scatterers expressed as a sum of offset Gaussian functions as derived much earlier by Wong et al. [34], and argued heuristically that the rotational components that spread the spectrum

resulted in power-law spectral shapes. To illustrate this hypothesis, Li numerically evaluated Wong's expression for three different cases in which Wong's statistical parameters were changed to ostensibly show effects of varying wind speed, and two different cases in which the statistical parameters were changed to ostensibly show effects of changing radar frequency. For all five cases, Li showed that the changing spectral shapes resulting from such parameter variations in Wong's formula could be well tracked by changing  $n$  in a simple power-law approximation. All such comparisons were shown over spectral dynamic ranges reaching 30 dB below zero-Doppler peaks. Li finally showed that two of his power-law approximations closely fit, respectively, two spectral measurements taken from the much earlier Rosenbaum and Bowles paper [45]. These two measurements were at UHF and L-band and were available to Rosenbaum and Bowles (who were Lincoln Laboratory investigators) from a 1972-era Lincoln Laboratory clutter spectral measurement program [47] to be discussed later. Li selectively showed the Rosenbaum and Bowles data only over upper ranges of spectral power (i.e., to -30 dB and -20 dB, respectively, or only over about one-half the spectral dynamic ranges of the original data), and Li also converted the Rosenbaum and Bowles data from a logarithmic to a linear Doppler frequency axis. Li's resulting plots show results, including both Rosenbaum and Bowles' experimental data and the power-law approximations to them, that are very linear on  $10 \log P$  vs  $f$  axes, that is, all would be reasonably matched with exponential functions, although Li matched them with power-law functions.

Recent measurements of decorrelation times [35], bistatic scattering patterns [36], and power spectra [37] of continuous-wave X-band backscatter from windblown trees were obtained by Narayanan and others at the University of Nebraska. These measurements were of individual trees (1.8-m-diameter illumination spot size on the tree crown) of various species at very short ranges (e.g., 30 m). Radar system noise is evident in these spectral data at levels 35 to 45 dB below the zero-Doppler spectral peaks and for Doppler frequencies  $f$  corresponding to Doppler velocities  $v \leq \sim 1$  m/s [37]. Over these relatively limited spectral dynamic ranges and corresponding low Doppler velocities, many of the measured spectral data appear to closely follow power-law behavior (i.e., the spectral data are very linear as presented on  $10 \log P$  vs  $\log f$  axes), although this apparent near-power-law behavior was not commented upon in the paper. As with Li [20], the Narayanan et al. starting point in modeling these data was the Wong et al. [34] formulation of the power spectrum for a group of moving scatterers, each with random rotational as well as translational motion. As previously discussed, Wong's spectral result consists of six Gaussian terms of which four are offset from zero-Doppler. Wong's expression depends on three parameters, the standard deviation  $\sigma_d$  of the translational drift velocity components, and the mean  $\bar{\omega}_r$  and standard deviation  $\sigma_r$  of the rotational components. Thus in Wong's expression  $\sigma_d$  determines the spectral width of the central Gaussian peak at zero-Doppler arising just from translation;  $\bar{\omega}_r$  determines the locations of the four offset peaks at  $\pm 2\bar{\omega}_r$  and  $\pm 4\bar{\omega}_r$ , respectively; and  $\sigma_d$  and  $\sigma_r$  together determine the slower-decaying spectral widths of all five additional Gaussians (four offset and one not offset from zero-Doppler) arising from rotation. In modeling his measured power spectral data from windblown trees using Wong's theoretical expression, Narayanan postulated each of the three parameters  $\sigma_d$ ,  $\bar{\omega}_r$ , and  $\sigma_r$  to be linearly dependent on wind speed, and specified the coefficients of proportionality for each specifically by tree type based on least-squared fits to measured autocovariance data. Narayanan et al. also provided extensive conjectural discussion associating  $\sigma_d$  with branch translational motion and  $\bar{\omega}_r$  and  $\sigma_r$  with leaf/needle rotational motion, although their results do not appear to be dependent on the validity of these associations. In this manner Narayanan et al. arrived at a six-term Gaussian expression for the power spectrum from windblown trees based on three coefficients of

proportionality to wind speed for which the coefficients are empirically specified for six different species of trees. This expression provided reasonable matches to measured clutter spectral data from individual trees over spectral dynamic ranges reaching 35 to 45 dB below the zero-Doppler peaks. Narayanan et al. also derived an expression for the MTI improvement factor for a single delay-line canceller based on their six-term Gaussian expression for the clutter power spectrum from windblown vegetation, and provided numerical results showing significant degradation in tree-species-specific delay-line canceller performance using their six-term (i.e., with rotation) spectral expression compared with the corresponding single-Gaussian (i.e., without rotation) spectral expression. In both spectral and improvement factor results, there is considerable variation in these results between different tree species. These short-range small-spot-size deterministic results applicable to specific tree species are in major contradistinction to the Phase One and LCE statistical results, which are applicable to larger cells at longer ranges and over greater spectral dynamic ranges, each cell containing a number of trees, often of mixed species.

Even more recently, a limited set of preliminary coherent X-band measurements of ground clutter spectra were obtained by Ewell [22] utilizing a different Lincoln Laboratory radar unrelated to the Phase One and LCE radars. This radar ( $1^\circ$  beamwidth and  $1\text{-}\mu\text{s}$  pulsewidth) was not specifically designed for measuring very-low-Doppler clutter signals—e.g., it uses a cavity-stabilized klystron as the stable microwave oscillator, which is less stable at low Doppler frequencies than modern solid state oscillators. The available ac spectral dynamic range provided by this radar for measuring clutter signals at low Doppler offsets was  $\sim 40$  to 45 dB. Measurements were made of three desert terrain types at ranges for the most part from 3 to 12 km on three different measurement days under winds gusting from 9 to 12 mph. Results were provided for both circular and linear polarizations. Over the available  $\sim 40$ -dB spectral dynamic range these measured data appeared to follow power-law spectral shapes, although with occasional hints in the data of faster decay at lower levels. Table 9 shows the resulting power-law shape parameters, averaged over a number of measurements within each of the three terrain types. These three desert clutter spectral shapes are quite similar; that is, when each is normalized to equivalent unit spectral power as per Equation (12), and the set of three is plotted together, they form a relatively tight cluster to levels  $\sim 40$  dB down. For example, all three curves reach the  $-30$  dB level at  $v \cong 1$  m/s, which point is very closely matched by the  $\beta = 8$  exponential shape factor provided by the spectral model of Section 2 for similar breezy wind conditions (see Figure 1). Also included for comparison in Table 9 are Fishbein's original power-law spectral shape parameters. The Fishbein power law is wider than the three desert power laws in Table 9 (e.g., the Fishbein power law reaches the  $-30$  dB level at  $v = 1.7$  m/s), although part of the reason for the wider Fishbein data is that they were noncoherent. Besides corroborating gross spectral extents of Phase One and LCE clutter spectra measured at upper ranges of spectral power under breezy conditions, the results of Ewell's spectral measurements shown in Table 9 also tend to substantiate the Phase One and LCE findings that ac clutter spectral shape, at least to first-order, tends to be approximately independent of terrain type, and that clutter spectral shape tends to be largely independent of polarization.

**Table 9.**  
**Comparison of Ewell [22] and Fishbein [9]**  
**Power-Law Clutter Spectral Shape Parameters**

Clutter Spectrum	Power-Law Spectral Shape Parameters	
	$n$	$v_d(\text{m/s})$
Ewell [22] <sup>a</sup>		
1) Scrub/brush	4.1	0.11
2) Mountain slopes (sparse vegetation/rocks)	3.7	0.10
3) Low-growing cedar trees	3.3	0.07
Fishbein [9] <sup>b</sup>	3.0	0.11
a. Spectral shape parameters shown are valid for approximating clutter spectra over ac spectral dynamic ranges reaching ~40 to 45 dB down from the zero-Doppler peak. b. Valid to ~ 35 dB down		

**Status (Power-Law Spectral Shape).** Many measurements of windblown clutter spectra that have been and continue to be obtained following the very early measurements of Barlow and others provide spectral dynamic ranges typically reaching  $\approx 30$  or  $\approx 40$  dB below zero-Doppler peaks. Such measurements, as reviewed in the preceding discussion, provide clutter spectral shapes that are frequently well represented as power laws. In contrast to the Gaussian spectral shape which theoretically arises from a random group of scatterers each of constant translational drift velocity, there is no simple physical model or fundamental underlying reason requiring clutter spectral shapes to be power law. All theoretical investigations of clutter spectra based on physical models that include oscillation and/or rotation in addition to translation of clutter elements provide expressions for clutter spectra that are to greater or lesser degree of complex mathematical form [13,19,30,34,44,45], although one such expression [13] is derived to be a negative power series in  $f$  (i.e., as a sum of elemental power laws) which at least does have a general power law-like behavior. Because the preponderance of the empirical evidence in spectral measurements to levels 30 or 40 dB down from zero-Doppler peaks has been for simple power-law spectral shapes, there has been some motivation by theoreticians either to reduce an initially derived complex formulation for clutter spectral shape to a simpler, approximately power-law formulation [19]; or to show that numerical evaluation of the complex formulation provides results that closely match a simple power law [20]. However, the evidence that clutter spectra have power-law shapes over spectral dynamic ranges reaching 30 to 40 dB below zero-Doppler peaks is essentially empirical, not theoretical.

### 5.1.3 Exponential Spectral Shape

Phase One [23] and LCE [32] ground clutter spectral measurements to levels 60 to 80 dB down indicate that the shapes of the spectra decay at rates often close to exponential. The two-sided exponential spectral shape is given by Equation (2), repeated here as:

$$P_{ac}(v) = \frac{\beta}{2} \cdot \exp(-\beta|v|) \quad , -\infty < v < \infty \quad , \quad (2)$$

where  $\beta$  is the exponential shape parameter,  $K = \beta/2$  is the normalization constant,  $k(v) = \exp(-\beta|v|)$ , and  $\int_{-\infty}^{\infty} P_{ac}(v) dv = 1$ . To convert to  $P_{ac}(f)$  in Equation (2), i.e.,  $P_{ac}(f)df = P_{ac}(v)dv$ , replace  $v$  by  $f$  and  $\beta$  by  $(\lambda/2)\beta$ . The standard deviation of the exponential spectrum of Equation (2) is given by  $\sigma_\beta = \sqrt{2}/\beta$  in units of [m/s]. The exponential shape is wider than Gaussian, but in the limit much narrower than power law, whatever the value of the power-law exponent  $n$ . Like the Gaussian, the exponential is simple and analytically tractable. For example, the Fourier transform of the exponential function is a power-law function of power-law exponent  $n = 2$  [7,41]. The exponential shape is easy to observe as a linear relationship in a plot of  $10 \log P_{ac}$  vs  $v$ . Figure 20 shows four cases of measured Phase One and LCE spectra that are remarkably close to exponential over most of their Doppler extents, and other examples of Phase One and LCE exponential or quasi-exponential clutter spectral decay are provided throughout this report. There is no known underlying fundamental physical principle requiring clutter spectra to be of exponential shape. Rather, the exponential shape is a convenient analytic envelope approximating the shapes of many of the Phase One and LCE measurements to levels 60 to 80 dB down.

In Equation (2), the independent variable  $v$  may itself be raised to a power, say  $n$ , as:  $\exp(-\beta|v|^n)$  to provide an additional degree of freedom in curve-fitting to measured data. When  $n > 1$ , this results in convex-from-above spectral shapes on  $10 \log P$  vs  $v$  axes, that is, in shapes that decay faster than exponential (e.g., when  $n = 2$  the shape becomes Gaussian). On the other hand,  $n < 1$  (i.e., fractional) results in concave-from-above spectral shapes on  $10 \log P$  vs  $v$  axes, which is the direction away from purely exponential that some of the measured Phase One and LCE spectra tend towards, especially at lower wind speeds. This idea of providing a more complex exponential-like expression to possibly enable improved curve-fitting capability to particular empirical data sets is not further pursued in this report since the simple exponential form (i.e.,  $n = 1$ ) satisfactorily captures the general shapes and trends in the data.

The Phase One data are shared with the Canadian government. Chan of Defence Research Establishment Ottawa (DREO) has issued a report [24] and subsequent paper [27] on the spectral characteristics of ground clutter as determined largely from his investigations of the Phase One data, but also including measured ground clutter spectra from a DREO rooftop S-band phased-array radar. Figure 34 shows some of Chan's results, taken from his report [24]. In the main, Chan's results agree with those of Lincoln Laboratory. In arriving at these results, Chan used a different set of the Phase One data than the long-time-dwell experiments used at Lincoln Laboratory in spectral processing. That is, in order to obtain a larger set of measurements, Chan used "repeat sector" Phase One data [25] which provided more spatial cells but shorter dwells, and performed maximum entropy spectral estimation on these data to obtain the necessary spectral resolution. Thus with different data, different processing, and, in the case of the DREO phased-array instrumentation, a different radar, Chan also arrived at exponential spectral decay for what he calls the "slow-diffuse" component of the ground clutter spectrum. Indeed, the spectra from the DREO radar shown in Figure 34 do appear for the most part to be highly exponential in spectral shape.

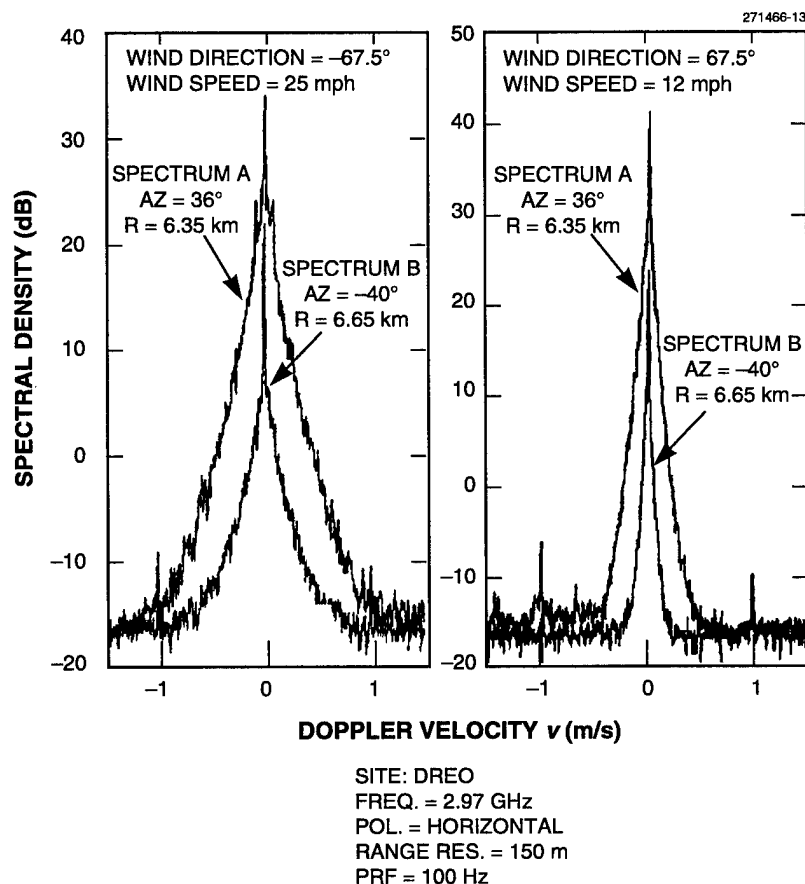


Figure 34. Measurements of radar ground clutter power spectra by Chan [24], 1989.

The Phase One clutter data were also made available to the government of the United Kingdom. Some U.K. clutter spectral results taken from Sarno [28] for the Phase One prairie rangeland site of Wainwright, Alberta, are shown in Figure 35. At Wainwright, the clutter sector was at  $\approx 2$ -km range and consisted of patches of trees (45-ft high aspen) and patches of shrubs (15-ft high willow) separated by open areas of herbaceous (grassy) rangeland. The open areas constituted about 14% of the total area in the clutter sector. The spectra in Figure 35 are each averaged over 76 contiguous 15-m range gates, one FFT per gate, at VV-pol. These Wainwright measurements were performed in late March/early April 1984 under late winter/early spring conditions before deciduous leaf emergence. More descriptive information of the Wainwright site is available in Billingsley and Larrabee [25]. Sarno's Wainwright spectra shown in Figure 35 are much narrower than normally observed in the Phase One and LCE data bases of clutter spectral measurements, particularly at X- and S-bands. A significant dc component exists in these spectra, presumably largely the result of geometrically visible open ground occurring between the patches of trees and shrubs. "Shoulders" are also evident in the spectral shapes at the onset of the ac spreading just at the base of the dc spikes. Such shoulders in spectral shape have been associated with the natural resonant frequency of the trees [47]. Beyond these shoulders, the rates of decay over the ac spectral tail regions in the spectra of Figure 35 are highly exponential (very linear as shown on  $10 \log P$  vs  $v$  axes). Often spectra as narrow as the S- and X-band spectra of Figure 35 in the Phase One and LCE spectral measurement data base are less well approximated as exponential (they have somewhat increased spreading compared with rigorous exponential shapes) than those of Figure 35 (but see also Chan's narrow exponential spectra in Figure 34).

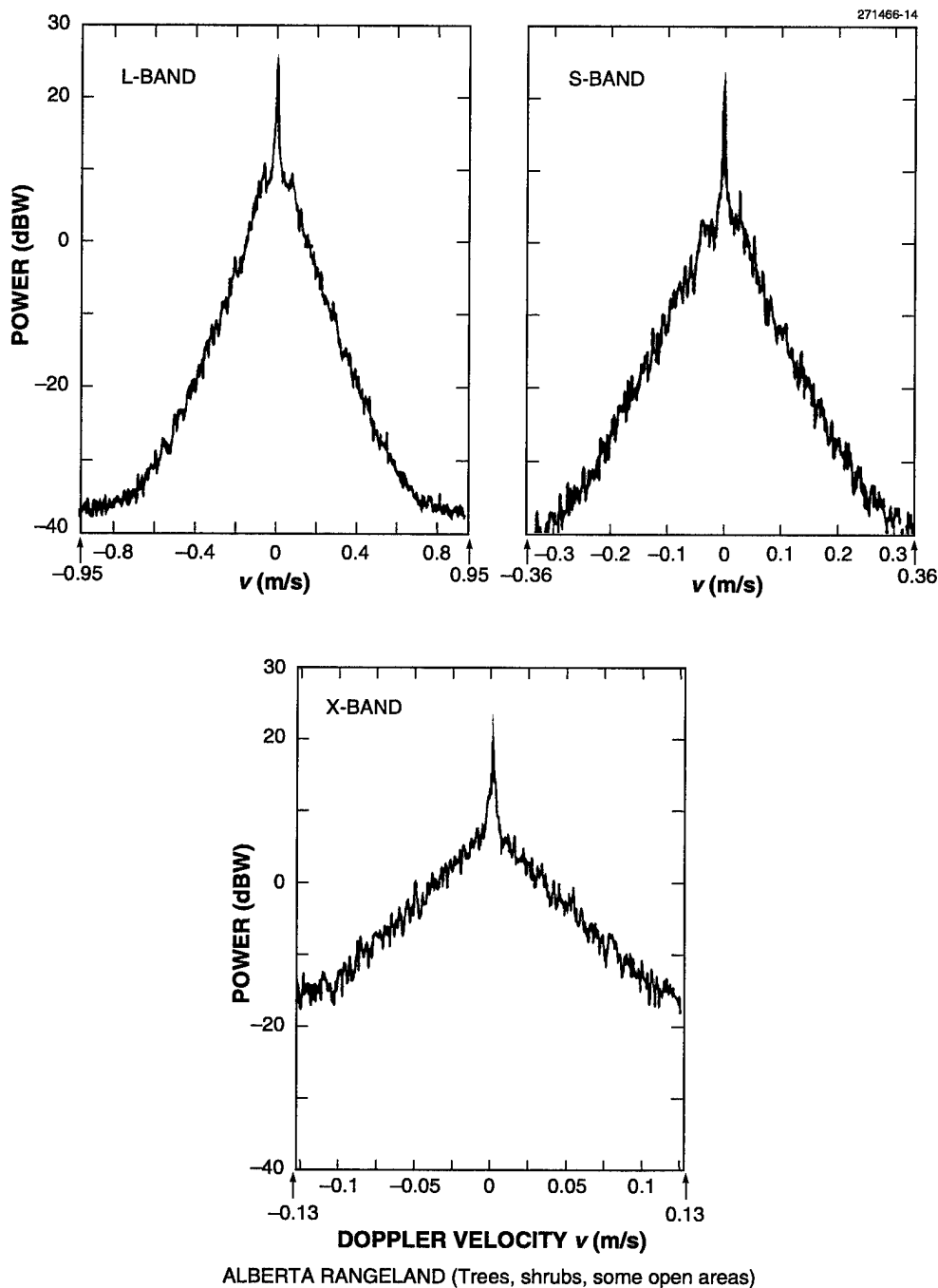


Figure 35. Phase One ground clutter spectra from Wainwright, Alta. (tree- and shrub-covered prairie rangeland, partially open) as processed by Sarno [28], 1991.

Sarno's Wainwright spectra were essentially reproduced at Lincoln Laboratory over all five Phase One frequency bands using different processing as shown in Figure 36. These spectra are averaged over the same 76 range gates as in the Sarno data, but also include averaging of a number of FFTs per gate (15, 5, 3, 1, and 1 FFTs averaged at X-, S-, L-, UHF, and VHF bands, respectively). The L-, S-, and X-bands spectra

of Figure 36 are very similar to Sarno's results, remaining very narrow and very exponential. The UHF and VHF spectra are very reminiscent of LCE desert spectral measurements on windy days (strong dc spike rising out of pronounced spectral shoulders) and quiet days (no spectral spreading whatsoever), respectively. Modeling information to approximate the spectra as exponential is provided in Table 10. It is apparent in Figure 36 and Table 10 that these Wainwright spectra are generally narrower and at S- and X-bands contain more modeled dc spectral power than predicted by the exponential clutter model of Section 2, although these data still retain a strong dependency of spectral width on wind speed. At Wainwright, the wind speed data were obtained at the radar location on an open hilltop about 100 feet higher than the measurement sector. One contributing factor to the narrowness of the Wainwright spectra, particularly at S- and X-bands, is that measurement sector wind speeds could have been considerably lower than those on the hilltop.

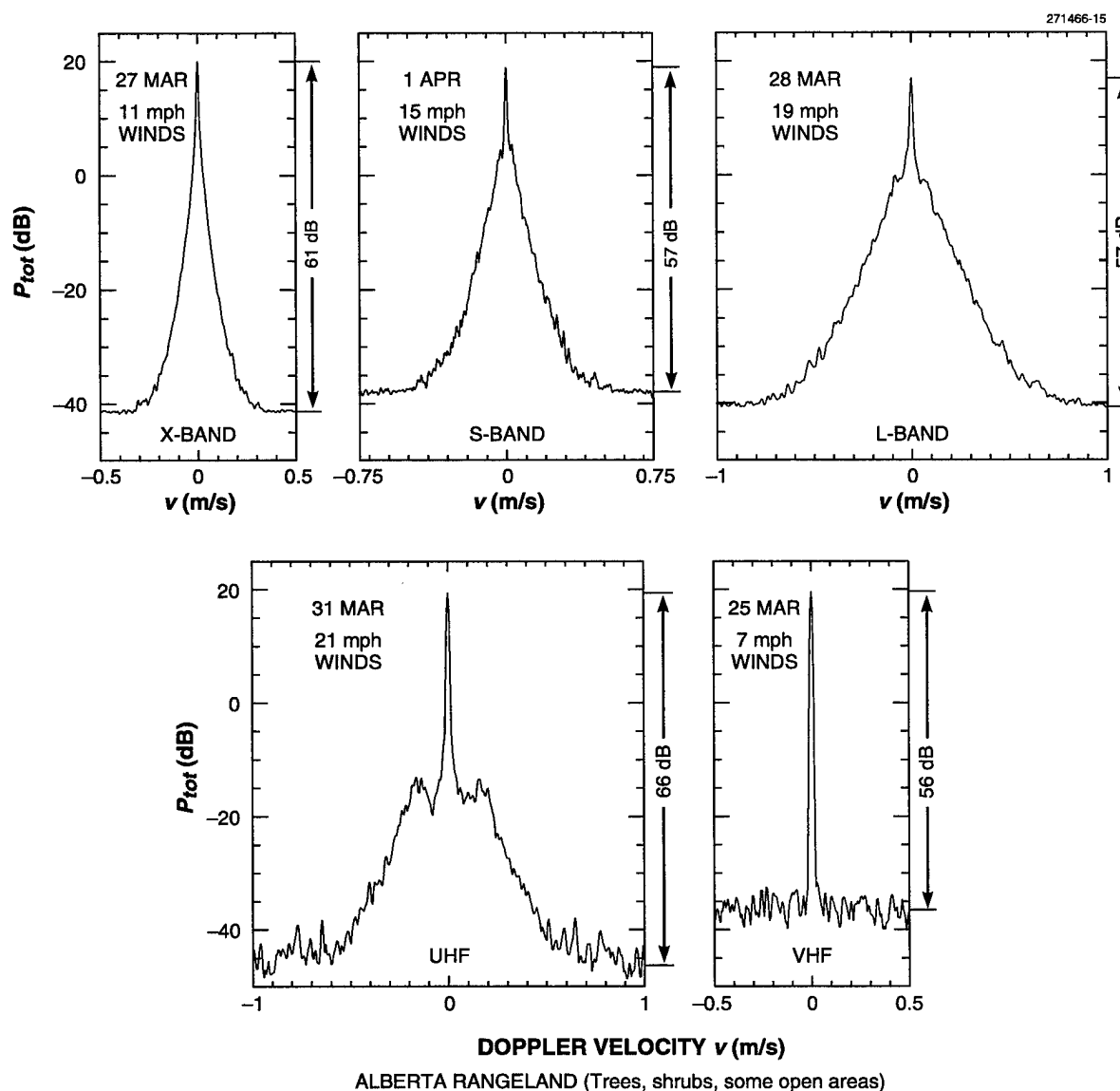


Figure 36. Phase One ground clutter spectra from Wainwright, Alta. (tree- and shrub-covered prairie rangeland, partially open) as processed at Lincoln Laboratory.



**Table 10.**  
**Exponential Approximations to Wainwright Clutter Spectra**

Frequency	Date Measured (1984)	Wind Speed, Radar Hilltop Location (mph)	Exponential ac Shape Parameter $\beta$	dc/ac Ratio $r$ (dB)	
				Measured (Direct Time-Domain Computation)	Modeled (Excess Quasi-dc Power in dc Delta Function Term)
X-band	27 Mar	11	34	3.6	19.3
S-band	1 Apr	15	25	0.5	10.6
L-band	28 Mar	19	17	1.8	6.5
UHF	31 Mar	21	17	14.4	15.1
VHF	25 Mar	7	—	24.8	—

The empirical observations of exponential decay in the Phase One and LCE clutter spectra recently motivated White [30] to develop a new first-principles physical model for radar backscatter from moving vegetation that also provides exponential spectral decay to conform in this respect with the experimental evidence. White's model assumes that an important element of the scattering arises from the tree branches. The key feature of the model is the representation of each branch as a cantilever beam clamped at one end. Distributions of branch lengths is Gaussian. Distribution of branch angles with respect to horizontal is uniform over  $\pi$  radians. Scattering centers are distributed uniformly over an outer (specifiable) portion of each branch. A mathematical expression for the Doppler spectrum of the radar return from such an assemblage of branches under a distributed wind forcing function is derived. This expression is a complex five-part multiple integral requiring numerical evaluation. When numerically evaluated, the resultant Doppler spectrum is shown to very closely provide exponential decay with increasing Doppler frequency.

In addition, the sensitivity of White's exponential spectral shape to a number of his model assumptions was tested numerically. It was found that the exponential shape was not very sensitive to a number of underlying assumptions concerning the beam modes of oscillation, but much faster than exponential decay occurred when the beams were not clamped (i.e., simple translation), when a nondistributed wind force was used, and when branch lengths were uniformly (as opposed to Gaussianly) distributed. Besides this exponential spectral component arising from branch motion, the model also postulates a rectangular wideband background spectral component at lower power levels arising from leaf motion (see Section 5.2.3). Although White's main thrust was the development of a theoretical clutter spectral model, he also provided [30] a small amount of measured radar clutter spectral data acquired with a rooftop C-band radar at DRA/Malvern of spectral dynamic range reaching  $\approx 30$  to 40 dB below zero-

Doppler peaks. White concluded from curve-fitting studies comparing power-law with exponential approximations to his measured data that “... the exponential model is the better fit” [30].

Measured results very similar to those of Phase One and LCE but over less wide, 40- to 60-dB dynamic ranges were obtained in a much earlier set of Lincoln Laboratory measurements of ground clutter spectra at UHF and L-band [47]. Figure 37 shows a typical measured result—an averaged clutter spectrum from five different range cells—from this earlier Lincoln program. The data displayed on the log-doppler axis to the right show an increasing rate of downward curvature (convex from above) for  $v > 0.08$  m/s as in the LCE and Phase One measurements, and evidence of the dc component window-function limiting resolution for  $v < 0.08$  m/s. By coincidence, this early Lincoln program [47] of 1972 and the Russian X-band investigations [12] going forward in very nearly the same time period (1973) both developed first-principle physical models of clutter spectra from forest. In both studies, the tree was modeled as a mechanical resonator excited by a turbulent wind field of known spectral content. Both programs involved measurements of tree motion. In both programs, the spectral content of tree motion decayed at low frequencies below a resonance maximum according to an  $n = 5/3$  power law; at higher frequencies above the resonance maximum, the decay was faster. The slightly later (1974), largely theoretical paper by Lincoln Laboratory authors [45] concerning electromagnetic scattering from vegetative regions included three measured clutter spectra from this 1972-era Lincoln measurement program.

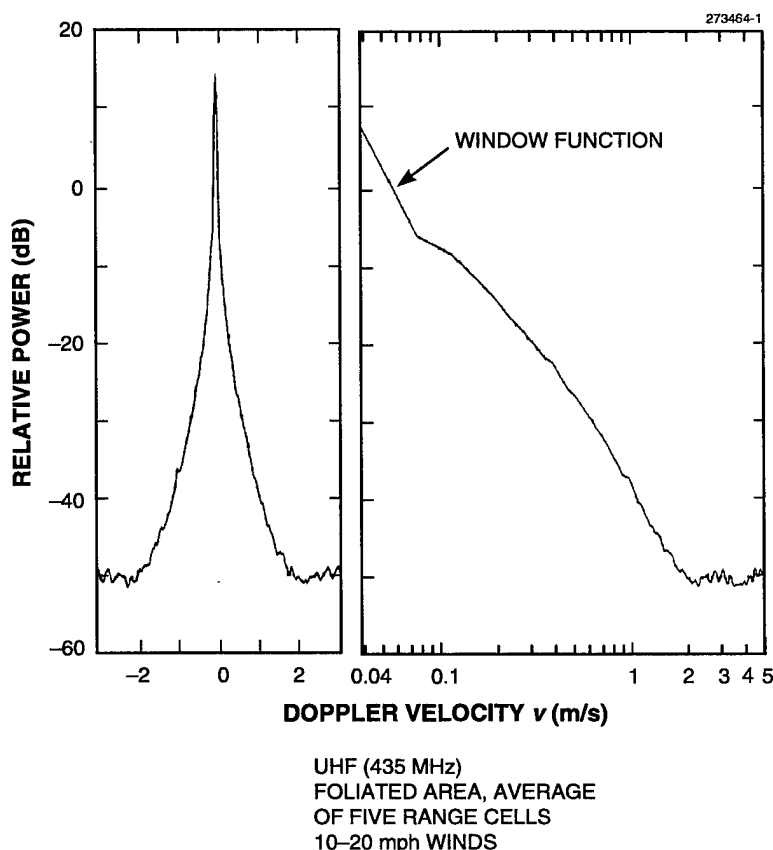


Figure 37. Measurements of radar ground clutter power spectra by Cartledge et al. [47], 1972.

Shoulders before the onset of faster decay such as those shown in some of the LCE- and Phase One-measured clutter spectra (Figures 17, 21, 23, 24, and 36; see also 34) are similar to those observed previously in the earlier Lincoln program [47] and explained as local resonance maxima associated with the natural resonant frequency of trees. In this program, the resonance shoulder was more pronounced at lower frequencies and lower wind speeds, and tended to diminish at higher frequencies and higher wind speeds. The reason is that, at lower wind speeds and longer wavelengths, the motion of the tree is a small fraction of a radar wavelength. Thus under these conditions the tree motion superimposes a phase modulation with low index of modulation, and as a result the clutter spectrum directly corresponds with that of the tree's physical motion. At higher frequencies and under stronger winds, the degree of phase modulation increases and the clutter spectrum no longer simply replicates that of the tree motion. These observations tend to be corroborated in LCE and Phase One results (see Figure 36). In addition, the LCE and Phase One data tend to have resonance shoulders to somewhat higher frequencies in measurements from partially open or open terrain (desert, farmland, rangeland) in which there is a significant dc component; the measurements from forested terrain tend to have distinct resonance shoulders only at the lower radar frequencies (VHF and UHF). The earlier Lincoln program also observed, in passing, that the shapes of some measured spectra beyond the resonance shoulder were highly exponential, but this observation was not elaborated upon.

It appears that the only other earlier explicit observation of exponential spectral shape is in the results of Andrianov, Armand, and Kibardina [15] (see Figure 32). In these results, exponential decay was observed 20 dB down from the maximum zero-Doppler level, followed by power law decay thereafter to -70 dB with reported values of  $n$  equal to 3.4, 3.8, and 5.6 for pine, alder, and birch, respectively. The equipment used was ostensibly of 70-dB dynamic range [14], although, to use their words translated to English, two dynamic range intervals were "sewn together" [15], as shown in Figure 31, to provide the full 70-dB range. In terms of gross spectral extent (e.g., 1.5 m/s, 70 dB down; 0.4 m/s, 20 dB down), these results of Andrianov et al. [14,15] fall closely within the range of measured LCE and Phase One spectral extents over similar spectral dynamic ranges. The earlier results of Kapitanov, Mel' nichuk, and Chernikov [12], as shown in Figure 30, were said to exhibit Gaussian decay down 10 to 15 dB, followed by power-law decay with  $n = 4$  down to -40 dB. The initial Gaussian decay was later stated to be erroneous by Andrianov et al. [15] because of early equipment limitations and that initial exponential decay as reported by them (see Figure 32) was more correct.

The exponent  $n$  of the power law is easy to estimate in measured spectral data as simply one-tenth the slope of the approximating straight line on  $10 \log P$  vs  $\log \nu$  axes in dB/decade. In Figure 32, the three measured spectral curves for pine, alder, and birch shown to the left do not exhibit decay anything like the quoted power-law slopes of  $n = 3.4$ , 3.8, and 5.6, respectively. These three curves are stated by the authors to be three particular examples of measured spectra, whereas their quoted values of  $n$  are averages over all measurements in which the value of  $n$  varies from 2.6 to 6.8. The rates of decay in the spectral tails of the data to the left in Figure 32 are much greater than any of these quoted values of  $n$ , and at least in qualitative appearance (increasing downward curvature) appear to be more exponential than power law. The data of Figure 31 appear to be more credibly of power-law behavior ( $n \approx 6$ ) in their tails, but the data plotted at the -68 dB level indicate slightly increasing curvature (rate of decay  $> n \approx 6$ ) at the lowest power levels shown. The data of Figure 30 closely match the  $n = 4$  power law attributed by the authors to these data.

Some confusion may arise because these Russian investigators [12-15] associate power-law shapes with lower ranges of spectral power in their measured data, whereas other investigators [9,10,16,19,20,22]

match their data to power-law shapes over upper ranges of spectral power. Measured clutter data in any particular regime of spectral power may be fitted with a power law, but the danger lies in extrapolating the power law beyond its regime of applicability.

**Status (Exponential Spectral Shape).** The significantly increasing rate of downward curvature (i.e., convex from above) observed in the general shapes of Phase One- and LCE-measured windblown ground clutter Doppler spectra on  $10 \log P$  vs  $\log \nu$  axes over spectral dynamic ranges reaching 60 to 80 dB below zero-Doppler peaks points to a general exponential characterization rather than a power-law characterization that plots linearly on such axes. Increasing rate of downward curvature in such plots has always been observed without exception in all measurements examined of clutter spectra from windblown trees and other vegetation under breezy or windy conditions taken from these extensive data bases. Other investigators [24,28] have corroborated that the exponential shape factor is generally representative of these data and is not the result of processing-specific particulars. Until recently, theoretical investigators have been attempting to reduce complex mathematical formulations of clutter spectra based on physical models incorporating oscillation and/or shadowing of elemental scatterers to simple power-law forms to conform with the experimental evidence at upper levels of spectral power (down 30 or 40 dB from zero-Doppler peaks). Only relatively recently with the increasing awareness of investigators of the Phase One and LCE spectral results has there been motivation to attempt to provide a theoretical basis for the observed exponential spectral shapes. Thus we have the interesting recent result of White [30] based on a physical model in which branches are represented as oscillating cantilever beams resulting in a formulation for the clutter Doppler spectrum, that, although mathematically complex, provides close to exponential decay under numerical evaluation. In addition, White observed that "the series solutions produced by Bass et al. [44], Armand et al. [13], and Wong et al. [34] probably have sufficient degrees of freedom to produce a function that would be a close approximation to ... exponential ..." [30]. Nevertheless, as for the power law for spectral dynamic ranges 30 to 40 dB down, the evidence of exponential clutter spectral shape for spectral dynamic ranges reaching 60 to 80 dB down is essentially empirical.

The only known measurements of windblown clutter spectra of spectral dynamic ranges equal to or exceeding those of the Phase One and LCE instruments are the Russian measurements of the 1970s [12-15] for which the results over lower ranges of spectral power were approximated as power laws. However, these results are power law only in a piece-part sense; the upper range of spectral power was concluded to be exponential. Hence these results are not very useful or analytically tractable, in that no single simple analytic function was provided to describe the complete clutter spectral shape over its full measured spectral dynamic range. Furthermore, little actual measurement data were shown in these papers, thus restricting possibilities for independent assessment of the data and conclusions by present-day readers.

Like the Gaussian function, the exponential function is simple and analytically tractable. The exponential function provides spectral shapes that are wider than Gaussian, as required by all the empirical evidence and by theoretical constructs involving oscillation, rotation, and shadowing of clutter elements; that are very much narrower at lower power levels (60 to 80 dB down) than extrapolations to lower levels of power-law representations of measurements accurate at higher levels of spectral power (30 to 40 dB down); and that are reasonably equivalent to the measurement data at high and low levels of spectral power.

### 5.1.4 Exponential vs Power Law

Figure 38 shows an LCE, VV-pol., windblown tree clutter spectrum measured on 11 September at Wachusett Mt. at range = 8.0 km. Also shown in the figure is the  $n = 3$ ,  $\nu_c = 0.1072$  power-law curve introduced by Fishbein et al. [9] to match their data as shown in Figure 28. This Fishbein power-law curve is shown dashed in Figure 38 to a level 35 dB down from the zero-Doppler peak, which is the region for which Fishbein et al. had data; at lower levels in Figure 38 the Fishbein power-law curve is shown dotted to indicate extrapolation. The LCE data in Figure 38 provide a remarkably close match to the Fishbein power-law curve at upper levels (viz., down 35 dB) over which Fishbein et al. had data. That is, these LCE spectral data confirm the historic Fishbein et al. spectral measurement [9] with modern measurement instrumentation. However, it is also very clear in Figure 38 that the Fishbein power-law curve cannot be extrapolated to lower levels. At lower levels the LCE measured spectrum in this figure decays much more rapidly than at upper levels.

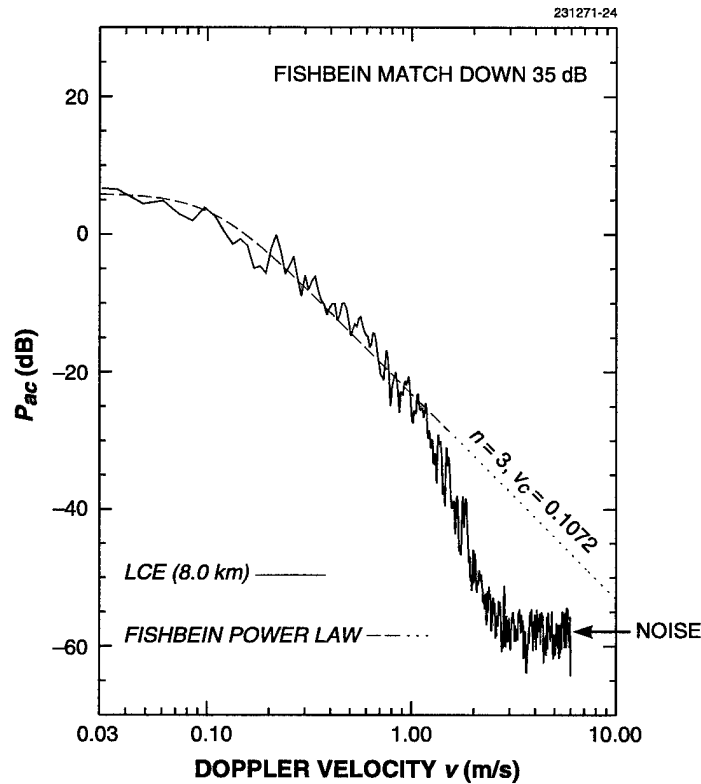


Figure 38. Comparison of an LCE windblown forest clutter spectrum with the Fishbein et al. power-law model [9].

Figure 20 shows measured LCE and Phase One clutter spectra as  $10 \log P_{tot}$  vs  $\nu$  from cells containing windblown trees on breezy and windy days. These results are among the widest windblown clutter spectra

measured by these instruments. In contrast with most of the other spectral measurements (historical and recent) discussed in Section 5.1, the measurements of Figure 20 over greater spectral dynamic ranges than were available in most of the other measurements have spectral shapes that are accurately representable as exponential. This accurate exponential representation is indicated by the good fits of the data to the straight lines drawn through the right sides of the spectra in Figure 20.

Figure 39 shows the right sides of Figures 20(a), (b), respectively, plotted as  $10 \log P_{tot}$  vs  $\log v$ . Recall that the power-law spectral shape [Equation (12)] plots as a straight line in the spectral tail region  $v \gg v_c$  using a log-Doppler velocity axis as in Figure 39. Certainly no single power-law straight line fits either of the spectral data traces in Figure 39, both of which exhibit strong downward curvature (convex from above) over their complete spectral extents. Even though the measurement data in Figure 39 exhibit strong downward curvature, a local power-law rate of decay can be defined for such data in a small Doppler interval  $\delta v$  as the value of power-law exponent  $n$  corresponding to the slope of the straight line tangent to the data curve in the region  $\delta v$ . The local power laws that thus fit the upper levels over historic dynamic range intervals in Figure 39 ( $n = 3$  or  $3.5$ ) cannot be extrapolated to lower levels. Much faster decaying local power laws ( $n = 7, 8$ , or  $10.5$ ) fit the lower levels.

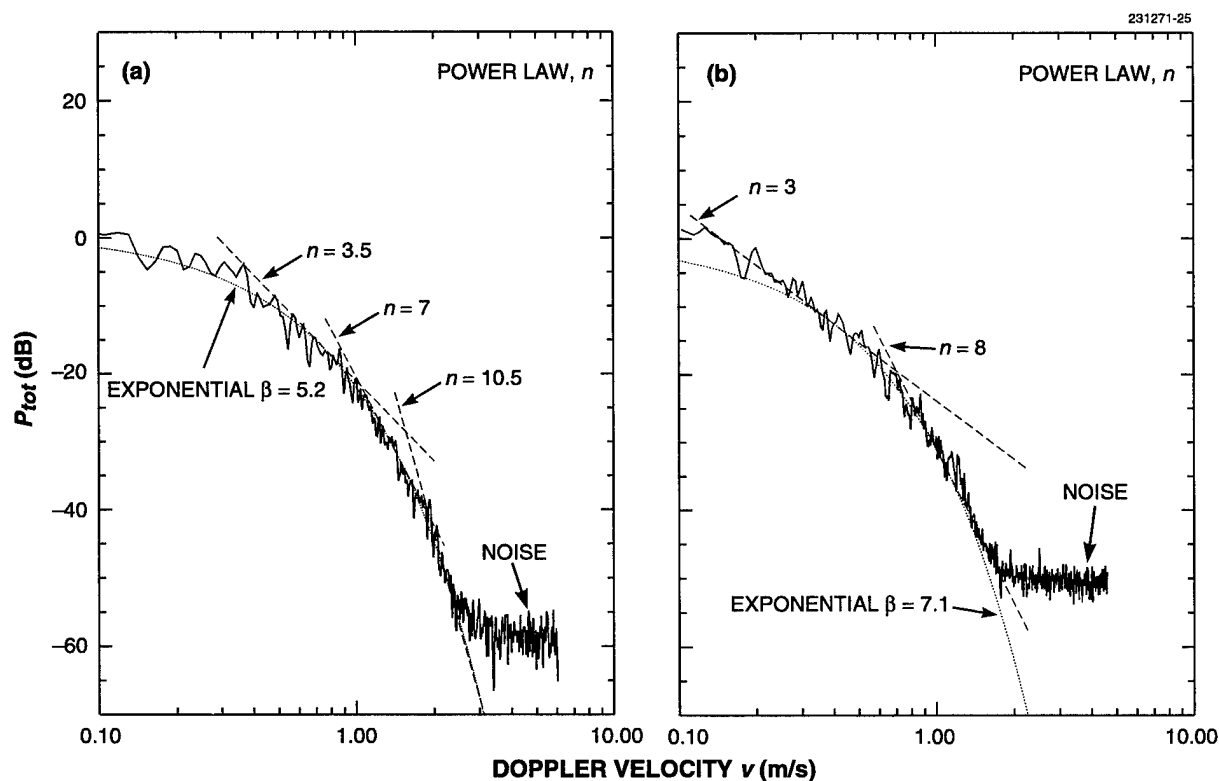


Figure 39. Two windblown forest clutter spectra for which exponential fits are compared with power-law fits: (a) LCE data, Wachusett Mt., 11 September 1991 and (b) Phase One (L-band) data, Katahdin Hill, 3 May 1985.

In both Figures 38 and 39, the more sensitive Phase One and LCE measurement instruments confirm measured rates of spectral power decay reported by other investigators at upper power levels, but in addition find that much faster local power-law rates of decay occur at lower power levels. Close examination of the spectral data in Figures 38 and 39 appear to indicate, in fact, two or more distinct rates of decay in the spectra, perhaps indicating different phenomenological regimes with different sets of scatterers and/or different mechanisms of scatter dominating at different spectral power levels. On the basis of these results it is not surprising that various early and recent investigators have characterized the rate of ground clutter spectral decay at relatively high spectral power levels (i.e., 35 to 45 dB down) as  $n = 3$  or  $n = 4$  power laws.

In Figure 39, exponential fits to the data are shown lightly dotted. The exponential shape  $\beta = 7.1$  closely fits the Phase One data of Figure 39(b) over its full ac spectral range away from its quasi-dc region (i.e.,  $|v| > \approx 0.2$  m/s), including both regions of local power-law fits; similarly, the exponential shape  $\beta = 5.2$  closely fits the LCE data of Figure 39(a) over its full ac range (i.e.,  $|v| > \approx 0.1$  m/s). In Figure 26, the exponential  $\beta = 6$  curve lying between Barlow's  $g = 20$  Gaussian curve and the Fishbein et al.  $n = 3$  power-law curve is now seen as reasonably representative of the data shown in Figure 39 from two different instruments at two different sites across more than six orders of magnitude of diminishing spectral power.

Figure 40 compares the  $\beta = 6$  exponential shape with  $v_c = 0.1$ ;  $n = 3, 4, 5$  power-law shapes both on  $10 \log P$  vs  $v$  axes [Figure 40(a)] and on  $10 \log P$  vs  $\log v$  axes [Figure 40(b)]. Each of the four spectral shapes shown is normalized to equivalent unit spectral power as per Equations (2) and (12). Figure 40(a) uses a linear Doppler velocity axis, making evident how all power-law shapes become slowly decaying at low levels of spectral power, whatever the value of  $n$ . Given that the maximum Doppler velocities observed in Phase One- and LCE-measured clutter spectra were in the 3- to 4-m/s range at levels 60 to 80 dB down, the power-law parameters  $v_c$  and  $n$  can certainly be adjusted to provide similar spectral extents at similar power levels. However, the resultant power-law shapes will not match Phase One- and LCE-measured data at higher levels of spectral power and will rapidly extrapolate to excessive spectral width at lower levels.

As plotted against the logarithmic Doppler velocity axis in Figure 40(b), the  $\beta = 6$  exponential shape demonstrates the increasing downward curvature (convex from above) with increasing Doppler velocity and decreasing power level that characterizes all the Phase One- and LCE-measured clutter spectra. In contrast, the power-law shapes in Figure 40(b) have little curvature. That is, on  $10 \log P$  vs  $\log v$  axes, power-law shapes are asymptotic to two straight lines with a maximum departure in curvature below these asymptotes of only 3 dB at the  $v = v_c$  breakpoint between them. This rapid rotation from near-horizontal to straight line spectral tails in which rapidly increasing downward curvature is constrained to a very narrow  $v \approx v_c$  Doppler regime is not generally characteristic of the Phase One- and LCE-measured clutter spectral shapes.

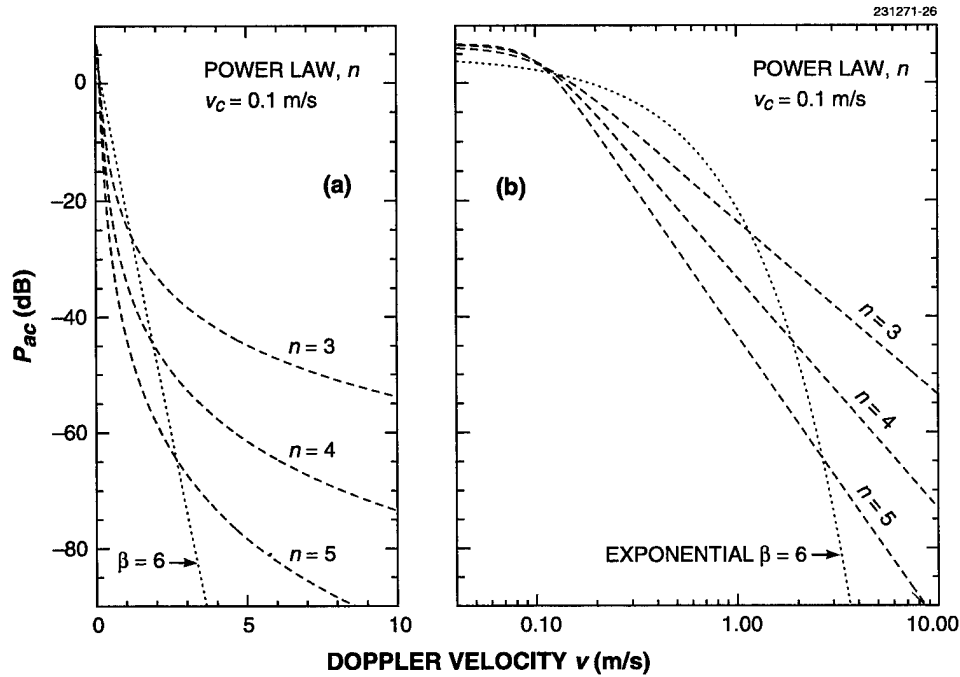


Figure 40. Comparison of exponential and power-law spectral shapes: (a) linear and (b) logarithmic Doppler velocity axis.

**Status (Exponential vs Power Law).** The Phase One and LCE measurements of ground clutter spectra presented in this report are displayed on both linear and logarithmic Doppler velocity axes. What is clear in these presentations, and what has not been generally recognized, is that if the clutter ac spectral shape  $P_{ac}$  is represented as a power law, the power-law exponent  $n$  is not constant but gradually increases from  $n = 3$  or 4 when  $P_{ac}$  is 35 or 40 dB down from its maximum to  $n = 5$  or 6 or even higher when  $P_{ac}$  is 60 to 80 dB down from its maximum. Recent uncertainty about whether “the law” of spectral decay is “ $n = 3$  or  $n = 6$  (or even exponential)” is abetted by the additional lack of general recognition that the shape of the spectrum to levels 60 to 80 dB down is usually not precisely representable by any single analytic expression. In the results presented herein, slight upward curvature (concave from above) often occurs on the  $10 \log P_{ac}$  vs  $v$  plots, hence the shape can be slightly broader than exponential, whereas strong downward curvature (convex from above) almost always occurs on the  $10 \log P_{ac}$  vs  $\log v$  plots, hence the shape is much narrower than constant power law. Thus there is no argument with Andrianov, Armand, and Kibardina that “It is [usually] impossible to [precisely match] the spectral density of the scattered signal by a single analytical function in the entire range of [Doppler] frequencies” [15]. However, much of the potentially ensuing difficulty in the general modeling of clutter spectra is overcome in this report not just by utilizing exponential shapes, but also by introducing the concept of a quasi-dc region and absorbing excess power in this region into the dc delta function term of the model. However the spectrum is modeled, the Phase One



and LCE results support the general existence of windblown clutter Doppler velocities only as great as  $\approx 3$  to 4 m/s for 15- to 30-mph winds to levels 70 to 80 dB down.

The evidence for both power-law and exponential clutter spectral shapes is essentially empirical. The concern in this report is not which of these two forms fits the data best over spectral dynamic ranges of  $-30$  or  $-40$  dB, or even whether such a question can be definitively answered. This report provides good examples of both power-law and exponential fits to measured clutter spectral data to levels 30 or 40 dB down, and in reviewing the technical literature finds it to be similarly bipartite on this matter. The concern is, however, in determining an appropriate functional form to describe clutter spectra over greater spectral dynamic ranges. The main observation in this regard, based on the Phase One and LCE data bases, is that no matter how good the power-law fits are over spectral dynamic ranges extending 30 to 40 dB below zero-Doppler peaks, they cannot be extrapolated to lower levels. That is, power-law shapes extrapolate rapidly to excessive spectral width. In contrast, the exponential form generally represents the Phase One and LCE measurements not only over their upper ranges of spectral power but also over their complete spectral dynamic ranges extending to levels 60 to 80 dB below zero-Doppler peaks. Thus radar system design for which ground clutter interference is of consequence at such low levels of spectral power is much more accurately based on an exponential clutter spectral shape approximation than on an extrapolated power-law approximation.

## **5.2 REPORTS OF UNUSUALLY LONG SPECTRAL TAILS**

Several historical reports of spectral tails in ground clutter at unusually high power levels and/or extending to unusually high Doppler velocities are considered in the following subsections.

### **5.2.1 Total Environment Clutter**

There has been concern in recent years with how to characterize clutter residues that might be left in Doppler filter banks in high sensitivity radars after MTI cancellation and that might cause false targets for subsequent multitarget tracking algorithms. Thus there is interest in specifying an overall environment clutter model that would include the Doppler interference from such things as aurora, meteor trails, cosmic noise, windblown material (leaves, dust, spray), birds and insects, rotating structures, rain and other precipitation, lightning, clear air turbulence, fluctuations of refractive index, etc. Often such phenomena are highly transient as they occur in measurements of radar Doppler spectra, so that it is difficult to causally and quantitatively associate unusual spectral artifacts directly with their sources. It is not suggested here that a specific program dedicated to measuring any one of these phenomena would not be successful—rather that in a general data base of spectral measurements collected from spatial ensembles of remote ground clutter cells, the occasional occurrence of causative agents different from windblown vegetation is difficult to determine. The main focus of interest in the Phase One and LCE spectral measurements is the general and continuous spectral spreading that occurs in ground clutter due to wind-induced motion of tree foliage and branches or other vegetative land cover. These clutter data bases have not been very extensively used for systematic searching for infrequent, spatially unusual, narrowband, or transient spectral features resulting from other causative agents in the total clutter environment because of their ephemeral nature and uncertain signature characteristics, although occasional evidence of birds, airplanes, automobiles, and other anomalies has been encountered in the spectral analyses of these data. The one concrete example encountered by

the LCE radar of clutter from the total environment over land with atypical spectral behavior was strong Bragg resonance at small, but nonzero Doppler frequencies in the returns from a small inland body of water [32]. Some of the unusually long spectral tails attributed to windblown clutter in the following discussions may actually originate from external sources other than windblown vegetation or even from internal instrumentation effects.

### 5.2.2 Chan's "Fast-Diffuse" Component

In addition to a "slow-diffuse" exponential component in ground clutter spectra, Chan [24] also introduced a "fast-diffuse" component at a relatively weak but constant power level out to a higher Doppler frequency cutoff than the slow-diffuse component. Both components are indicated in Chan's idealized diagram (Chan [24]) of a composite ground clutter model shown in Figure 41. The fast-diffuse component is based on the observation of very infrequent or narrowband spectral features usually observed in isolated cells and for short-duration time intervals. The amplitude and cut-off frequency of the fast-diffuse component are not specified by Chan; however, for all his fast-diffuse examples, the maximum, or cutoff Doppler velocity, although greater than the slow-diffuse component present, was  $\leq 2.5$  m/s. Such occasional spectral features may often be caused by total environment clutter (birds, etc.).

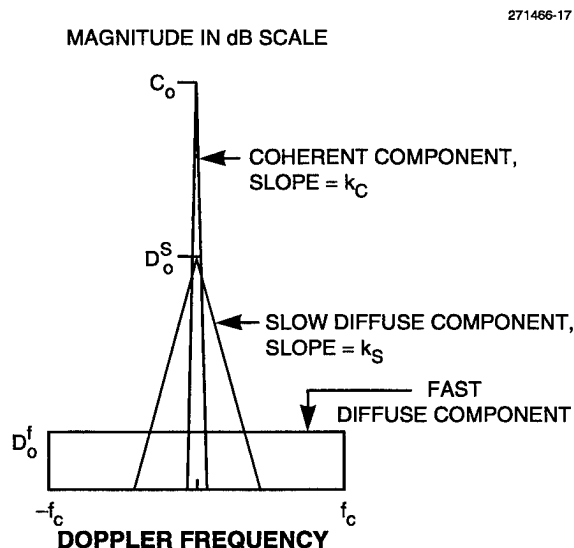


Figure 41. Chan's [24,27] conceptual composite clutter model, including a fast-diffuse component.

Chan's discussion of several of these unusual spectral features is interesting. Transient, isolated, narrowband spectral features at low Doppler that do not exist symmetrically to either side of zero-Doppler can often, with some degree of confidence, be attributed to birds. Chan also speculated that "regular oscillatory motion of [crop] vegetation, arising from restricted freedom of travel and natural elasticity" [24] might ex-

plain some unusual symmetrical features. Similar features have not been observed at Lincoln Laboratory, although Chan was using different Phase One data (repeat sector) and different processing (maximum entropy). Nonlinear superresolution processing techniques (such as maximum entropy) usually require large S/N ratios—not available at low levels in measured clutter spectra—to avoid spurious results. Spectral contaminants from the measurement instrument or from external RF sources of interference may also be present. Spectral features that are not isolated but exist in all spatial resolution cells, and/or that exist symmetrically to either side of zero-Doppler, are likely to be instrumentation or processing contaminants.

Probabilities of occurrence, which would be difficult to determine, would eventually be required in a model for fast-diffuse spectral features. In any event, experience has indicated that Chan's fast-diffuse spectral component is easily misunderstood to imply the existence of a long, continuous, low-level, uniform amplitude spectral tail in ground clutter that is always there for all cells and all times. In fact, the fast-diffuse component was based on the observation of infrequent spectral artifacts.

### **5.2.3 White's Wideband Background Component**

White's physical model [30] for windblown trees, which provides an exponential spectral component, also provides a rectangular wideband background spectral component at lower power levels. White essentially postulated the existence of his background component on the basis of Chan's fast-diffuse component [24, 27]. In so doing, White—as others have done—appears to have misinterpreted Chan's fast-diffuse component in the manner discussed earlier. Thus whereas Chan's fast-diffuse component was based on the observation of infrequent spectral artifacts out to a maximum observed Doppler velocity of 2.5 m/s, White took this as the basis for postulating a wideband noise-like spectral component with "... a uniform spread of spectral power over all [Doppler] frequencies up to about 1 kHz" [30]. A cut-off frequency of 1 kHz corresponds to Doppler velocities of 15 and 50 m/s for the X- and S-band radars, respectively, that White was considering, which is well beyond Chan's observed cutoff.

White provided heuristic argument for the existence of a wideband background spectral component based on leaf (as opposed to branch) motion. In particular, he argued that rapid decorrelation in the returned signal resulting from the shadowing of one leaf by another and by leaf rotation can be expected to give rise to a wideband noise component. White did not derive a mathematical expression for the wideband component, and its absolute level was not specified.

White did attempt to provide some experimental evidence for the wideband background spectral component in C-band clutter data measured at DRA/Malvern. This experimental evidence is unconvincing. The spectral dynamic range of the measurement radar was not shown or specified, but it was stated that the radar had a "... reasonably high radar noise floor" [30]. Results were provided for a quiet day and a windy day. In both sets of results what was claimed to be the wideband background component also has the appearance of a system or processing noise floor. In both sets of results, cells with significantly spread clutter spectra, cells with little, and cells with no clutter Doppler spread were separately combined to provide averaged clutter spectra with wide, some, and no clutter spread. It was observed that the noise-like background component was somewhat higher in spectral power level for the wide averaged spectrum than for the other two averaged spectra with little or no spread. In the quiet-day results, this difference in background level was small, and it was concluded that "the apparent white noise component ... is due to ... Fourier sidelobes and system noise" [30]. In the windy-day results, the difference was somewhat greater. It was argued that in this

case this difference indicates “a real white-noise scatterer motion within the band limits of the radar” [30]. In White’s plotted results, what was claimed to be the white-noise spectral component occurs about 38 dB below the zero-Doppler peak.

The Phase One and LCE data bases of clutter spectral measurements provide no evidence for the existence of a noise-like wideband background spectral component within the spectral dynamic ranges of these instruments, which reach 60 to 80 dB below the zero-Doppler spectral peaks. The Armand et al. [13] measured clutter spectral data (discussed later in this report) at 4-mph wind speed show a noise-like component at a constant level of  $\sim -115$  dB extending over the range  $2.5 < v < 20$  m/s. At the higher wind speeds of 13 and 31 mph, the Armand et al. data decay continuously and reach the  $-115$ -dB level only at the limit of the measured data as  $v$  reaches  $\sim 20$  m/s. No convincing evidence is provided by Armand et al. that the  $-115$ -dB level in these data is not a noise level. The bare-hill data of Warden and Wyndham [10] show a hint of a possible constant noise-like tail beginning at the  $-24$ -dB level ( $0.55 < v < 0.65$  m/s), which is almost certainly a noise level or other corruptive influence (see Figure 29). In a recent private communication, White agreed that some degree of skepticism was warranted concerning his postulated wideband noise-like background component and indicated that he was “... in the process of looking at this area again” [31].

#### 5.2.4 Simkins’ “Lowland” Data of Wide Spectral Extent

This discussion concerns the Seek Igloo L-band measurements of clutter spectra by Simkins, Vannicola, and Ryan [16] shown in Figure 33. The modeling information for spectral shape derived from these measurements was based on upper-bound approximations to worst-case spectra. These worst-case spectra came from resolution cells causing false alarms in a three-pulse-canceller MTI channel. These cells causing false alarms led to  $v^{-3}$  and  $v^{-4}$  power-law estimates of spectral shape. Spectra from adjacent cells with similar intensity but which did not cause false alarms were narrower, with  $v^{-5}$  or exponential shape.

Relative frequencies of occurrence of false alarm cells compared with non-false alarm cells were not specified. False alarms can be caused by transient events in the total clutter environment other than generally pervasive windblown vegetation. False alarms that moved measurable distances over several PPI scans were called angels; possible associations of angels, primarily with birds, but also with insects, clear air turbulence, and aurora, were discussed. Other false alarms were due to anomalous propagation, for which no spectral data were taken. Stationary ground clutter false alarm cells upon which the ground clutter spectral modeling information was based were not associated with such total environment causes.

Consider first the Seek Igloo ground clutter spectral data for “partially wooded hills” in 10- to 20-knot winds. The  $v^{-4}$  power-law shape attributed to these data in Figure 33 is an approximate upper-bound to an underlying scatter plot of data points. These data points, as typified by  $\approx -30$  dB at 0.25 m/s and  $\approx -40$  dB at 0.5 m/s, are not out of line with Phase One and LCE data. It is not the characterization of the bounding shape of these data as  $v^{-4}$  over the indicated 45-dB dynamic range that leads to difficulty, but the extrapolation of a constant  $v^{-4}$  power-law shape to power density levels significantly lower than  $-45$  dB. Phase One and LCE also often show  $v^{-3}$  and  $v^{-4}$  rates of decay 35 to 40 dB down, but these become  $v^{-5}$  and  $v^{-6}$  rates of decay 60 to 80 dB down.

Consider next the Seek Igloo ground clutter spectral data for “heavily wooded valleys” or “lowlands” in 10- to 20-knot winds also shown in Figure 33. A wider  $v^{-3}$  power-law shape was attributed as an upper bound approximation to these data. These heavily wooded valley data, as typified by  $\approx -7$  dB at 0.5 m/s and  $\approx -15$  dB at 1 m/s, are significantly wider than Phase One- and LCE-measured spectra (the widest LCE spectrum is  $\approx -20$  dB at 0.5 m/s and  $\approx -30$  dB at 1 m/s). The maximum measured Doppler velocity among the measured Seek Igloo heavily wooded valley spectral data points is 5.8 m/s, 40 dB down; 5.8 m/s is almost twice the maximum Doppler velocity of  $\approx 3$  m/s for windblown trees consistently seen by LCE in 15- to 30-mph winds, 70 to 80 dB down, and almost four times the Doppler velocity of 1.5 m/s seen in the widest LCE spectrum, 40 dB down. No other known measurement of a ground clutter spectrum approaches such high spectral power at such high Doppler velocity as given by the 5.8 m/s, -40-dB point of the Seek Igloo heavily wooded valley data.

On the basis of the many Phase One and LCE results in 15- to 30-mph winds, attributing Doppler velocities of 5.8 m/s, 40 dB down, to windblown trees would conjecturally require wind velocities much greater than the nominal 10- to 20-knots associated with the Seek Igloo heavily wooded valley data. The only other known measurements of ground clutter spectra in which spectral power decays as slowly with increasing Doppler velocity as in the Seek Igloo heavily wooded valley data are early results reported by Goldstein [8] for trees in gale-force winds, discussed in Section 5.2.5; however, these measurements only extend to a maximum Doppler velocity of 1 m/s. The only other known measurements of ground clutter Doppler velocities approaching or exceeding the 5.8 m/s maximum Doppler velocity shown at the -40-dB spectral power level in the Seek Igloo heavily wooded valley data (besides White’s improbable wideband noise-like component) are the highly questionable results of Armand et al. [13] discussed in Section 5.2.6; however, spectral extent  $\geq 5.8$  m/s in the Armand et al. data is at dubiously low spectral power levels in the range of -90- to -120-dB. Otherwise, the Phase One and LCE measurements and the rest of the published literature [6,9-12,14,15,19,20,22,24,37,39], including the other Seek Igloo data [16] and the Armand et al. data [13] at higher, less questionable spectral power levels, are in general agreement in terms of gross spectral extent (as opposed to details of spectral shape), measured over equivalent spectral dynamic ranges.

Since these high Doppler velocity heavily wooded valley or lowland data are worst-case results from false alarm cells, they are probably caused by some phenomenon other than windblown trees. The fact that a  $v^{-3}$  power-law spectrum at low Doppler frequencies typically results from poor stability in a radar (in particular, the oscillator) might suggest possible equipment limitations. However, Simkins, Vannicola, and Ryan [16] discuss their efforts to quantify the spectral contamination contributed by their measurement instrumentation, including spreading of observed spectra due to oscillator instability. Further assurance that the heavily wooded valley data were indeed of external origin and important consequence would be provided if they could be confirmed through routine replication in independent measurements. In any event, whether internally or externally caused, these high Doppler velocity heavily wooded valley data should not be misconstrued as generally representative of clutter spectra from windblown trees. The further extrapolation of these heavily wooded valley data as an upper bound,  $v^{-3}$  constant power-law dependency to levels significantly below -40 dB (e.g., to Doppler velocities of 30 m/s, 60 dB down), while retaining their general association with windblown trees, is even more unrealistic on the basis of the LCE and Phase One measurements.

### 5.2.5 Goldstein's Spectral Measurements in Gale Force Winds

Goldstein [8] describes three measurements in gale force winds (39 to 54 mph). The actual maximum Doppler velocities to which spectral power was measured in these results are low ( $\leq 1$  m/s), but the corresponding power levels are very high. The first two measurements were at X- and K-bands for which the power spectra are shown much as originally plotted in Figure 42 on linear scales of normalized spectral power density (0 to 1) vs Doppler velocity. The two spectra are quite similar; both are typical bell curves. The X-band spectrum is slightly wider than the K-band spectrum. At 0.5 m/s, the power levels in those spectra are 0.36 (−4.4 dB) and 0.28 (−5.5 dB) for X- and K-bands, respectively. At higher Doppler velocities, power levels in these bell-curve spectra diminish: at 0.85 m/s, the K-band curve is shown to reach zero power (−∞ dB); and at 1 m/s the X-band curve is at power level = 0.04 (−14 dB), this latter point being the maximum Doppler velocity provided in Goldstein's gale force spectral results. This point is nearly equivalent to corresponding points provided by the exponential spectral model of this report for gale force winds at 1 m/s (i.e., −15.4 and −13.7 dB for  $\beta = 4.3$  and 3.8, respectively; see Section 2).

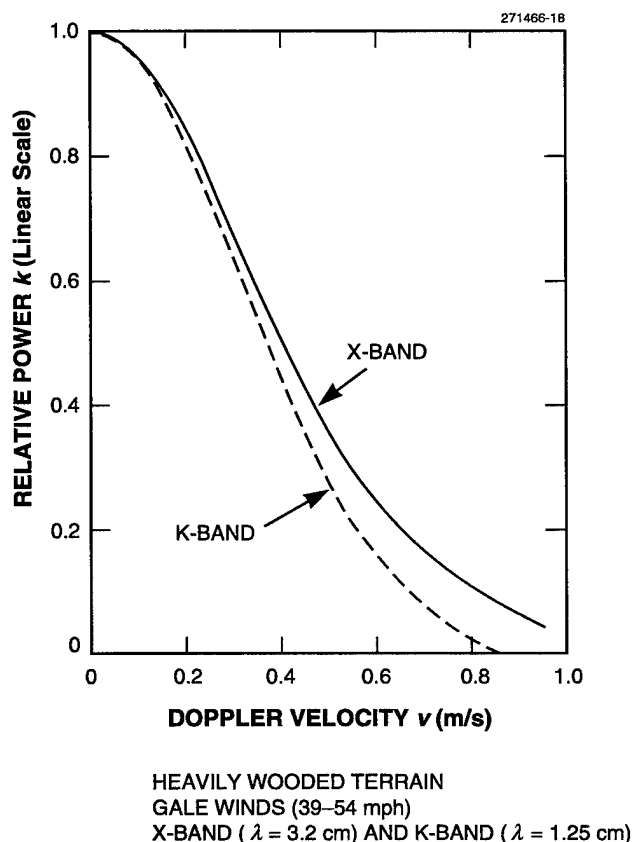


Figure 42. Measurements of radar ground clutter power spectra by Goldstein [8], 1951, under gale force winds.

Goldstein's third measurement was at S-band in 50-mph winds. This spectrum, reported by Goldstein to be of "strange shape" and "markedly out of line with the others" [8], was not shown, although three points were provided, viz., -1dB at 0.1 m/s, -3dB at 0.2 m/s, and -10 dB at 0.7 m/s. However, the autocorrelation function for this measurement was provided by Goldstein and shows a long, slowly diminishing tail plotted on linear scales. Subsequently, Wong, Reed, and Kaprielian [34] computed a corresponding power spectrum as the Fourier transform of a theoretical autocorrelation function incorporating scatterer rotational motion that was a very close match to Goldstein's unusual experimental autocorrelation function. Wong, Reed, and Kaprielian's computed spectrum is reproduced in Figure 43 together with the three actual spectral points specified by Goldstein. The computed spectrum shows a long, slowly diminishing tail. Initially, it rapidly drops to power level = 0.2 (-7 dB) at 0.5 m/s, and thereafter slowly diminishes at a rate approximated by a power law of  $n = 3.3$  to power level = 0.02 (-17 dB) at 2 m/s. In comparison, at 2 m/s the widest measured LCE spectrum is at -53 dB. In discussing these curves of correlation function and power spectrum, Wong, Reed, and Kaprielian noted that they "deviate significantly from the usual expected Gaussian shape. Instead, they drop very slowly toward zero" [34]. Thus these data have contributed to the concept of a long spectral tail, here at an usually high power level.

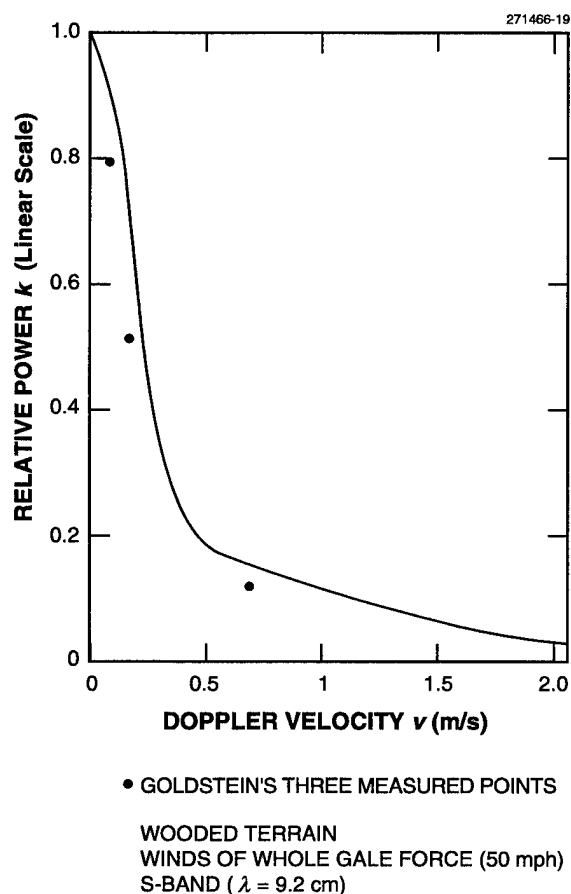


Figure 43. A radar ground clutter power spectrum computed from Goldstein's measured correlation function by Wong et al. [34], 1967, showing a long spectral tail under gale force winds.

Some reservations must be accorded to Goldstein's results, due to their very early origin. Goldstein was attempting to establish only the most basic general characteristics and, indeed, just the very existence of spectral spreading of ground clutter in these early results. Conversion of values from near the limits of Goldstein's plots on linear scales to decibel quantities for comparison with modern measurements to much lower power levels where the concern is with detailed behavior of spectral tails is using Goldstein's data out of historical context. In particular, Goldstein's unusual S-band gale force data and their further elaboration by Wong, Reed, and Kaprielian [34] now appear to be best regarded as historically anomalous (i.e., anything can happen in an isolated measurement), at least until the unlikely occurrence of their consistent confirmation with modern measurements. Unfortunately, no modern measurements of windblown tree clutter spectra under gale force winds are known to exist. On 19 August 1991, during the time of LCE clutter measurement on Wachusett Mt., Hurricane Bob swept through Massachusetts with gale force winds occurring in the clutter measurement sectors. However, radar operating personnel were unable to remain on Wachusett Mt. during the hurricane, and measurements were not acquired. Similarly, on another occasion the Phase One crew were evacuated from their operations van by local police because of severe blizzard conditions (e.g., wind gusts to 50 mph) in the area, before they could collect the stormy weather measurement data [25].

#### 5.2.6 Armand's Long, Low-Level Clutter Spectral Tail

Armand et al. [13] ostensibly measured X-band clutter spectra from windblown trees to very low levels of spectral power ( $-120$  dB) and correspondingly very high Doppler velocities (20 m/s). Their results are reproduced in Figure 44. Armand et al. stated that these ground clutter spectra were measured with CW equipment in which the power received from the sidelobes of the transmitter was an order of magnitude higher than that reflected from the trees. Instabilities were reported eliminated through use of klystrons stabilized by cooling with liquid helium. Results were obtained in the 40- to 2500-Hz Doppler frequency band (i.e., not near the carrier). Spectral results are shown for three wind speeds—4, 13, and 31 mph—over the range from 40 to  $\approx 1300$  Hz (0.6 to  $\approx 20$  m/s). Over this range, the spectral power density levels are between  $-50$  and  $-120$  dB (i.e., are much lower than any other known spectral measurements). For the 4-mph spectrum, the power drops to  $-120$  dB at 2.5 m/s, and thereafter stays at  $\approx -120$  dB all the way out to 20 m/s (i.e., exhibits a long spectral tail at a uniform low level, like White's [30] conceptual wideband noise-like spectral component). The 13- and 31-mph spectra drop gradually from  $-63$  and  $-52$  dB, respectively, at 0.6 m/s to  $\approx -115$  dB at 20 m/s. At power levels 80 dB down, Doppler velocities in the Armand et al. results of Figure 44 are  $\approx 0.9$ , 1.4, and 2.5 m/s for 4-, 13-, and 31 mph winds, respectively; these spectral widths are a very close match to those measured by Phase One and LCE at similar levels of spectral power (i.e., near their limits of sensitivity).

Armand et al. [13] claimed that their spectral shapes were power law, with an average value of power-law exponent  $n = 3$  in the 110- to 2500-Hz band averaged over all tests and with  $n$  varying inversely with wind velocity between 3 and 6 in the 40- to 110-Hz band. The authenticity of these very long, very low-level clutter spectral tails is open to question; what was measured may have been effects of internal system instabilities. Before undue credibility is ascribed to these results, they certainly need to be confirmed by independent and consistent replication using modern measurement instrumentation. However, these results arguably keep open the possibility of long spectral tails at very low power levels below Phase One and LCE



sensitivities. As previously discussed, spectral power at large Doppler velocities is theoretically accounted for by Armand et al. through amplitude modulation via leaf rotation and shadowing of one leaf by another, in addition to phase modulation caused by leaf oscillatory motion in the direction of the radar. Note that the Russian spectral measurements [14,15] that followed those of Armand et al. [13] were performed specifically to obtain information close to the carrier. Although the Phase One and LCE results do not agree with this series of Russian results [12–15] in their assessments of spectral shape as power law, none of these Russian measurements show inordinately wide spectra over the ranges of spectral power measured by Phase One and LCE.

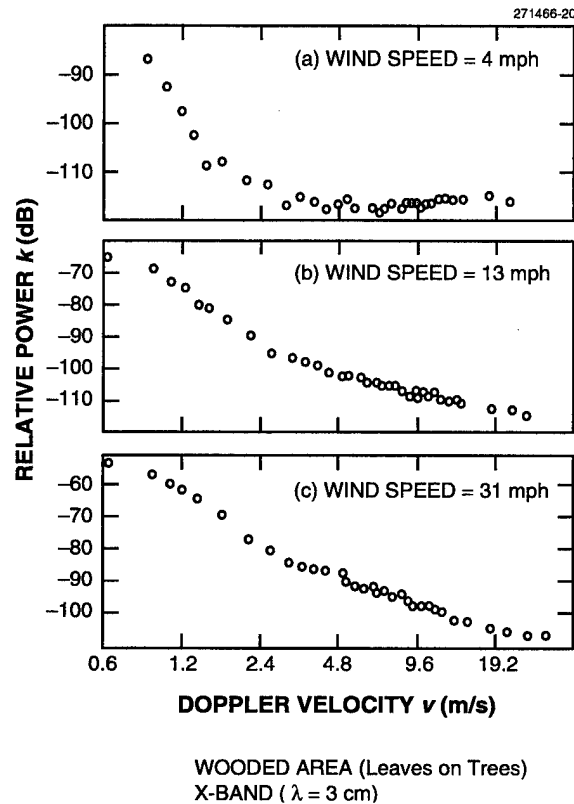


Figure 44. Measurements of radar ground clutter power spectra by Armand et al. [13], 1975, showing very long, low-level spectral tails.

### 5.2.7 Instrumentation and Processing Effects

Internal effects from the measurement radar often have contaminated and corrupted attempted measurements of clutter frequency spectra to low spectral power levels. The fact that the shape of the spectrum

resulting from oscillator instability is an  $n = 3$  power law can raise suspicion of measured clutter spectra with  $n = 3$  power-law characteristics. For example, the Simkins et al. [16] heavily wooded valley or lowland data of unusually wide spectral extent follows an  $n = 3$  power-law shape, as do the Armand et al. [13] data at very low power levels (70 to 120 dB down) and at very high Doppler velocities (1.65 to 37.5 m/s). Care must be taken to isolate and avoid spectral contamination from system instabilities. Quantification of spectral contamination is required for every measurement at the actual range at which the clutter measurement is performed, since instability of the stable local oscillator (STALO) produces a greater effect at longer ranges (the phase has more time to change when the STALO is used to upconvert on transmit and downconvert on receive). If the STALO is not used on receive, but the signal is merely envelope-detected prior to spectral analysis (as in the results of Goldstein [8] and Fishbein et al. [9]), the full STALO instability spectrum or that of the transmitter is impressed on the received clutter signal. Goldstein's [8] early measurements were undoubtedly made using a klystron or magnetron as the transmitter, resulting in relatively poor stability. In the Armand et al. [13] results, transitions are observable in the spectral data at low power levels (at 1.5 m/s Doppler velocity for 4-mph wind speed, and at 2.4 m/s Doppler velocity for 13-mph wind speed). For Doppler velocities greater than those of these transition points, it is conceivable that the data result from system instabilities. Note that the results of Armand et al. were obtained using a CW transmitter; use of pulsed radar can introduce additional instability due to noise contamination of trigger pulses. Nonlinearities in circuitry or processing can also spread the frequency spectrum. For example, in the Seek Igloo results of Simkins et al. [16], a lin-limit amplifier was used in the receiver, which conceivably might limit and spread the spectrum under strong signal (strong clutter) conditions. Data in saturation result in significant spectral spreading caused by the actual spectrum convolving with itself in such circumstances. Discounting this possibility for the stationary false alarm cells underlying the Simkins et al. heavily wooded valley data is the reported fact that spectra from adjacent non-false alarm cells of similar intensity were narrower. Unwanted antenna motion caused mechanically, and/or by the wind, can also spread the frequency spectrum by modulating the clutter signal. This modulation may go unobserved if stability testing is performed in low-wind conditions.

A few cases of long spectral tails extending to Doppler velocities  $\gg 3$  m/s were observed during the course of examining the Phase One data base of spectral measurements. In every case, the long spectral tail was isolated to some sort of instrumentation problem (e.g., sticking bits on the A/D converter generating minute sample-and-hold stairsteps on the temporal signal; occasional saturations; external interference). One excessively wide Phase One spectral measurement caused by undetected saturation was inadvertently included in a set of "windy" spectra in a previous publication (spectrum 4, Figure 8, in Billingsley and Larabee [23]). Thus any unusually wide measured spectra should always be very carefully examined in the time domain before accepting the wide frequency domain result. Attempts to improve Phase One stability by sampling the transmitted signal and correcting (i.e., subtracting) transmitted phase variations in the received signal were unsuccessful (i.e., proved to be not simple to implement). The LCE radar was a spectrally purer system than Phase One and was never observed to generate an excessively wide spectral tail due to system or processing contamination. Some new windblown clutter spectral measurements by another investigator were recently reviewed that at first contained obviously corrupted clutter spectral tails of excessive width and extremely slow ( $n \approx 3$ ) decay; subsequent investigation found these long spectral tails to be caused by an error in processing involving the window function.

In considering all the possible ways in which instrumentation limitations or processing errors can broaden measured clutter spectra, it is well to bear in mind that of two measured spectra—one narrow and one wide—ostensibly characterizing the same clutter phenomenon, the narrower spectrum is always more

credible since all corruptive influences due to instrumentation limitations or processing errors can only broaden the spectrum, not narrow it.

Because of all the potential uncertainties (i.e., potential contaminants of internal and external origin) in radar ground clutter spectral measurements as exemplified in the preceding discussions of Section 5.2, the use of such data requires the exercise of judgment. Ground clutter spectral models should reflect, for the most part, central repeatable trends in measured data, not unusual or isolated artifacts or aberrations.

## 6. SUMMARY

Accurate characterization of radar ground clutter spectral shape is important in radar technology applications in which target signals compete with strong ground clutter returns. Ground clutter spectral spreading can limit the performance of MTI/Doppler processors, including both conventional one-dimensional fixed-parameter designs and modern two-dimensional displaced phase-centered antenna or space-time adaptive techniques for detecting and tracking moving targets in clutter backgrounds. Internal clutter motion can also cause defocusing in SAR processing, and indeed can degrade any radar processing technique that assumes the clutter to be stationary. Such reasons motivate us to understand clutter spectral spreading and the accurate characterization of the shapes of clutter spectra to very low levels of spectral power. Until recently, the state of knowledge of windblown ground clutter spectral shape has been rather poor, and considerable disagreement has existed concerning the extent to which Doppler spreading occurs in such spectra.

Lincoln Laboratory measurement data indicate that ground clutter power spectra over spectral dynamic ranges reaching 60 to 80 dB below the zero-Doppler peaks are relatively narrow and reasonably characterized as of exponential shape. Exponential decay was first observed in Air Vehicle Survivability Evaluation (AVSE) program studies at Lincoln Laboratory as broadly characterizing the shapes of measured ground clutter spectra in the early examination of windblown foliage clutter spectra obtained with the Phase One clutter measurement radar at western Canadian sites [23] from 1982 to 1984. These first AVSE observations of exponential decay remained valid in the general representation of a much more complete set of L-band spectral measurements over various regimes of wind speed obtained during 1985 with the Phase One radar at the Lincoln Laboratory measurement site of Katahdin Hill in eastern Massachusetts [23]. It subsequently became known that some measured clutter spectra had been observed to be very exponential in shape in a much earlier Lincoln Laboratory measurement program [47]. The only other known earlier instance of using the exponential function to characterize the shape of a measured ground clutter spectrum came to light in a literature search that uncovered four Russian papers [12–15] from 1973–76, in which the fourth paper [15] revised the rate of decay over the first 20 dB of spectral decay from Gaussian as originally specified [12] to exponential; the rate of decay thereafter to lower power levels was modeled in these papers as power law. Subsequent processing of Phase One clutter data by Chan [24,27] in Canada and Sarno [28] in the U.K. also concluded that ground clutter spectra were generally best-fitted with exponential shapes. In addition, Chan also observed exponential spectral decay in independent clutter measurements obtained with an S-band phased-array radar at the DREO site in Ottawa. Recently, White [30] developed an interesting first-principles physical model characterizing tree branches as cantilever beams clamped at one end which leads to spectral decay that is closely exponential. White also observed exponential decay in a small amount of C-band clutter measurement data obtained at the DRA/Malvern site in the U.K. Exponential decay was also concluded to be the best overall characterization of windblown ground clutter spectral shape covering several thousand spectral observations taken from the extensive L-band data base of clutter spectral measurements obtained by Lincoln Laboratory with the LCE clutter measurement radar in further AVSE studies. The LCE radar was a major L-band-only 1991 upgrade of the five-frequency Phase One radar with new, much improved receiver and data recording units, lower phase noise levels, and very clean and reliable spectral response.

The very earliest indications were that windblown ground clutter spectra were of Gaussian spectral shape [6–8]. Many subsequent measurements to lower power levels 30 to 40 dB below the peak zero-Doppler level indicated spectral shapes that were significantly wider than Gaussian in their tails and that

appeared to be well approximated with power-law functions [9–16,19,20,22]. The Phase One and LCE ground clutter spectral measurements, over such limited spectral dynamic ranges, also can be adequately modeled as of power-law shapes. However, the Phase One and LCE measurement data also clearly indicate that the power-law rates of decay at upper levels of spectral power do not continue to lower levels of spectral power reaching 60 to 80 dB down from the zero-Doppler peak. The measured power-law rates of decay at lower power levels are always much faster than at the upper levels. An exponential representation generally captures, at least approximately and occasionally highly accurately, the major attributes of the windblown clutter ac spectral shape function over the entire range from near the zero-Doppler peak to measured levels 60 to 80 dB down. In contrast, the windblown clutter ac spectral shape is not at all representable by any power law over such a wide spectral dynamic range. The maximum Phase One- and LCE-measured Doppler velocity spectral extents from windblown foliage at levels 60 to 80 dB down are  $\approx 3.3$  m/s. Power-law models can extrapolate data of 40-dB spectral dynamic range to spectral extent as great as 30 m/s, 60 dB down. Such extreme windblown foliage spectral extents have never been corroborated by any results in the extensive Phase One and LCE data bases of windblown clutter spectral measurements.

This report provides a new empirical model for windblown ground clutter Doppler spectra based on many clutter spectral measurements obtained with the Lincoln Laboratory LCE and Phase One five-frequency (VHF, UHF, L-, S-, and X-band) radars. This model is complete, including both ac and dc components of the spectrum. The important parameters incorporated in the model are wind speed and radar carrier frequency. Ac spectral shape is specified as exponential, with the Doppler-velocity exponential shape factor strongly dependent on wind speed but independent of radar frequency, VHF to X-band. This surprising fact, that ac spectral spreading occurs at VHF in windblown clutter Doppler-velocity spectra more or less equivalently as at X-band, is illustrated through representative measurement results; many other examples of VHF-measured clutter spectra with similar spectral spreading exist at Lincoln Laboratory. The difference between VHF and X-band clutter spectra is that a much larger dc spectral component exists at VHF compared with X-band. The ratio of dc to ac spectral power in the model is determined by an analytic expression empirically derived from the measurements which captures the strong dependencies of dc/ac ratio on both wind speed and radar frequency. This report includes both a complete specification of the clutter spectral model, and a thorough comparison of model predictions with many examples of measured windblown clutter spectra under various combinations of radar parameters and measurement circumstances. Besides wind speed and radar frequency, other parameters that might be thought to significantly influence clutter spectra but that appear to be largely subsumed within general ranges of statistical variability in the measurement data include tree species, season of the year, wind direction, cell size, polarization, range, and grazing angle. The exponential model is explicitly derived to be applicable to windblown trees, but examples are also provided of measured clutter spectra from scrub desert, rangeland, and cropland vegetations which indicate that the model can also perform adequately for other windblown vegetation types by suitably adjusting its dc/ac term.

Although it is now generally accepted that radar ground clutter spectral shapes are wider than Gaussian in their tails, nevertheless the simple Gaussian continues to be how clutter spectra are usually represented in radar system engineering, at least as a method of first approach in representing effects of intrinsic clutter motion, based on reasons of simplicity and analytic tractability. The Gaussian spectral shape is theoretically generated by a group of moving scatterers, each of random translational drift velocity [20]. Theory also suggests that the origin of the increased spreading observed in measured ground clutter spectra beyond that predicted by Gaussian is largely due to the random oscillatory motion of leaves and branches, in contrast to simple random translational motion [20,34,37]. Like the Gaussian spectral shape, the

exponential spectral shape is also simple and analytically tractable, and has the advantage of being wider than Gaussian as required by experiment and supported by theory.

There is no underlying fundamental physical principle requiring clutter spectra to be precisely of exponential shape. Many of the Phase One and LCE clutter spectral measurements, particularly many of the narrower spectra occurring at lower wind speeds, are less exponential overall than some of the wider measured spectra. To be clear on this matter, almost none of the Phase One- and LCE-measured clutter spectra can be accurately represented by any single simple analytic function, including exponential, over their complete spectral dynamic ranges, from the point of view of passing rigorous statistical hypothesis tests. Use of the exponential shape in this report is as a convenient analytic bounding envelope that empirically approximates, occasionally very accurately, many of the LCE and Phase One measurements over most of their spectral dynamic ranges, including the lowest power levels measured. The resulting model overcomes much of the difficulty in modeling clutter spectra not only by using exponential shapes, but also by introducing the concept of a quasi-dc region and absorbing the excess power measured in the quasi-dc region into the dc delta function term of the model. This approach allows the model the flexibility of using the exponential representation to optimally match the measured spectral spreading in the spectral tail regions without regard to the narrow near-zero-Doppler quasi-dc region, which often displays a different rate of decay than occurs in the broad spectral tail.

It is evident on the basis of the Phase One and LCE measurements that the current state of knowledge regarding the extent of spectral spreading in windblown ground clutter has been advanced to the point where it is relatively incontrovertible that clutter spectra from windblown vegetation, although wider than Gaussian, are still generally relatively narrow and spread to Doppler velocities  $< \approx 3$  or 4 m/s over spectral power levels reaching to 80 dB below zero-Doppler peaks for wind speeds in the 15- to 30-mph range. Investigators who may wish to continue to argue for much wider spectra over such ranges are faced with proving spectral purity in their wider measurements, since unknown corruptive instrumentation or processing effects can only widen spectra, not narrow them. Presumably, most of the spectral spreading that does occur in the Phase One and LCE data is caused by the velocity distribution (translational and/or oscillatory) of the foliage, that is, by the radial motion of individual scatterers (leaves and branches) toward and away from the radar causing phase modulation in the returned signal. To whatever extent other effects are also at work in the Phase One and LCE data such as leaf rotation or the shadowing of one leaf by another causing more complex amplitude modulation effects, such effects are also constrained to cause limited spreading to levels 80 dB down.

This report also provides a relatively thorough review of the available literature of clutter spectral measurements which generally brings it and the Phase One and LCE results into conformity and agreement. There remain hints in the literature, however, not only from theoretical reasoning but also in various poorly substantiated measurement results, of long spectral tails existing in ground clutter data to Doppler velocities greatly exceeding the maximum  $\approx 3$  to 4 m/s observed in the Phase One and LCE data. Arguments for the existence of such wide tails often are based on postulated leaf-rotation and leaf-shadowing effects. Such long tails have never been observed, whether as slowly decaying power laws or as uniform-amplitude wide-band noise-like components, in any of the several thousand spectra that have been examined from the extensive Phase One and LCE data bases of ground clutter spectral measurements to levels reaching 60 to 80 dB below zero-Doppler peaks. What might occur at lower levels remains conjectural.

## REFERENCES

1. M. I. Skolnik, *Introduction to Radar Systems*, 2nd ed., New York: McGraw-Hill (1980).
2. J.A. Scheer and J.L. Kurtz (eds.), *Coherent Radar Performance Estimation*, Boston, Mass.: Artech House, Inc. (1993).
3. J. Ward, "Space-Time Adaptive Processing for Airborne Radar," Lexington, Mass.: MIT Lincoln Laboratory, Technical Rep. 1015 (13 December 1994), DTIC AD-A293032.
4. P. Richardson, "Relationships between DPCA and adaptive space-time processing techniques for clutter suppression," *Proc. International Conf. Radar*, SEE 48 rue de la Procession, 75724 Paris Cedex 15 (May 1994), pp. 295-300.
5. L.N. Ridenour (ed.), *Radar System Engineering*, Vol. 1 in the MIT Radiation Laboratory Series, New York: McGraw-Hill (1947). Reprinted, Dover Publications (1965).
6. E.J. Barlow, "Doppler Radar," *Proc. IRE* **37**, 4 (1949).
7. J.L. Lawson and G.E. Uhlenbeck (eds.), *Threshold Signals*, Vol. 24 in the MIT Radiation Laboratory Series, New York: McGraw-Hill (1950). Reprinted, Dover Publications (1965).
8. H. Goldstein, "The Fluctuations of Clutter Echoes," pp. 550-587, in D. E. Kerr (ed.), *Propagation of Short Radio Waves*, Vol. 13 in the MIT Radiation Laboratory Series, New York: McGraw-Hill (1951). Reprinted, Dover Publications (1965).
9. W. Fishbein, S.W. Graveline, and O.E. Rittenbach. "Clutter Attenuation Analysis," Fort Monmouth, N.J.: U.S. Army Electronics Command, Technical Rep. ECOM-2808 (March 1967). Reprinted in *MTI Radar*, D.C. Schleher (ed.), Boston, Mass.: Artech House, Inc. (1978).
10. M.P. Warden and B.A. Wyndham, "A Study of Ground Clutter Using a 10-cm Surveillance Radar," Royal Radar Establishment, Technical Note No. 745, Malvern, U.K. (1969). DTIC AD 704874.
11. N.C. Currie, F.B. Dyer, and R.D. Hayes, "Radar Land Clutter Measurements at Frequencies of 9.5, 16, 35, and 95 GHz," Engineering Experiment Station, Georgia Institute of Technology, Technical Report No. 3, United States Army, Contract DAAA-25-73-C-0256, April 1975. DTIC AD-A012709.
12. V.A. Kapitanov, V. Mel' nichuk, and A.A. Chernikov, "Spectra of radar signals reflected from forests at centimeter waves," *Radio Eng. and Electron. Phys.*, **18**, 9 (1973).
13. N.A. Armand, V.A. Dyakin, I.N. Kibardina, A.G. Pavel'ev, and V.D. Shuba, "The change in the spectrum of a monochromatic wave when reflected from moving scatterers," *Radio Eng. and Electron. Phys.*, **20**, 7 (1975).
14. V.A. Andrianov, I.S. Bondarenko, I.N. Kibardina, V.K. Prosshin, and D.Y. Shtern, "Characteristics of measurement of spectra of radio signals scattered by an underlying surface," *Radio Eng. and Electron. Phys.*, **21**, 2 (1976).
15. V.A. Andrianov, N.A. Armand, and I.M. Kibardina, "Scattering of radio waves by an underlying surface covered with vegetation," *Radio Eng. and Electron. Phys.*, **21**, 9 (1976).
16. W.L. Simkins, V.C. Vannicola, and J.P. Ryan, "Seek Igloo Radar Clutter Study," Rome Air Development Center, Technical Rep. RADC-TR-77-338 (October 1977). Updated in FAA-E-2763b Specification, Appendix A (May 1988). See also FAA-E-2763a (September 1987), FAA-E-2763 (January 1986, July 1985).

17. M.W. Long, *Radar Reflectivity of Land and Sea*, 2nd ed., Norwood, Mass.: Artech House, Inc. (1983).
18. N.C. Currie and C.E. Brown, eds., *Principles and Applications of Millimeter-Wave Radar*, Norwood, Mass.: Artech House, Inc. (1987).
19. J. Jiankang, Z. Zhongzhi, and S. Zhong, "Backscattering power spectrum for randomly moving vegetation," *Proc. IGARSS Symposium*, Zurich (August 1986), pp. 1129–1132.
20. N.J. Li, "A study of land clutter spectrum," *Proc. 1989 International Symp. on Noise and Clutter Rejection in Radars and Imaging Sensors*, T. Suzuki, H. Ogura, and S. Fujimura (eds.), IEICE, Kyoto (1989), pp. 48–53.
21. F.E. Nathanson, *Radar Design Principles*, 2nd ed., New York: McGraw-Hill (1991).
22. G.W. Ewell, private communication (December 1995).
23. J.B. Billingsley and J.F. Larrabee, "Measured Spectral Extent of L- and X-Band Radar Reflections from Windblown Trees," Lexington, Mass.: MIT Lincoln Laboratory, Project Rep. CMT-57 (6 February 1987), DTIC AD-A179942.
24. H.C. Chan, "Spectral Characteristics of Low-Angle Radar Ground Clutter," Ottawa, Canada: Defence Research Establishment Ottawa, Report No. 1020 (December 1989), DTIC AD-A220817.
25. J.B. Billingsley and J.F. Larrabee, "Multifrequency Measurements of Radar Ground Clutter at 42 Sites," Lexington, Mass.: MIT Lincoln Laboratory, Technical Rep. 916, Volumes 1, 2, 3 (15 November 1991), DTIC AD-A246710.
26. J.B. Billingsley, "Radar ground clutter measurements and models, part 1: Spatial amplitude statistics," *AGARD Conf. Proc. Target and Clutter Scattering and Their Effects on Military Radar Performance*, Ottawa, AGARD-CP-501 (1991), AD-P006 373.
27. H.C. Chan, "Radar ground clutter measurements and models, part 2: Spectral characteristics and temporal statistics," *AGARD Conf. Proc. Target and Clutter Scattering and Their Effects on Military Radar Performance*, Ottawa, AGARD-CP-501 (1991), AD-P006374.
28. G.C. Sarno, "A model of coherent radar land backscatter," *AGARD Conf. Proc. Target and Clutter Scattering and Their Effects on Military Radar Performance*, Ottawa, AGARD-CP-501 (1991), AD-P006375.
29. J.B. Billingsley, "Ground Clutter Measurements for Surface-Sited Radar," Lexington, Mass.: MIT Lincoln Laboratory, Technical Rep. 786, Rev. 1 (1 February 1993), DTIC AD-A262472.
30. R.G. White, "A model for MTI radar clutter," *Proc. SEE Int. Radar Conf.*, Paris (May 1994), pp. 540–545.
31. R.G. White, private communication (11 September 1995).
32. J.B. Billingsley and J.F. Larrabee, "Bragg Resonance in Measured L-band Radar Clutter Doppler Spectra from Inland Water," Lexington, Mass.: MIT Lincoln Laboratory, Technical Rep. 1019 (1 August 1995), DTIC AD-A297680.
33. F.J. Harris, "On the use of windows for harmonic analysis with the discrete Fourier transform," *Proc. IEEE* **66**, 51–83 (January 1978).
34. J.L. Wong, I.S. Reed, and Z.A. Kaprielian, "A model for the radar echo from a random collection of rotating dipole scatterers," *IEEE Trans. AES* **3**, 2 (1967).



35. R.M. Narayanan, D.W. Doerr, and D.C. Rundquist, "Temporal decorrelation of X-band backscatter from wind-influenced vegetation," *IEEE Trans. Aerosp. Electron. Syst.* **28**, 2 (1992), pp. 404–412.
36. R.M. Narayanan, S.E. Nelson, and J.P. Dalton, "Azimuthal scattering pattern of trees at X-band," *IEEE Trans. Aerosp. Electron. Syst.* **29**, 2 (1993), pp. 588–593.
37. R.M. Narayanan, D.W. Doerr, and D.C. Rundquist, "Power spectrum of wind-influenced vegetation backscatter at X-band," *IEE Proc.-Radar, Sonar Navig.*, **141**, 2 (1994), pp. 125–131.
38. J.B. Billingsley, "A Handbook of Multifrequency Land Clutter Coefficients for Surface Radar," Lexington, Mass.: MIT Lincoln Laboratory, Technical Rep. 958 (in preparation).
39. G.P. de Loor, A.A. Jurriens, and H. Gravesteijn, "The radar backscatter from selected agricultural crops," *IEEE Trans. on Geoscience Electronics*, **12**, 70–77 (April 1974).
40. D.K. Barton, *Modern Radar System Analysis*, Boston, Mass.: Artech House, Inc. (1988), p. 246.
41. A. Papoulis, *The Fourier Integral and its Applications*, New York: McGraw-Hill (1962).
42. W.B. Davenport, Jr., and W.L. Root, *An Introduction to the Theory of Random Signals and Noise*, New York: McGraw-Hill (1958).
43. S. Goldman, *Frequency Analysis, Modulation, and Noise*, New York: McGraw-Hill (1948). Reprinted, Dover Publications (1967).
44. F.G. Bass, P.V. Bliokh, and I.M. Fuks, "Statistical characteristics of a signal scattered from randomly moving reradiators on a plane section," translated from *Radiotekhnika i Elektronika* (USSR), **10**, 5 (May 1965), pp. 731–739.
45. S. Rosenbaum and L.W. Bowles, "Clutter return from vegetated areas," *IEEE Trans. Ant. Propag.*, **AP-22**, 2 (March 1974), pp. 227–236.
46. J.A. Scheer, "Coherent Radar Performance Estimation," IEEE National Radar Conference, Tutorial Notes, Atlanta (1994).
47. L. Cartledge, M. Labitt, J.H. Teele, and R.D. Yates, "An Experimental UHF Ground Surveillance Radar, Volume 2," Lexington, Mass.: MIT Lincoln Laboratory, Technical Rep. 497 (12 October 1972), DTIC AD-757565.

# REPORT DOCUMENTATION PAGE

Form Approved  
OMB No. 0704-0188

Public reporting burden for this collection of information is estimated to average 1 hour per response, including the time for reviewing instructions, searching existing data sources, gathering and maintaining the data needed, and completing and reviewing the collection of information. Send comments regarding this burden estimate or any other aspect of this collection of information, including suggestions for reducing this burden, to Washington Headquarters Services, Directorate for Information Operations and Reports, 1215 Jefferson Davis Highway, Suite 1204, Arlington, VA 22202-4302, and to the Office of Management and Budget, Paperwork Reduction Project (0704-0188), Washington, DC 20503.

1. AGENCY USE ONLY (Leave blank)		2. REPORT DATE 29 July 1996		3. REPORT TYPE AND DATES COVERED Technical Report	
4. TITLE AND SUBTITLE Exponential Decay in Windblown Radar Ground Clutter Doppler Spectra: Multifrequency Measurements and Model				5. FUNDING NUMBERS  C — F19628-95-C-0002 PR — 331 PE — 63003F	
6. AUTHOR(S)  J. Barrie Billingsley					
7. PERFORMING ORGANIZATION NAME(S) AND ADDRESS(ES)  Lincoln Laboratory, MIT 244 Wood Street Lexington, MA 02173-9108				8. PERFORMING ORGANIZATION REPORT NUMBER  TR-997	
9. SPONSORING/MONITORING AGENCY NAME(S) AND ADDRESS(ES)  Department of the Air Force      DARPA SAF/AQL                                  3701 N. Fairfax Dr. The Pentagon                              Arlington, VA 22203-1714 Washington, DC 20330				10. SPONSORING/MONITORING AGENCY REPORT NUMBER  ESC-TR-95-098	
11. SUPPLEMENTARY NOTES  None					
12a. DISTRIBUTION/AVAILABILITY STATEMENT  Approved for public release; distribution is unlimited.				12b. DISTRIBUTION CODE	
13. ABSTRACT (Maximum 200 words)  A new empirical model for windblown radar ground clutter Doppler spectra is developed based on many clutter spectral measurements obtained with Lincoln Laboratory's L-Band Clutter Experiment (LCE) and Phase One five-frequency (i.e., VHF, UHF, L-, S-, and X-band) instrumentation radars over spectral dynamic ranges reaching 60 to 80 dB below zero-Doppler peaks. The model includes both ac and dc spectral components. Ac spectral shape is specified as exponential, with the Doppler-velocity exponential shape factor strongly dependent on wind speed but independent of radar frequency, VHF to X-band. The exponential shape is intermediate in spectral extent between the Gaussian shape of historical usage (now acknowledged as being too narrow) and power-law shapes of more recent usage (which are too wide when extrapolated to levels 60 to 80 dB down). The ratio of dc to ac spectral power in the model is determined by an empirically derived analytic expression that captures the strong dependencies of dc/ac ratio on both wind speed and radar frequency in the measurement data. Many examples of windblown clutter spectra are provided and compared with model predictions, encompassing variations in wind speed and radar frequency, as well as in other parameters such as polarization, range, cell size, grazing angle, wind direction, measurement site, and season of the year. Although the exponential model is explicitly derived to be applicable to windblown trees, examples are also provided of measured clutter spectra from scrub desert, rangeland and cropland vegetations which indicate that the model can also perform adequately for other windblown vegetation types by suitably adjusting its dc/ac term. In addition, the moving target indicator (MTI) improvement factor for a single delay-line canceller in exponentially distributed clutter is derived and compared with that for Gaussian clutter; and the theoretical and experimental literature on windblown radar clutter is reviewed, including the somewhat apocryphal evidence that spectral tails very much wider than exponential might exist at spectral power levels well below LCE and Phase One radar sensitivities.					
14. SUBJECT TERMS radar ground clutter Doppler frequency spectra intrinsic clutter motion spectral shape  spectral purity windblown trees vegetative land cover clutter measurements  clutter spectral models multifrequency MTI				15. NUMBER OF PAGES 114	
				16. PRICE CODE	
17. SECURITY CLASSIFICATION OF REPORT Unclassified	18. SECURITY CLASSIFICATION OF THIS PAGE Unclassified	19. SECURITY CLASSIFICATION OF ABSTRACT Unclassified	20. LIMITATION OF ABSTRACT Same as Report		